The University Of Sheffield.

Design of novel adaptive magnetic adhesion mechanism for climbing robots in ferric structures

By:

Francisco Ochoa Cardenas

A thesis submitted in partial fulfilment of the requirements for the degree of Doctor of Philosophy

The University of Sheffield
Faculty of Engendering
Department of Automatic Control and Systems Engineering

November 2016

Abstract

The work presented in this thesis proposes a novel adaptive magnetic adhesion mechanism that can be implemented in most locomotion mechanisms employed in climbing robots for ferric structures. This novel mechanism has the capability to switch OFF and ON its magnetic adhesion with minimal power consumption, and remain at either state after the excitation is removed. Furthermore, the proposed adhesion mechanism has the ability to adapt the strength of the adhesive force to a desired magnitude. These capabilities make the proposed adhesion mechanism a potential solution in the field of wall climbing robots.

The novel contributions of the proposed mechanism include the switching of the adhesive force, selectivity of the adhesive force magnitude; determination of the parameters that have an impact in the final adhesive force. Finally, a final prototype is constructed with customised components and it is subject to a set of simulations and experiments to validate its performance.

Acknowledgments

Firstly, I would like to express my deepest gratitude to my supervisor, Prof. Tony J. Dodd, for all his support, guidance through the PhD and specially for his patience.

All my gratitude to the people that encouraged me on pursuing the PhD and that always were present.

- My wife, whose support, patience and encouragement where vital for reaching the end.
- My daughter and son, which are the motor that push me go further and never give up.
- My parents, whose care, support and guidance in life have driven me to reach the unimaginable.
- My aunts Cuca and Pina Ochoa, and uncle Luis Ochoa, who set the basis, along with my parents, that allowed me be where I am, and more important to be who I am

Last but not least, I would like to thank my two Mexicans sponsors, CONACyT and SEP (under Becas Complemento SEP grant), for the great opportunity to going abroad to study and contribute the future of my country.

Contents

List of Figures

List of Tables

Nomenclature

A	Cross sectional area
B	Magnetic flux density
F	Magnetomotive force
H	Magnetic field intensity
Hc	Coercivity / Intensity of the magnetic field (Oe)
I	Current flowing through the coil
i(t)	Electric current
L	Inductance
N	Number of turns in a coil
Oe	Oersted
R	Resistance
S/s	Samples per second / Sampling rate
t	Time
V	Voltage
ℓ	Length of the coil
τ	Time constant
ρ	Resistivity of a given material

List of Acronyms

Alnico	Aluminium-Nickel-Cobalt
AWS	American Wire Gauge
EM	Electro Magnet
emf	Electromotive force
EPM	Electro-Permanent Magnet
EPMAM	Electro-Permanent Magnet Adhesion Mechanism
FEA	Finite Element Analysis
L-T H	Legs-Tracks Hybrid
L-W H	Legs-Wheels Hybrid
L-W-T H	Legs-Tracks-Wheels Hybrid
M/EMAM	Magnetic/Electro-Magnetic Adhesion Mechanism
MFVF	Magnetic Field Viewing Film
MR	Mobile Robots
NdFeB	Neodymium-Iron-Boron
PM	Permanent Magnet
SWG	Standard Wire Gauge
T-W H	Tracks-Wheels Hybrid
UAVs	Unmanned Aerial Vehicles
UGVs	Unmanned Ground Vehicles
USVs	Unmanned Surface Vehicles
UUVs	Unmanned Undersea Vehicles
UV	Unmanned Vehicle
WCMR	Wall Climbing Mobile Robot

Chapter 1

Introduction

Since the beginning of modern civilization, humans have pursued the development of new technologies which can allow them to simplify work and increase productivity, among other objectives. These new technologies are intended to carry out repetitive, heavy, dull or dangerous tasks, where humans are at risk or cannot be involved.

As a result of the industrial revolution, new technologies were developed in fields like metallurgy, steam power, textile manufacturing and machine tools, among many others. Although these breakthrough technologies have increased productivity and reduced physical work for humans, they have also augmented the complexity of machineries, and all related components and structures that make them operational. As a result of this progress, lots of infrastructure were developed and constructed, such as manufacturing and storage buildings, bridges and railways for transportation of goods. Since then, the complexity and quantity of these structures has increased exponentially.

The majority of the infrastructure developed from the late 19^{th} century until these days has been made from steel. These often require constant maintenance and inspection in order to remain functional. Up to now most of these maintenance and inspection tasks were performed by humans,

which in many cases is risky and life threatening for humans, and requires lots of resources.

To deal with this situation, some of these fixed-base systems started migrating to mobile systems. This provides more flexibility to deal with the tremendous growth of new technologies, and in order to keep structures and equipment in working conditions, with minimum risk for the users.

In the last couple of decades, inspection, maintenance and surveillance tasks have become very challenging, risky and high cost. Some of the main reasons for this are: the exponential growth in the number of structures that are being built, the increasing complexity of these structures (either for aesthetic or efficiency reasons), the scenario surrounding the structures (dangerous, dull, etc.), among others.

1.1. Motivation

These circumstances have opened up new fields of opportunity to satisfy the increasing need of more efficient, less expensive and faster inspection procedures. One particular new technique to address this is the employment of Unmanned Vehicles (UV) or Mobile Robots (MR) for inspection, maintenance and surveillance tasks. Most of the MRs developed up to now have being designed for a particular task, or to be employed in a specific scenario. Although these MRs are highly valued by military and commercial entities, the need of a multi-task MR has been increasingly pursued in the last decade. Unfortunately, up to now, there is still no MR that can satisfy this specific need (multitasking). The Unmanned Ground Vehicles (UGVs) are the likely to be the closest to reach multitasking capabilities.

A particular, and very important case, is the development of a multi-task UGV for inspection of vertical and complex structures such as, bridges, industrial plants, and building frames. This particular type of UGVs are commonly referred to as, wall climbing UGVs. More recently, some researchers are referring to UGVs capable to move on, and climb vertical

structures as “Scansorial mobile robots”. This last term, is taken from zoology, and refers to any creature capable or adapted for climbing.

Most of these scansorial UGVs have been designed for a specific task and scenario. This is mainly because of the limitations of locomotion and adhesion mechanisms available for the case of climbing structures.

The main motivation for the present research is the development of a novel adhesion mechanism, which can be integrated into most of the locomotion mechanisms used by MRs for inspection in ferric structures. This adhesion mechanism must ensure manoeuvrability in complex structures, and enhance the MR capability to overcome different types of obstacles.

In recent years, the development of these MRs has been fostered by the exponential growth and innovation of new technologies such as high-speed/low-cost computing, high-bandwidth and reliable wireless communications (Fish & Sitzman 2009).

The development of most of these Mobile Robots (MR) was inspired by the military (US DoD 2013; Defense 1992; Carroll et al. 2004; Clapper et al. 2009), which normally invests in these technologies to cover areas such as surveillance missions. This development is followed by a commercial use, which is normally carried out by big companies.

These unmanned MRs can be grouped in three main domains: Air Domain - Unmanned Air Vehicles (UAVs); Maritime Domain - Unmanned Surface Vehicles (USVs) and Unmanned Undersea Vehicles (UUVs); and Ground Domain - Unmanned Ground Vehicles (UGVs). These three domains will be covered in more detail through the literature review, Section 2.1.

Although the new technologies in the construction and structural fields are moving more towards increased use of composites, up to now most of the structures are still built using steel or ferrite materials. These structures are expected to remain in use for at least a few more decades. That is the reason for developing systems or vehicles for inspection all these structures, with tasks such as: looking at corrosion, fatigue, damages, among

others, that could put at risk the safety of these structures. The focus of the present research is to employ electromagnetic technology, as the adhesion mechanism, for the specific case of ferric structures.

1.2. Problem definition

The research proposal for the present PhD is the design and development of a scansorial Mobile Robot (MR) for inspection of ferric structures. Two key components of the MR will be the main focus. First of all, to develop a novel active adhesion mechanism for ferromagnetic surfaces by means of a new "Electro-Permanent Magnet" (EPM) technology. This novel technology will enhance the adhesion system, with an active mechanism for attaching, detaching or adjusting the adhesion force, depending to the conditions. This new approach for the magnetic adhesion mechanism, which is being explored for this particular case, is a combination of two Permanent Magnets (PM) with different properties (magnetically hard and semi-hard) coiled together with a magnetic wire. In fact, it can be referred as an Electro-Magnet (EM) with a core formed from two PMs.

1.3. Aims and objectives

The aim of this research is to develop a novel active magnetic adhesion mechanism capable of switching OFF and ON, and varying the strength of its magnetic adhesive force. This novel adhesion mechanism has to be suitable for being integrated into most of the locomotion mechanism used in MR for inspection of ferric structures

The objectives of the research are:

1. Design and development of a novel magnetic adhesion mechanism, by the use of Electro-Permanent Magnets (EPMs), which can be implemented in different locomotion systems e.g. legged, tracked or wheeled.

2. Simulation and validation of the novel adhesion mechanism, to determine the influence of the parameters on the performance of the adhesion mechanism, such as: voltage, number of turns in the windings, gage of the enamelled wire.
3. Optimization of the critical components and their influence in the performance of the adhesion mechanism.
4. Testing and characterization of the novel adhesion mechanism, to determine the curve for the force versus electrical pulse magnitude.

1.4. Contributions

The contributions of the proposed research are:

1. Novel active adhesion mechanism: Designed using EPM technology. This active adhesion mechanism has the advantage of being active, allowing the regulation of the magnetic adhesion force required in a particular situation.
2. Determination of the parameters that have an impact in the performance of the adhesion mechanism in order to perform an optimization of the mechanism.
3. Testing a wheel that integrates the EPM adhesion mechanism, to be implemented in a MR.

Publications

The work performed in this thesis has contributed the following publications:

- F. Ochoa-Cardenas and T. J. Dodd, "Design of an active magnetic wheel with a varying Electro-Permanent Magnet adhesion mechanism," *Intelligent Robots and Systems (IROS), 2015 IEEE/RSJ International Conference on*, Hamburg, 2015, pp. 3340-3345. doi: 10.1109/IROS.2015.7353842

- F. Ochoa-Cardenas and T. J. Dodd, "Design of a Continuously Varying Electro-Permanent Magnet Adhesion Mechanism," *Towards Autonomous Robotic Systems (TAROS 2015), 16th Annual Conference*, Liverpool, UK, 2015, Proceedings, pp. 192-197. doi: 10.1007/978-3-319-22416-9.

1.5. Thesis outline

The structure of the thesis is set to provide a literature review and theoretical background in Chapters 2 and 3, the main research derived from the theory is presented in Chapters 4 and 5. Finally, the concluding remarks and future work are presented in Chapter 6. A more detailed description of each chapter is presented next:

- Chapter 2 presents the state-of-the-art of MR used for inspection tasks. These MR are classified by their domain, and the most suitable domain for a MR for inspection of vertical ferric structures is selected. From the selected domain, wall climbing robots chosen as the best option. Furthermore, the different locomotion and adhesion mechanisms used in climbing robots are presented and a novel adhesion mechanism using Electro-Permanent Magnets (EPM) is proposed.

- Chapter 3 presents the theoretical background for EPM and their working principles are explored. Based in the presented theory, an EPM device is constructed using off-the-shelf components and the EPM concept is validated by Finite Element Analysis (FEA) simulations and the corresponding experiments, on the EPM device.

- Chapter 4 presents the possible configurations for integrating the EPM concept as the main adhesion mechanism for a previously selected locomotion mechanism. A new EPM device is constructed and the corresponding FEA simulations and experiments are performed in order to validate the feasibility of the proposed EPM-Locomotion mechanism integration.

- Chapter 5 presents an EPM wheel design using customised components and detailed analysis of the influence of each component on the final adhesive force is performed. From the outcomes from the analysis a final EPM adhesion mechanism is designed and manufactured. A set of FEA simulations and experiments to validate the design. Finally a functional EPM wheel is built using 3D printed components for the assembly.
- Chapter 6 summarises the content of the thesis and presents the concluding remarks. Finally, different ideas are presented for a possible future work.

Chapter 2

Literature Review

As mentioned in Chapter 1, there exists an increasing need for systems that help humans carry out inspection, maintenance and surveillance tasks for existing infrastructure. Over the years these tasks have been performed by humans, which in some cases can be dangerous for personnel involved. Furthermore, the cost of the safety systems and equipment required to guarantee the protection of the personnel, increases dramatically with the size, complexity and age of the structure inspected. The time and cost to mount the infrastructure needed to perform the inspection or maintenance task is another factor that impacts considerably. For these reasons the development of MRs, which help to reduce the amount of resources and personnel involved in these tasks, is becoming an important field of research.

Steel structures are an essential part of modern life. From mere aesthetic design or as a touristic landmark, such as the Eiffel tower, to vital infrastructure like bridges, manufacturing plants, storage vessels, and structural frames, among others. Whether they are new, or have been erected decades ago, these structures require a continuous inspection and maintenance in order to remain functional. The execution of these inspection and maintenance activities comprise dangerous, dull or dirty tasks, which in some situations are unsafe for humans to perform.

The employment of MR is becoming more and more common in the field of inspection and maintenance of steel structures. This is greatly thanks to the recent development of new technologies in different fields, which are being applied as adhesion mechanisms for the MRs.

The present chapter presents the current state-of-the-art on the development of MRs for close inspection tasks, in complex structures and unstructured environments, with a particular emphasis on the technologies used in MR employed in ferric structures. In Section 2.1 an introduction of the evolution of inspection robots is presented and the MRs are categorized into the three main areas according to their main environmental domain. The most suitable category for an MR for close inspection of large, complex structures, is selected. The specific group of climbing robots is then explored in Section 2.2, and the two main mechanisms (locomotion and adhesion) that allow them to climb structures are presented. Next, in Section 2.3, the state-of-the-art of Wall Climbing Mobile Robot (WCMR) used for inspection of ferric structures is explored. Finally, the concluding remarks are presented in Section 2.4

2.1. Classification of the unmanned vehicles

In today's society, there exists an increasing need for systems for monitoring, cleaning, maintenance, and surveillance tasks of existing old and new infrastructure such as: power plants, bridges, platforms or self-standing structures (Kolhalkar & Patil 2012). Most of these tasks are performed by humans, which results in risky, high cost, dull activities, and the need of lots of resources.

One way to minimize the negative impacts of these tasks is the employment of MRs (Perhinschi et al. 2010; Clapper et al. 2009; Defense 1992). These inspection and maintenance tasks, among others such as providing aid in public safety or military activities, are the main incentives leading the design and development of these type of MRs.

By definition any vehicle without humans on-board is considered an MR. They can be:

- Remotely operated, fully controlled by an operator.
- Semi-autonomous, with remote assistance of an operator for specific tasks or manoeuvres.
- Autonomous, capable of navigating on their own, and decision making, to some extent.

The last couple of decades have seen a significant progress in areas such as computational power, communications, vision systems, navigation, systems miniaturisation, and energy storage (Bruch et al. 2005). All these advancements have allowed the development of new technologies, which have led to the design of MRs and boosted their implementation in all kind of scenarios (De Sousa & Andrade Gonçalves 2011).

MRs are categorised according to the environmental domain where they are being employed:

- Aerial domain for Unmanned Aerial Vehicles (UAVs).
- Maritime domain (aquatic) which is subdivided into two classifications: Unmanned Underwater Vehicles (UUVs) and Unmanned Surface Vehicles (USVs).
- Ground domain (terrestrial) for Unmanned Ground Vehicles (UGVs) that contains all on-ground locomotion systems for flat, rough and inclined environments.

All MR, employed for inspection or maintenance tasks, have constraints that are inherent to the domain to which they belong, these can enhance or limit their implementation depending on the circumstances. These constraints, for each domain (aerial, maritime and ground), are presented next and the most suitable type of MR is selected for the case of close inspection of large, complex structures.

Aerial domain

In the aerial domain case, UAVs are mainly used when an inspection outside the structure is needed. These systems have experienced a great growth in recent years (Clapper et al. 2009), pushed by the military seeking new ways to enhance surveillance tasks and to assist troops in combat operations (Khurshid & Bing-rong 2004; Defense 1992; US DoD 2013). In the case of non-military use, UAVs are implemented in applications, such as: rescue and surveillance tasks (Burri et al. 2012); building and structure inspection (Winkvist et al. 2013); or power transmission lines inspections (Smith 2001; Hrabar et al. 2010), (Wang et al. 2010).

This type of UAVs present a major limitation, they are not suitable for close and detailed inspection of complex structures such as bridges, industrial plants or inside structures. These limitation is essentially due to the turbulence that their propulsion mechanism generates. When the UAV is in an open space, with no close obstacles, turbulence is not a problem. But being surrounded by a huge diversity of existing obstacles, mainly inside the structures, becomes a major problem. This results in the impossibility of getting close enough for a detailed inspection of the targets. Although these issues have been addressed in recent years (Gunetti et al. 2011; Winkvist et al. 2013), key challenges remain before they are reliable and trustable for commercial use. Hence, UAV's are not a practical solution to be implemented in the field of close inspection and maintenance, up to now.

Maritime domain

In the case of the maritime domain, USV are limited to a 2D spatial domain. They are suitable for approaching structures that are in their domain but are impeded to get into the structure for a detailed examination. On the other hand, UUV move in a 3D spatial domain, which extends their operation range compared to USV. However, this type of MRs exhibit issues similar to those on the aerial domain (AUVIS 2013; Manley 2008). Specifically, for UUV an analogy can be made to a UAV, in the way they

approach structures or targets. Their spatial domain is essentially the same (three-dimensional domain), changing only the medium from air to water.

UUVs and USVs have been developed mainly for military purposes (Agoros 1994; Gogarty & Robinson 2011; US DoD 2013). Additionally, the scientific need for the exploration of the vast immensity of the deep seas (Hobson et al. 2001; Pascoal et al. 2000), along with offshore industry, like oil or deep sea-mining companies (Damus et al. 2002; AUVIS 2013), or the growth of optical communications, that connect continents (Bannon 2000; Santos et al. 2013) have pushed the development of these types of vehicles (Manley 2008). However, these MR are only capable of inspecting the outside of structures, having difficulties to go inside them for a closer approach. In addition to a lesser quantity of structures that exist underwater, compared to those on ground, the use UUV and USV for the case of the present work is excluded.

Ground domain

Now, for the case of the ground domain, the development of UGVs has a similar history to UAVs, UUVs and USVs. They were first developed for military purposes (Haas et al. 1997; Defense 1992; Carroll et al. 2004), but quickly, scientific, commercial and civilian uses were established. This category of MRs is the most researched and has the widest range of applications, as well as, shapes and locomotion mechanisms (Caprari & Breitenmoser 2012; Okamoto et al. 2012; Kim et al. 2010; Haraguchi et al. 2005; Granosik et al. 2005; Byrd & DeVries 1990; Asano et al. 1983).

UGVs, compared to UAVs or UUVs, have the ability to move through the area of interest, approaching structures closer and maintaining a fixed position with minimal power consumption. Furthermore, they can navigate inside and through the constructions, in an unstructured, confined scenario (Caprari & Breitenmoser 2012).

Most of the UGVs are conceived for solving a specific problem or performing a particular task, such as, maintenance, inspection, surveillance,

or safety tasks. Examples of these include: power plants and nuclear facilities (Zwicker et al. 2010; Guo et al. 2010; Fulbright & Stephens 1995; Roman 1991; Byrd & DeVries 1990), power transmission lines and bridges (Katrašnik et al. 2010; Debenest et al. 2008; Cho et al. 2013; Yun et al. 2013; Liu et al. 2008; Wang et al. 2010), pipes and sewage (Yoon & Park 2012; Kwon et al. 2010; Tavakoli et al. 2010; Lee et al. 2012) or vertical structures (Kalra et al. 2006; Kalra & Gu 2007; Fernández et al. 2010; Yoshida & Ma 2010; Schoeneich et al. 2011; Menon et al. 2004). Hence, the need of a UGV capable of travelling around most of the existing structures, and especially able to climb the structure to reach areas inaccessible for humans, or that requires huge amounts of time and resources to approach, was observed.

Through next section WCMRs are discussed in more detail, dividing them by their type of locomotion and adhesion mechanism.

2.2. Wall climbing mobile robots

A particular challenging area for inspection UGVs, is the inspection of vertical structures. Places exist that are not reachable by humans, or where direct human access is potentially dangerous, dull, expensive, or requires a considerable amount of time (Schmidt & Berns 2013). The UGVs employed in these scenarios are commonly called "Wall Climbing Mobile Robots (WCMR)", alternatively "Scansorial Robots" (Desbiens et al. 2010; Autumn et al. 2005). They can be classified as a specialised subcategory of UGVs, whose main characteristic is to remain adhered to the structure they are inspecting, performing against gravity and moving in an unstructured 3-D scenario. This particular characteristic is achieved by the integration of an adhesion mechanism along with the locomotion mechanism (Balaguer et al. 2005). Depending on the scenario, type of structure and obstacles that the MR might face, the type of locomotion mechanism implemented in the MR will vary. Furthermore, in order to be able to operate in vertical structures, and remain attached to the structure, the MR must possess a special type of adhesion mechanism. This is the element that allows them to remain attached to the structure on which they are operating. The adhesion

mechanism needs to be strong enough so the MR can support its full weight (including the payload from instruments required for the task), when placed in an upside-down position. Both, locomotion and adhesion mechanism, are presented in Sections 2.2.1 and 2.2.2 respectively.

In order to have a clearer idea of the importance of an adhesive mechanism, Figure 2.1 presents three different scenarios for a WCMR, where F_A represents the adhesive force of the WCMR, F_g is the gravity force acting on WCMR (as weight), F_T represents the traction force produced by MR when moving, F_{fr} is the friction force produced by the contact between the MR and the surface where is moving, F_N is the normal force produced by the surface against the WCMR and θ_i is the angle of the incline with respect to the horizontal.

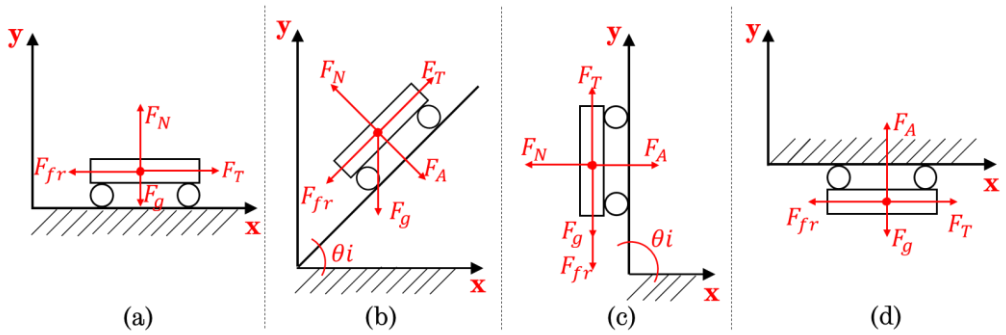

Figure 2.1: Force digram for a WCMR in four different scenarios. (a) On the floor, no need for adhesive forces. b) On a slope of $\theta_i < 90°$, the adhesive force increases as the slope reaches the 90°. c) On a vertical. d) On a ceiling, for the case of $\theta_i \geq 90°$ the adhesive force must be stronger than the WCMR weight plus its payload.

Based on the force diagrams from Figure 2.1 (b) the equations for the equilibrium of forces are the following:

$$\Sigma F_x = F_A \sin\theta_i - F_N \sin\theta_i + F_T \cos\theta_i - F_{fr} \cos\theta_i = 0 \quad (2.1)$$

$$\Sigma F_y = F_T \sin\theta_i - F_{fr} \sin\theta_i - F_g - F_A \cos\theta_i + F_N \cos\theta_i = 0 \quad (2.2)$$

$$F_{fr} = \mu F_N \quad (2.3)$$

where μ is friction coefficient of the surface where MR will move.

From the eq. 2.1, 2.2 and 2.3 it can be observed that the need of an adhesive mechanism becomes critical for scenarios where the slope approaches the 90° with respect to the horizontal. For the cases of a wall and ceiling climbing the adhesion is essential otherwise the WCMR will fall to the floor.

For the case of the MR is moving on a vertical, $\theta_i = 90°$, equations can be simplified to:

$$\Sigma F_x = F_A - F_N = 0 \tag{2.4}$$

$$\Sigma F_y = F_T - F_{fr} - F_g = 0 \tag{2.5}$$

$$F_{fr} = \mu F_N \tag{2.6}$$

In order for MR to remain attached to a vertical structure the adhesive force must meet the following condition.

$$F_A > (F_g - F_T)\mu \tag{2.7}$$

Similarly, for the case of the MR moving on a ceiling, $\theta_i = 180°$, the governing equation is:

$$\Sigma F_y = F_A - F_g = 0 \tag{2.8}$$

In order for the MR to maintain adherance to the ceiling the following condition must be met, $F_A > F_g$.

A description of the evolution WCMR and the state-of-the-art of the technologies used as adhesion mechanism will be presented next.

The first wall climbing robots developed for inspection of vertical structures, made use of vacuum suction and aerodynamic attraction technologies, to stay adhered to the structures with varied types of surfaces and substrates (Nishi 1996; Briones et al. 1994; Bahr et al. 1996). In the particular case of ferric structures, one of the first designs used permanent magnets to keep the WCMR attached to the structure (Hirose & Tsutsumitake 1992). Even though these WCMRs were modular, compact and relatively small when compared with earlier technologies, they were noisy,

constrained to very specific scenario, and needed to be tethered to a power supply and for communications.

Since then, and thanks to the development of new technologies and novel adhesive materials in different fields, the study of new adhesion mechanisms has opened up, leading to a significant growth in the field of WCMRs. These strategies include: electro-adhesion materials (Wang et al. 2012; Prahlad et al. 2008; Schmidt & Berns 2013) and Gecko inspired materials (Santos et al. 2008; Lab n.d.; Menon et al. 2004); vacuum and aerodynamic adhesion (Elliott et al. 2007; Xiao et al. 2006; Xiao & Zhu 2009; Koo et al. 2013), electro-magnetic and magnetic adhesion (Tavakoli et al. 2013; Fischer et al. 2011; Zhang & Dodd 2011; Fischer et al. 2010; Oliveira et al. 2010).

Six main technologies that are implemented in the design of adhesion mechanism for climbing robots exist, whose strengths and weaknesses are explored in Section 2.2.2.

Some of the first designs for a WCMR were presented in the mid-1990s by (Briones et al. 1994) and (Nishi 1996). Both works proposed three different configurations that used suction as their main adhesion mechanism that allowed them to perform on flat or slightly curve areas. Nevertheless, they were not able to overcome obstacles or make transitions between perpendicular planes. Another limitation was the need to be permanently attached to a power supply due to the high energy consumption that is inherent to the suction adhesion technology.

Since then there has been a fast growth in research and development of WCMRs, most of them being conceived to perform a specific task (Xiao & Zhu 2009; Kalra et al. 2006; Fernández et al. 2010), to move in a particular scenario (W. Fischer et al. 2007) or overcome a specific type of obstacle (W Fischer et al. 2007). Some of the designs are quite simple, for example a single actuator (Degani et al. 2007), whilst others are small enough to fit inside places smaller than 1" (2.5 cm) (Gilbert et al. 2007).

In recent years, surveys on climbing robots have been presented (Chu et al. 2010; Schmidt & Berns 2013), both works explore the current state-of-the-art on climbing robots. (Chu et al. 2010) classified climbing robots into

six groups according to their locomotion mechanism, and rearranged them into five groups given their adhesion mechanism. Finally, presenting a chart divided by their industrial field of application and their main characteristics. Alternatively (Schmidt & Berns 2013), examined over a hundred WCMRs used in fields such as: inspection, maintenance or construction. Also, WCMRs were classified by their adhesion mechanism in combination with their locomotion mechanism.

WCMR are categorized into three main groups by their locomotion mechanism: 1. legged; 2. tracked; and 3. wheeled. Each locomotion mechanism has advantages and disadvantages, depending on the scenario (type of terrain) and assignment for which they are developed. These characteristics are discussed in more detail in Section 2.2.1.

2.2.1. Locomotion mechanisms

When a MR is being developed, the appropriate selection of its locomotion mechanism represents a crucial part in the design. Whether or not the MR will efficiently operate on the scenario they are intended to be implemented depends heavily on the correct selection.

The locomotion systems implemented in UGVs are divided into three main categories, Figure 2.2:

- Legs (Palmer et al. 2009; Byrd & DeVries 1990; Menon et al. 2004).
- Wheels (Oliveira et al. 2010; Koo et al. 2013; Xu et al. 2015).
- Tracks (Carroll et al. 2004; Kalra et al. 2006).

Additionally, four sub-categories (hybrids) can be derived from combinations between these main categories, Figure 2.2:

- Legs-Wheels Hybrid (L-W H) (Shiroma et al. 2006; M. Lauria; Y. Piguet and R. Siegwart 2002).
- Tracks-Wheels Hybrid (T-W H) (Kato 2005; Michaud et al. 2005).

- Legs-Tracks Hybrid (L-T H) (Michaud et al. 2005; Michaud et al. 2003; Xingguang et al. 2006).
- Legs-Tracks-Wheels Hybrid (L-W-T H) (Michaud et al. 2005).

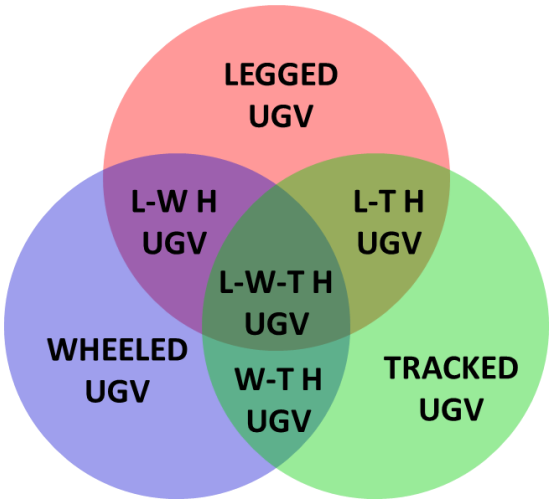

Figure 2.2: Locomotion main categories: Legged, Wheeled and Tracked. Subcategories: Legged-Wheeled Hybrid (L-W H), Tracked-Wheeled Hybrid (T-W H), Legged-Tracked Hybrid (L-T H), and Legged-Tracked-Wheeled Hybrid (L-W-T H).

The purpose for the hybrid locomotion mechanisms is to enhance the MR performance in a specific scenario. A hybrid takes advantages of the key features of the main categories from which they are derived.

In order to get a better understanding of the strengths and weaknesses, the main features from each locomotion mechanism are presented in Table 2.1. This table presents in a more compressive way how good or poorly each mechanism performs in the main scenarios MR face, based on the results presented by (Jahanian & Karimi 2006; Bruzzone & Quaglia 2012).

Legged locomotion mechanisms are the most suitable for unstructured scenarios, however, they have a great diversity of obstacles due to the number of degrees of freedom. This type of mechanism is still in development and require complex control systems for the operation, have high power consumption due to the servos required for the degrees of freedom, which also increases the weight of the MR (Shen & Seipel 2012).

Table 2.1: Comparison of locomotion mechanisms. (Top six) Motion performance of each of the locomotion categories and subcategories through most common scenarios. (Bottom three) Design characteristics from each category and subcategory.

	TRACKED	WHEELED	LEGGED	L-W H	L-T H	W-T H	L-W-T H
SPEED	Moderate/ High	High	Poor/ Moderate	Moderate /High	Moderate	Moderate/ High	Moderate/ High
OBSTACLE EVASION ABILITY	Moderate/ High	Poor	High	Moderate /High	High	Moderate	High
STEP/STAIR CLIMBING ABILITY	Moderate	Poor	High	High	High	Moderate	High
INCLINE CLIMBING ABILITY	High	Poor/ Moderate	Moderate /High	Moderate /High	High	Moderate/ High	High
MOVEMENT ABILITY ON SOFT GROUNDS	High	Poor	Poor/ Moderate	Poor/ Moderate	Moderate /High	High	Moderate/ High
DRIVE ABILITY ON ROUGH GROUNDS	Moderate/ High	Poor	High	High	High	Moderate/ High	High
ENERGY CONSUMPTION	Moderate	Low	Moderate /High	Low/ Moderate	Moderate	Low/ Moderate	Low/ Moderate
MECHANICAL COMPLEXITY	Low	Low	High	Moderate /High	Moderate /High	Low/ Moderate	High
CONTROL COMPLEXITY	Low	Low	High	Moderate /High	Moderate /High	Moderate	High

A similar situation happens with hybrid mechanisms, they are still under research, besides most of they are developed for very specific tasks (Mae & Ohara 2009; Smith et al. 2006; Bruzzone & Fanghella 2014; Tavakoli et al. 2015; Desbiens et al. 2010). This makes hybrid mechanism unsuitable for inspection of large structures.

The wheeled and tracked locomotion mechanism are the most researched (Nie et al. 2013; Ting Wang et al. 2005; Wang & Gu 2007). Moreover, their technology can be considered to be in a mature state, which means most of the gaps and issues in their design and implementation have been investigated.

Wheeled locomotion mechanism can be considered the most popular mechanism among the field of robotics thanks to their mechanical

simplicity, low power consumption, high speeds, and stability (Nie et al. 2013; Wang & Gu 2007). For these reasons wheeled locomotion mechanism are the most appropriate mechanism to be implemented in a WCMR used in the close inspection of large structures. Compared to wheeled locomotion, tracked locomotion mechanisms are used in scenarios where a large area of contact is needed, and the presence of big obstacles are a concern. Although tracked mechanisms are not as fast and efficient as wheeled locomotion. Therefore, if obstacles are not a significant concern, the best option is the wheeled locomotion mechanism, furthermore, by implementing an articulated frame to the MR, its ability to overcome complex obstacles is enhanced.

The next section explores the types of adhesion mechanisms that can be implemented in a WCMR, which along with locomotion mechanisms, are the two key components that allow the MR to adhere and move around the structure.

2.2.2. Adhesion mechanisms

The adhesion mechanism in the case of WCMR is the most important part of the design, without it WCMR would not be able to perform or to keep adhered on vertical structures. When we talk of adhesion mechanisms for climbing robots, different principles can be discussed, e.g. magnetic, electrostatic, vacuum, suction, elastomer, mechanical griping or aerodynamic adhesion. A more detailed description and performance of these mechanisms is presented next:

Electro-adhesion

Electro-adhesion makes use of electrostatic forces that act between the target surface material (e.g. brick wall) and the electro-adhesive material (elastomers) integrated to the locomotion mechanism (Legs, Wheels, etc.) (International 2010). The electro-adhesive material is composed of embedded micro conductive electrodes. By inducing opposite (positive and negative)

charges in neighbouring electrodes, the electric field generated produces the opposite charges in the target surfaces. Therefore, an electrostatic adhesive force is produced between the electrodes and the target structure surface (Prahlad et al. 2008). These working principle is comparable to electrostatic chucks employed to grip silicon wafers, or other specialized grippers for robotic handling of materials (International 2010).

Some of the advantages of the electro-adhesion technology are: 1. adjustable adhesion to different surfaces with a low steady energy consumption; 2. high adhesive forces on a diverse range of materials such as: glass, concrete, plastics, drywall and wood); 3. quick attachment and detachment response; 4. no damage produced in the substrates where it is being used; and 5. ability to adapt to the surface coarseness, shape and cracks that might be present (Prahlad et al. 2008; Wang et al. 2012)

On the other hand, the disadvantages of this technology are: 1. remains an expensive technology; 2. it is still in development stage; 3. it has limited payload capacity, only suitable for small and light MRs; and 4. it requires a continuous supply of the power to maintain adherence (Prahlad et al. 2008; Wang et al. 2012).

Dry adhesives/synthetic Gecko feet

Dry adhesion uses Van der Waals forces as adhesion mechanism. This type of adhesives mimic the mechanism gecko lizards use for attachment and detachment in nature. This is done by emulating the setae present in a gecko's toes (Peyvandi et al. 2013; Sahay et al. 2015; Murphy et al. 2011; Menon et al. 2004). Surface material is not important, which means that this technology will perform on most surfaces, similar to the electro adhesive mechanism.

Dry adhesives, compared with the electro adhesive technology have advantages such as: 1. no energy required to stay attached to surface (Prahlad et al. 2008; Wang et al. 2012); 2. allows moderate velocities for locomotion (Menon et al. 2004); 3. attachment and detachment occurs almost

instantaneously (Menon et al. 2004; Lab n.d.; Santos et al. 2008); and 4. self-cleaning mechanism of the setae (Menon et al. 2004).

In the case of the disadvantages of this technology, they are similar to the case of the electro adhesion technology: 1. remains an expensive technology; 2. it is still in the early stage of development; 3. it has limited payload capacity, only suitable for small and light MRs; and 4. it requires a continuous supply of the power to maintain adherence (Prahlad et al. 2008; Wang et al. 2012).

Suction-vacuum and aerodynamic suction adhesion

This type of adhesion mechanism is one of the most used and earliest mechanisms used in the field of WCMRs. The adhesion is accomplished by suction cups, in which a vacuum pump generates the depressurization. This produces a negative pressure which maintains the system adhered to surface where it is being used (Bahr et al. 1996). This adhesion mechanism allows bigger payloads for the MRs, compared to the two previous adhesion mechanism. Even though this adhesion mechanism has been in use for few decades, it has major drawbacks when compared with the other types of mechanisms, such as: 1. it has to be used in MR that move on smooth surfaces to avoid air leaking; 2. MR that use this technology are slow, noisy and heavy due to the pumps that are carried; 3. have a high power consumption (Hu et al. 2009; Kim et al. 2008; Xiao & Zhu 2009; Koo et al. 2013; Xiao et al. 2006; Elliott et al. 2007); and 4. therefore require a tethered connection to a power supply due to their high power consumption.

Mechanical adhesion

Robots with the mechanical adhesion mechanisms either grip or clamp to the structures. Usually mechanical grippers, connectors or claws are employed (e.g., small hooks) to keep attached on rough surfaces (Hu et al. 2009; Kim et al. 2008; Xiao & Zhu 2009; Koo et al. 2013; Xiao et al. 2006; Elliott et al. 2007).

This type of adhesion has the main disadvantage of potentially damaging the areas where the attachment is performed. This limits its employment to situations where the side effects of the clamping is not a concern.

Magnetic adhesion mechanism

Magnetic adhesion mechanisms make use of Permanent Magnets (PM) in order to generate the adhesion forces. Similarly, to electromagnetic adhesion, magnetic adhesion is exclusively suitable for ferric structures. The strength of the adhesive forces depends from the type and size of the PM employed in the mechanism.(Carrara et al. 1992; Fischer et al. 2011; Tavakoli et al. 2013; Tache et al. 2007).

This adhesion mechanism has the advantages such as: 1. strong adhesive forces, allowing bigger payloads (Chu et al. 2010); 2. reliable form of adhesion (Chu et al. 2010); 3. a relatively low cost compared to other adhesion mechanisms due to its development maturity (Fernández et al. 2010; Khirade et al. 2014); 4. works on most types of surfaces (e.g. rough, smooth) providing the structure is ferric (Khirade et al. 2014); and 5. no energy required for attachment/detachment (Chu et al. 2010; Khirade et al. 2014).

Some of the limitations this technology possess are: 1. it presents a fixed adhesive force, that cannot be modified once a specific design is selected (Chu et al. 2010); 2. MRs that use this technology may present a poor manoeuvrability if the adhesive mechanism is not properly designed (Chu et al. 2010); and 3. it is suitable exclusively for ferric structures.

Electromagnetic adhesion

This type of mechanism uses Electro Magnets (EM) for adhering exclusively to ferric structures. The electromagnetic adhesion is generated by the magnetic field produce by an electric current flowing in a solenoid.

Compare to the magnetic adhesion mechanism, electro-magnets have advantages such as: 1. large adhesion forces; 2. different forces can be generated by a single mechanism; and 3. the adhesive force can be controlled by varying the magnitude of the electric current applied to the solenoid.

The disadvantages of electromagnetic adhesion are: 1. power consumption due to the continuous power supply needed to maintain a desired adhesive force (Fischer et al. 2010; Fischer et al. 2011; Oliveira et al. 2010; Tavakoli et al. 2013; Zhang & Dodd 2011); 2. high temperature rise due to the heat dissipation of the electric current flowing through the windings of the solenoid; and 3. not suitable for untethered MR.

In order to have a more comprehensible comparison amongst the described adhesion mechanisms, Figure 2.3 presents the advantages and disadvantages for each adhesion technologies.

Based on Figure 2.3, the most appropriate technology for the application on which the MR will perform can be selected. For example, in the case of a smooth and clean surface, vacuum, suction, dry adhesive or electro-magnetic can be used. But, the first two have the limitation of the power consumption (the same case for electro-magnetic adhesion), which becomes a big issue on cordless vehicles, as well as the noise generated. For the case of dry adhesives, they tend to degrade with use over time.

For the specific situation of inspection on ferrite/ferric structures, the Magnetic/Electro-Magnetic Adhesion Mechanism (M/EMAM) seems to be the ideal choice. However, this adhesion mechanism has a major restriction in the case of PM use, which is a fixed (passive) attraction force. This means that it is not possible to vary the adhesion force. This becomes a major problem in situations where this ability is required, e.g. to overcome certain obstacles or move through a complex path. By employing EMs instead of PMs we can solve these issues. However, another concern arises, which is the power consumption. This is because an EM requires a permanent supply of energy to generate the (active) adhesion forces, and this condition will lead to a quick battery drain, for the case of cordless MRs. Some researchers addressed this problem by designing a switchable device (ROCHAT et al.

2010), which is a PM that can be rotated by a servo in different configurations to vary its adhesion force. Although, the use of this switchable device is an improvement, limitations exist, such as, mechanical complexity, control and energy consumption of the servo.

Technology	Weight	Repeated use on dusty surfaces	Works on both rough and smooth, substrates	Energy require-ments (attach-ment)	Energy require-ments (detach-ment)	Works on wide range of materials	Quiet / Non-damaging / no residue	Cost
Electro-static adhesion								
Dry adhesives / Synthetic Gecko feet								
Suction / vacuum								
Aerodynamic Suction								
Mechanical Adhesion								
Electro-Magnets								
Permanent Magnets								
Electro-Permanent Magnet Adhesion								

	Excellent Performance		Moderate Performance		Poor Performance

Figure 2.3: Comparison of existing adhesion technologies according to most common situations a WCMR might encounter. Electro Permanent Magnet adhesion will be presented section 2.3.1.

2.3. WCMR for inspection of ferric structures

In the specific scenario of ferric structures, different adhesion mechanisms can be implemented in the development of a WCMR. Magnetic adhesion offers a great advantage over other mechanisms.

One of the first designs that used magnetic adhesion in a WCMR was presented by (Hirose & Tsutsumitake 1992), where permanent magnet discs were used as the wheels of the vehicle. Even though this design was innovative and represented a step forward in the development of climbing robots, it was limited to operate on flat surfaces, and was not able to overcome obstacles.

A different approach employed in the design of an adhesion mechanism for ferric structures was presented by (Grieco et al. 1998). In this work researchers used electro-magnets combined with a legged locomotion mechanism in the development of a WCMR that was capable to carry a high payload (100kg) and able to manoeuvre in a complex 3-D scenario. The advantage on the use of electro-magnets over permanent magnets is that EM allows switching OFF and ON the adhesion force, making possible the legged locomotion and consequently permitting the WCMR to overcome obstacles and move in a 3-D scenario. The downside is, as in the case of the suction technology, the need of a constant supply of energy in order to keep EMs operative, constraining the range of operation.

Based on both principles, permanent magnets and electro-magnets, numerous designs have been proposed. Most of them to perform a specific task. Kalra et al. 2006 made use of PMs along with a tracked locomotion mechanism in the design of a platform for inspection of oil tanks; or to work in a similar scenario, W. Fischer et al. 2007 proposed a “mother-child” configuration for inspecting very thin and fragile structures, in this approach the “child” has magnetic wheels as adhesion mechanism, the “mother” component has the function to help the “child” to overcome ridges or any obstacle.

In recent years, there have been some studies in what are called “Electro-Permanent Magnets” (EPMs), in the fields of programmable matter. These are small magnetic actuators, or stepper-motors in the centimetre scale. Although, the principle of EPM has been used in a big scale in the improvement of electro-magnet lifters, its use in the centimetre scale is a novel field of study.

2.3.1. Electro-permanent magnets

This research is focused on the use of the EPM principle to develop a novel adhesion mechanism for MRs, which is called “Electro-Permanent Magnet Adhesion Mechanism” (EPMAM). This mechanism uses the advantages from both EM and PM combined in a single device. As a result, the new mechanism will have the ability to remain attached to a ferric/ferromagnetic surface by means of the PM force (no power consumption). In addition, it will have the ability to modify (increase, decrease, or nullify) the attracting magnetic force. To do this it will only require a small-width pulse (milliseconds) for modifying the magnetic field, resulting in lowered power consumption. This mechanism means a huge breakthrough in the field of magnetic adhesion, enhancing the mobility and manoeuvrability of MRs. Figure 2.3 at the bottom of the Table there is a comparison of magnetic/electro-magnetic versus electro-permanent magnet adhesion mechanisms. It can be observed that the limitations concerning power consumption, for electro-magnetic technology, and manoeuvrability for both magnetic and electro-magnetic adhesion mechanism, are overcome with the implementation of EPMAM.

The implementation of EPMs in the adhesion mechanism of WCMRs could signify a major advancement. Allowing the MR to move through intricate structures and to overcome obstacles that are not accessible with conventional magnetic adhesion mechanisms.

Electro-permanent magnets history

EPMs were first mentioned in a paper in 1952 (Hadfield & Mawson 1952), where they were part of the development of a spectrograph. It consisted of an electro-magnet in parallel with a permanent magnet. By applying an electrical pulse through the electro-magnet its magnetic field was added or subtracted (depending of the polarity of the electrical pulse) from the magnetic field of the permanent magnet. Thus, allowing the variation of the

net magnetic field of the system as needed, giving more stability to the system compared to only using an electro-magnet.

It was not until the 1980's, with the development of new magnetically semi-hard materials (e.g. Alnico or Alcomax), that innovative applications started to be researched for this type of device. The main incentive was the capability of an EPM to change its external magnetic field and maintain it when the energy power supply is removed. Another advantage compared to EMs is the low energy consumption, as they require a short electrical pulse to change (increase or decrease) their magnetic adhesion force. In contrast to electro-magnets, which require a constant supply power maintain their magnetic adhesion force.

The main commercial use for EPM technology has been its implementation in the electro-magnetic lifter field (Lee et al. 2008; Ltd 2014; Cassing et al. 2008). The objective is to enhance the safety of the electro-magnetic lifters, preventing them to fail when power supply (electrical current) was removed from the EM, either by mistake or a failure in the supply itself. In recent years, EPMs have been implemented in the design of electro-magnetic locks, griping cargo systems and reconfigurable matter (Piranda et al. 2013; Fu et al. 2012; Knaian et al. 2012).

In 1995, the basic working principle of EPMs was explored by Shirazee and Basak to develop a suspension system for acquiring large air gaps in suspended loads (Shirazee & Basak 1995). In this work, the arrangement of a hard and a soft material, coiled with a magnetic wire is still used.

From 2000 to 2010, Chang Hyeon Ji et al. developed a micro optical switch, which used a micro EPM to move a set of micro-mirrors (Ji et al. 2004). Tjahjo Pranoto et al. implemented an EPM in the mechanism of a vibration suppression device (Pranoto et al. 2007). Jan Bydžovský et al. proposed an EPM chuck, in which, the working principle of an EPM was applied (Ondreička & Paľa 2010).

Up to now, the most extensive work on EPMs has been done by Knaian (2010). He proposed the use of EPMs to construct connectors and actuators, in a centimetre scale, to build "Micro Electro-Mechanical Systems" or MEMS.

This work resulted in the development of: 1. “The Robot Pebbles” (Gilpin et al. 2010) in the programmable matter field, which are 1cm cubes that use EPMs to connect, communicate and share power with neighbouring cubes in order to form shapes; 2. “Electro-Permanent Actuators” (Marchese et al. 2011), where EPMs are used to build small valves that are then employed to construct actuators for soft robots. By applying a 5ms electrical pulse the EPM valves are able to drive the pressurization and depressurization of fluidics within the actuators; and 3. “The Milli-Motein” (Knaian et al. 2012), which is a chain of programable matter with 1cm pitch, in the mini robot field. This mini robot uses a mini stepper motor built with EPMs, which enable motor to maintain its position without any energy consumption, contrary to what happens with regular stepper motors.

The work of A. Knaian in these three devices has motivated others, specifically in the field micro devices, for developing novel connection or adhesion systems based on the EPM principle. Guoqiang Fu, et al. designed a miniature switchable connection system for modular robots (Fu et al. 2012). Andrew D. Marchese, et al. developed a programmable connection mechanism for robots separated by a surface (Marchese et al. 2012).

In 2012, based on the thesis of Knaian, Peter Ward replicated the basic experiments on EPMs presented by Knaian and suggested their possible use as adhesion mechanism for climbing robots in ferric structures (Ward & Liu 2012). This work consisted in some experiments presenting the behaviour of the EPMs in a centimetre scale and based on the results he proposed that EPM technology could be integrated with different locomotion mechanism employed in MR for climbing ferric structures. No further work was undertaken.

Therefore, the work presented in the following chapters goes further and explores in more detail the viability of different designs of MR with EPM technology as adhesion mechanism.

EPMs theory and their working principle will be discussed in more detail in Chapter 3.

2.4. Concluding remarks

Through this chapter, it has been shown that in most of the designs of a MR, there exist constraints that limit their development and implementation. In the particular case of WCMR, what has limited their development in the last decades are two main factors: 1. a versatile locomotion system (Ting Wang et al. 2005; Jahanian & Karimi 2006); and 2. an efficient adhesion mechanism (Schmidt & Berns 2013), (Miyake et al. 2007). However, the development of novel technologies in recent years, that can be applied into both, the locomotion and adhesion mechanisms, have contributed to overcome these constrains, up to some extent. This has allowed developing systems that can be used in more than one specific scenario. Therefore, the development of multitask vehicles capable of moving in an unstructured scenario with the ability to overcome different obstacles, although is a big challenge, will bring key benefits for the inspection robots field

To conclude, it can be seen that there does not exist a general WCMR as such. Additionally, the requirements for its development can be contradictive, for instance, a small (light weighted) and fast WCMR is not be able to carry a big payload or sensors, moreover, a system with a big payload requires a strong adhesion mechanism that will likely render it slow and difficult to manoeuvre.

In Chapter 3, the theory and working principles of the EPMs are introduced. A set of simulations and the corresponding physical experiments are performed and their results presented in order to validate the EPM concept as a viable adhesion mechanism for WCMRs.

Chapter 3

Electro-Permanent Magnets as an Adhesion Mechanism

Electro-Permanent Magnets (EPM) have the potential to be implemented as part of the adhesion mechanism in WCMRs. In the present chapter the theory behind the main concepts that enable the operation of EPMs is presented in Section 3.1. Then, the working principles of EPMs, and the OFF and ON states along with the variable magnetic adhesion, are presented in Section 3.2. Once the theory and working principles are presented, a set of Finite Element Analysis (FEA) simulations and corresponding experiments are performed with the purpose to validate the viability of EPMs as adhesion mechanism, and are presented in Section 3.3. Finally, results from both, simulations and experiments, are discussed and the concluding remarks are presented in Section 3.4.

3.1. Theory

Formal theory for Electro-permanent magnet (EPM) is limited at the moment (Marchese et al. 2011; Knaian et al. 2012; Knaian 2010; Marchese et al. 2012; Ondreička & Paľa 2010). However, based in the working principles of Permanent Magnets (PM) and ElectroMagnets (EM) the working principle of EPMs can be deducted.

An Electro-permanent magnet (EPM) is a bi-stable, solid-state magnetic device. It has the capability to be switched OFF and ON by applying a short electrical pulse. An EPM is composed of a particular arrangement of two magnetically different materials, one hard and one semi-hard. Both materials are PMs which are coiled together with magnetic (enamelled) wire, and topped at their magnetic poles with ferromagnetic keepers, Figure 3.1.

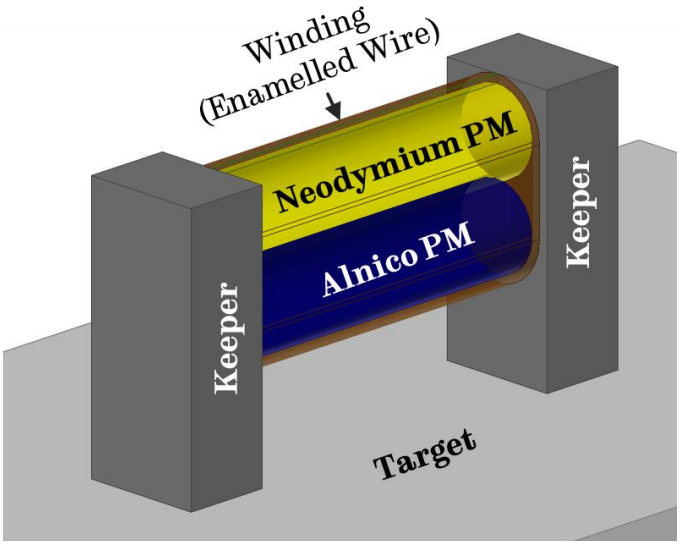

Figure 3.1: Electro-Permanent Magnet design: yellow, NdFeB PM (hard magnetic material); blue, Alnico PM (semi-hard magnetic material).Both PMs are coiled together with enamelled wire; capped with two ferromagnetic (steel) keepers placed at the poles of the PMs.

A key property of PMs is their coercivity, this property determines how magnetically hard or soft a PM is. Moreover, the difference in coercivity between the two PMs is what enables the bi-stability in EPMs

3.1.1. Important concepts

Magnetic Fields

The space adjacent to any magnet (electromagnet or permanent magnet) where magnetic forces, which have a direction and a magnitude, act is called the magnetic field. There exist two, closely related, fields that are denoted by B and H.

The B-field, or magnetic flux density, is the force on a moving charge and its units in the SI s the Tesla and is produced by currents according to Ampere's Law and Biot-Savart Law.

The H-field, or magnetic field strength, is the field produced when a magnetic field B passes through a magnetic material. The magnetic field strength SI units are the A/m (ampere per meter).

Both, B-field and H-field are proportional and their relationship is determined by the following equation:

$$B = \mu_m H \tag{3.1}$$

and

$$\mu_m = K_m \mu_0 \tag{3.2}$$

where μ_0 is the magnetic permeability of free space and K_m is the relative permeability of the material where the magnetic field is acting (Nave 2017).

Magnetic saturation

Magnetic saturation is the state reached in a magnetic material when an increase in the external magnetic field is applied but the magnetization of the material cannot increase further, is it can be observed in Figure 3.2.

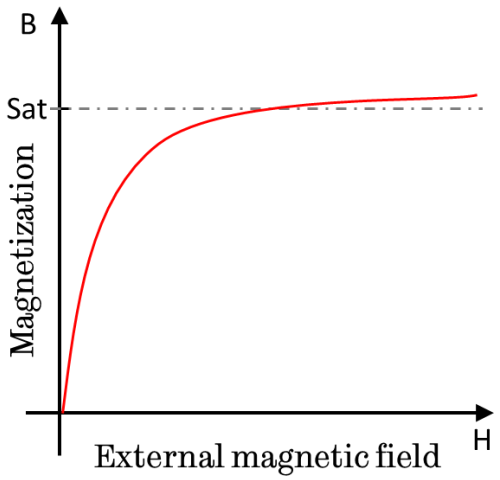

Figure 3.2: Magnetization curve of a magnetic material.

Coercivity

For ferromagnetic materials, coercivity measures the ability of the materials, previously driven to saturation, to resist demagnetization in the presence of an external magnetic field. This value is denoted **Hc**. Table 3.1 shows typical values of coercivity of three magnetically different materials.

Magnetically hard materials have high coercivity, which means a strong magnetic field is required in order to demagnetise them. Magnetically semi-hard materials have medium coercivity, and are therefore relatively easy to demagnetise by applying an external magnetic field. On the other hand, soft materials have low coercivity, thus they do not retain magnetization, which means they lose it as soon as the external magnetic field is removed.

Table 3.1: Typical values of coercivity for different magnetic materials (Online 2016).

Material	**Coercivity Hc (kA/m)**	
Neodymium (NdFeB)	880 - 960	Magnetically hard
Alnico (AlNiCo)	46 - 126	Magnetically semi-hard
Mild Steel	0.15 - 0.50	Magnetically soft

Inductance of a solenoid

Inductance is the opposition of a conductor to the change of the electrical current flowing through it and the SI units are the Henry (H). A solenoid or inductor is a device made from loops (or windings) of wire. If for a given solenoid the number of loops is increased, then for the same current flowing through it, the magnetic flux will increase hence its inductance, as shown in the following equation (Nave 2017):

$$L = \mu_0 \frac{N^2 A}{\ell} \tag{3.3}$$

where L is the inductance in henries, μ_0 is the permeability of free space, N is the number of turns in the solenoid, A is the inner core area of the solenoid in square meters and ℓ is the length of the solenoid in meters.

Electric current and magnetic field in a conductor

When an electric current flows through a conductor, a magnetic field is generated around the conductor. The intensity of the magnetic field is proportional to the magnitude of the electric current. This magnetic field forms in concentric circles perpendicular to the direction of the electric current.

Now, when the conductor is coiled forming a solenoid the magnetic flux lines around the conductor are distorted forming closed loops around the whole solenoid. As a result, the pattern produced by the magnetic flux lines, resembles the magnetic field in a permanent magnet bar, with a higher concentration of magnetic flux lines inside of the solenoid.

When the electric current flowing in a coil is fixed (no changes over time), the magnetic field generated by the solenoid is also constant. On the other hand, when a change in the magnitude of the current is produced, the magnetic field will vary in the same proportion. Furthermore, according to Faraday's law of electromagnetic induction, a changing magnetic field in a coil will induce an electromotive force (emf) across the coil. In addition with Lenz's law of electromagnetic induction, when an emf is induced, in accordance to Faraday's law, the direction of the emf will oppose the source from which it is produced. This is also known as inductance.

Due to the self-inductance present in every inductor, when a voltage is applied to the terminals of the solenoid the electric current that flows through the windings increases in an exponential way, Figure 3.3.

$$i(t) = \frac{V}{R}\left(1 - e^{\frac{R}{L}t}\right) \tag{3.4}$$

where i(t) is the current flowing through the windings, V is the voltage applied to the solenoid terminals, R is the resistance of the solenoid and L is the inductance of the solenoid.

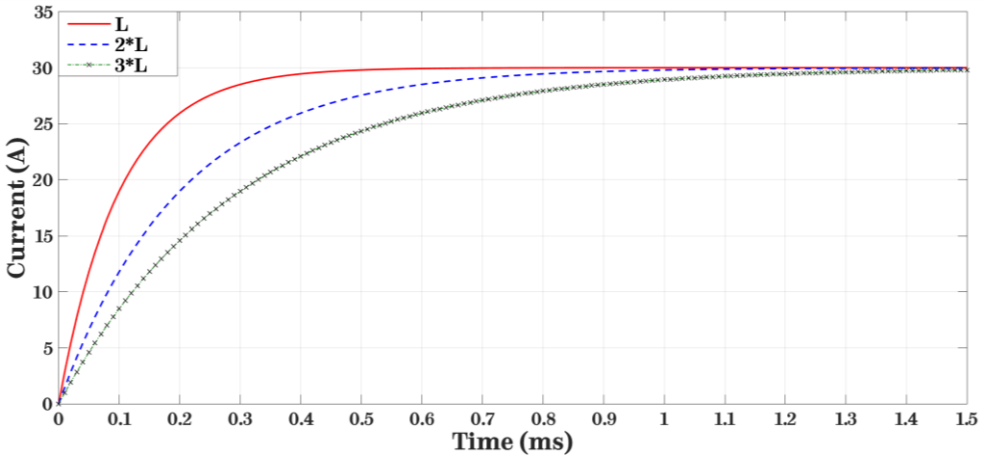

Figure 3.3: Electric current in an inductor. Bigger values of inductance increase the time that it takes the current to reach a steady state value. The red line represents an inductor with an inductance "L", and it takes approximately 0.5ms to reach the maximum current. Blue line represents an inductor with twice, 2*L, the original inductance, and it reaches the steady state in approximately 1.0ms. For the green line, an inductor with an inductance three times the initial is represented, in this case the time for reaching the maximum current value is 1.5ms.

From Figure 3.3 it can be observed that time to reach the maximum current depends on the inductance of the solenoid. Larger values of L mean it will take a longer time to reach the maximum current. From equation 3.4 it is possible to extract the time constant, which is $\tau = \frac{R}{L}$. By general rule, any exponential signal reaches 99.99% of the final value within 5τ. This time constant is an important part in the working principle of the variable EPM design, because it determines how fast the current, needed produce the external magnetic field, reaches the maximum magnitude. Hence, the period the electrical pulse is applied.

Magnetomotive force produced by a current

The magnetomotive force "F" produced by a magnetic field can be expressed by:

$$\boldsymbol{F = NI} \tag{3.5}$$

$$\boldsymbol{F = H_c \ell} \tag{3.6}$$

where N is the number of turns in the coil, I is the current flowing through the coil, H_C is the intensity of the magnetising field and ℓ is the mean length of the coil.

Both equations can be solved for H_C in terms of N, I and ℓ

$$\boldsymbol{H_c = \frac{NI}{\ell}} \tag{3.7}$$

From eq. 3.7 it is can be deduced that the intensity of the magnetic field generated by the coil depends from the number of turns N in the coil, the amplitude of the current I flowing through them, and its mean length. Considering N and L fixed parameters in an EPM, Hc depends from the magnitude of the electric current I.

Force calculation

In order to compute the holding force produced between the keepers and the target, is possible to use equation derive by (Knaian 2010):

$$F = \frac{B_{sat}^2 ab}{\mu_0} \tag{3.8}$$

where F is the magnetic force, μ_0 is the permeability of free space, B_{sat} is the saturation value for the flux density of the PMs and ab is the keepers bottom area.

3.2. Working principles

Coercivity can be considered as the crucial property in the development of EPMs, through the combination of two PMs with different coercivity. If a single type of PM, either magnetically hard or semi-hard, is used to build an EPM, it will result in a device with undesirable characteristics. The two most important affected characteristics are the

magnetic force and the energy consumption of the device, depending on the PM employed (magnetically hard or semi-hard).

For example, if the PM used is made of a magnetically hard material (e.g. NdFeB), it will exhibit strong adhesive force. However, the energy required for switching the adhesive force OFF and ON would be quite large, and thus not suitable to be employed in a WCMR.

On the other hand, if the PM is made of a magnetically semi-hard material, the energy required for performing the switching between states is reduced. But the adhesive force would not be enough to keep the whole device attached to the structure. Furthermore, the EPM would be vulnerable to influence of any external magnetic field as it may easily be demagnetised.

However, if both types of PMs (magnetically hard and semi-hard PM) are assembled into a single device, the strengths of both PMs will add up, and their weaknesses nullified. In other words, the resulting EPM would exhibit a strong adhesive force, small energy consumption and would not be influenced by external magnetic fields.

Based on this, the EPM device shown in Figure 3.1 can be implemented. The device consists of two magnetically different PMs, one hard PM (e.g. NdFeB) and the other semi-hard PM (e.g. Alnico). Both PMs are coiled together with magnetic (enamelled) wire and topped at their magnetic poles with two pieces of a magnetically soft material (e.g. iron, electric steel, hiperco), which act as keepers for the EPM.

3.2.1. OFF and ON configurations

An EPM has two basic configurations, OFF and ON, Figure 3.4. In both cases the PMs are placed in parallel with respect to the orientation of their magnetic fields. The ON configuration occurs when both magnetic fields are pointing in the same direction (both north poles are facing the same keeper, the same with the south poles).

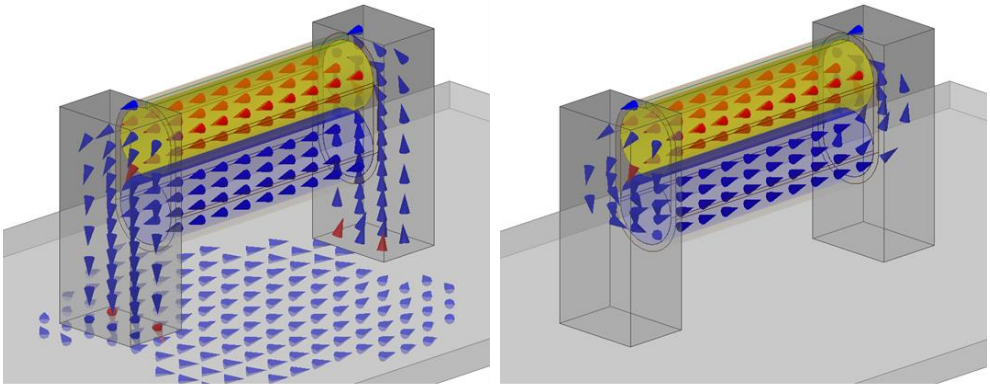

(a) ON State (b) OFF State

Figure 3.4: EPM basic configurations. (a) ON State - Both PMs are in parallel and their magnetic flux lines (blue and red arrows) are aligned in the same direction. The magnetic fluxes add up and flow through the left keeper. Then, the magnetic flux lines are exerted from the bottom of the left keeper and flow through the target re-entering the EPM through the bottom of the right keeper, closing the magnetic circuit. The magnetic flux coming out and in from the bottom of the keepers produces the attracting force on the target. (b) OFF State - PMs are in parallel, similar to the ON state, however, their magnetic flux lines are aligned in opposing directions (blue and red arrows). In this case, the magnetic flux lines coming out of the north pole of the top PM flow through the south pole of the bottom PM, using just the upper part of the left keeper. The magnetic flux comes out of the bottom PM's north pole and re-enters into the upper PM's south pole closing the magnetic circuit. As a result no external magnetic flux is generated and consequently no attracting magnetic force.

The magnetic flux lines coming out of each north pole add up, flow through the keeper next to them and come out at the bottom of the keeper. The magnetic flux lines then re-enter the EPM from the bottom of the keeper capped to the PMs' south poles. The exerted external magnetic field produces an attracting magnetic force that is used by the device to adhere to a ferromagnetic surface.

The OFF configuration forms when the magnetic flux lines of both PMs have opposite directions with respect to each other. In this case, magnetic flux lines coming out of the north pole of the first PM go into the south pole of the second PM that is next to it, through the upper part of the keeper. The magnetic flux flows through the PM and comes out again through the north pole and enters in the adjacent PM south pole. Therefore, the magnetic flux

is kept in a closed loop inside the EPM and no external magnetic field is generated, consequently no attracting magnetic force is produced.

Transitions between states

In order to perform the transitions from OFF to ON states, and vice versa, an electrical current pulse must be applied to the windings (solenoid) coiled around the PMs. This current pulse is indispensable to generate the external magnetic field that re-magnetises the Alnico magnets, reverting the direction of the PM's magnetic field. Which enables the main property of EPMs, switching between OFF and ON states. The operation hysteresis of an EPM in an OFF-ON working cycle is presented in Figure 3.5.

In order to perform the switching between the OFF and ON states an electrical pulse must be applied through the enamelled wire (coil). When the initial condition of the EPM is the OFF state and the electrical pulse has a positive polarity the EPM will switch from the OFF to the ON state. Conversely, when the initial condition of the EPM is the ON state and the pulse has a negative polarity the EPM will transition from ON to OFF state. The generated external magnetic field must to be strong enough to drive the Alnico5 PM to saturation. Due to the different coercivity, between the PMs, the magnetic field will not affect the NdFeB magnet because of its high coercivity.

In order to ensure that the Alnico PM is driven to saturation, the external magnetic field must be at least twice the value of the PM's intrinsic coercivity Hc. As shown in Section 3.1.1 the intensity of the magnetic field produced by a solenoid depends proportionally on the electric current, flowing through the windings, and the number of turns of the solenoid.

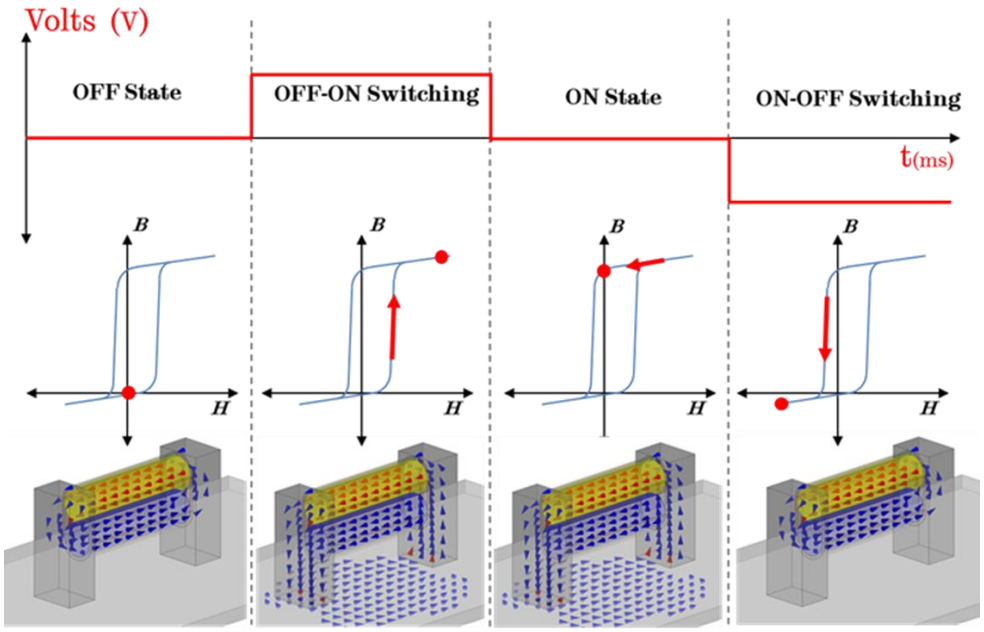

Figure 3.5: Hysteresis loop of an EPM, in an OFF – ON – OFF working cycle (Knaian 2010). (a) During the OFF state, both PMs (NdFeB and Alnico) are magnetized in opposite directions. As a result the magnetic flux lines flow in a closed loop between both PMs (inside the device) and no external magnetic field is generated. (b) The Off-On switching happens when an electrical pulse (with positive polarity) is applied through the coil. A magnetic field is generated reversing the magnetic field direction of the Alnico PM. As a result, the magnetic field of both PMs (Alnico and NdFeB) point in the same direction. The magnetic flux lines add up and flow through the keepers. An external magnetic field is generated, which produces the magnetic adhesive force. (c) In the ON state the electrical pulse is no longer present, but both PMs maintain the same magnetizing direction. Keeping the external magnetic field generated in the Off-On switching step. (d) For the On-Off switching step the operation principle is the same as in step (b), but with the electrical pulse applied with a negative polarity.

3.2.2. Variable magnetic adhesive force

Additionally, in EPMs it is possible to set a specific value for its magnetic adhesive force, between its minimum and maximum values. This characteristic is a major advantage over conventional PMs, which have a fixed magnetic force, or EMs that required a continuous supply of power to maintain a desired magnetic force. This characteristic has not been addressed in previous work by other researcher's, in the different areas where EPM principle has been applied. Those works only have explored the

EPM main characteristic of being able to be switched OFF and ON by single electrical pulse. Leaving out the capability of EPM to vary their magnetic adhesive force between OFF and ON values.

Adjustable magnetic adhesive force is a major breakthrough in the area of magnetic adhesion mechanism for ferric structures. Such adhesion mechanism enables WCMR to overcome complicated transitions or complex obstacles by varying its adhesive force as required.

To achieve a specific value of magnetic adhesive force the amplitude of the electric current pulse has to be varied. Taking into account equation 3.4, if the amplitude of the electric current pulse applied to the windings is varied, Alnico PM can be partially magnetised. Which results in a particular value for the magnetic adhesive force, between zero and maximum values.

3.2.3. Characteristics of the EPMs

EPMs have the following characteristics (Knaian 2010):

- **Bi-stability:** They can maintain the maximum or minimum magnetic adhesive force after the switching pulse has been applied. Therefore, they do not need a continuous supply of energy.
- **Switching:** EPMs have a switching period in the order of milliseconds to change states. For practical terms this can be considered as instantaneous.
- **Operation period:** EPMs are suitable for applications where the switching frequency is small and no repeated changes of states (ON-OFF or OFF-ON) in short time lapses are needed.
- **Power consumption:** EPMs require just a short electrical pulse (lasting a few milliseconds) to switch between states and maintain the final state. The instantaneous power required is just a fraction of what an EM needs to perform the same task (switching between OFF and ON states and preserving the final state). This characteristic translates to

significant savings in the power required for their operation compared with other technologies.

- **Low increase in temperature:** EPMs have a low temperature rise due to their short working cycle (they are active for a very short periods of time). The main components, PMs and Steel Keepers, also act as a heat sink dissipating the heat generated through the windings.

- **Scalability:** EPMs are scalable in two ways: 1. volume versus power; and 2. area versus attracting force. This means that the power needed for the switching scales with volume, whilst, the magnetic attraction force varies with the poles area (Knaian 2010). Increasing the area of the poles whilst reducing the volume of the EPM results in an increase of efficiency, with higher adhesion force and smaller power consumption.

3.3. Validation of the electro-permanent magnet concept

In order to validate the EPM concept and its implementation as an adhesion mechanism for WCMRs, a basic device is constructed using off-the-shelf components. Once the device is built the corresponding CAD model with the actual components dimensions is created with the intention to perform FEA simulations using ANSYS Maxwell software and the corresponding experiments are conducted to validate the EPM concept.

To physically observe the magnetic field in the EPM, a Magnetic Field Viewing Film (MFVF) was used. The latter is a sheet coated with micro-capsules containing nickel chips suspended in oil. In the presence of a magnetic field, the MFVF becomes darker in areas where the magnetic flux lines are perpendicular to the sheet. On the other hand, when magnetic flux lines parallel to the sheet, that area will appear bright.

Section 3.3.1 describes the components used for the experiment and Section 3.3.2 explains equipment and setup employed to perform the experiments.

3.3.1. Basic configuration and components of the EPM

The device constructed for validation purposes consists of two 5mm diameter x 20mm PMs rods (one Alnico5 and the other NdFeB N42) and two keepers made of mild steel, Figure 3.6 (a). Both PMs were placed in parallel one on top of the other and capped at both ends with the steel keepers as shown in Figure 3.6 (b). To complete the basic EPM device, both PMs are coiled with enamelled wire Figure 3.7.

Figure 3.6: Components of the EPM used for validation of the concept. (a) EPM components: one Alnico5 PM, one NdFeB N42 PM and two mild steel keepers. (b) Basic EPM configuration: NdFeB PM is placed on top of the Alnico PM, both PMs are topped with a keeper at each magnetic poles. (Coin shown for scale purposes).

Enamelled wire gauge

Enamelled wire (also magnet wire) is a coated wire made from copper or aluminium. This type of wire is mainly used in the fabrication of inductors, motors, electromagnets or transformers, among many other applications. Similar to other wires, enamelled wire is classified by its diameter by either American Wire Gauge (AWS) or Standard Wire Gauge (SWG).

Copper and aluminium, as any material, present a natural resistance to the flow of an electrical current. This resistance R can depends on the

resistivity of the material ρ, length of the wire ℓ and the cross sectional are of the wire

$$R = \frac{\rho \ell}{A} \tag{3.9}$$

From eq. 3.9, it is possible to observe that resistance is proportional to the length wire and inversely proportional to the cross sectional area. Therefore, the selection of most appropriate wire for the EMP wheel design is crucial. A wire with a small cross sectional area allows to fit more turns in a fixed length, however its resistance increases which reduces the maximum possible current that can flow through it. On the contrary, a large cross sectional area means lower resistance; however, less turns can be fitted in a fixed length. Table 3.2 shows seven wire gauges that are suitable to be used in an EPM wheel design.

The diameter of the AWG 26 enamelled wire is 0.404mm, which only allows to fit 44 turns around the 20mm long PMs, in one layer. In order to produce a sufficient magnetomotive force, three layer are coiled around the PMs resulting in 132 turns. Once the basic EPM is built, the corresponding CAD model was created, Figure 3.7. The purpose of the latter is to perform the FEA simulations needed for the validation.

Table 3.2: AWG enamelled copper wire size and data chart for the seven wire gauges considered for the EPM wheel design.

Gauge	**R (Ω/m)**	**Diameter**	**Weight (gr/m)**
32	0.5383	0.202	0.2846
30	0.338	0.255	0.4601
28	0.22	0.321	0.7227
26	0.133	0.405	1.1443
24	0.084	0.511	1.8349
22	0.053	0.644	2.8944
20	0.021	0.812	4.6013

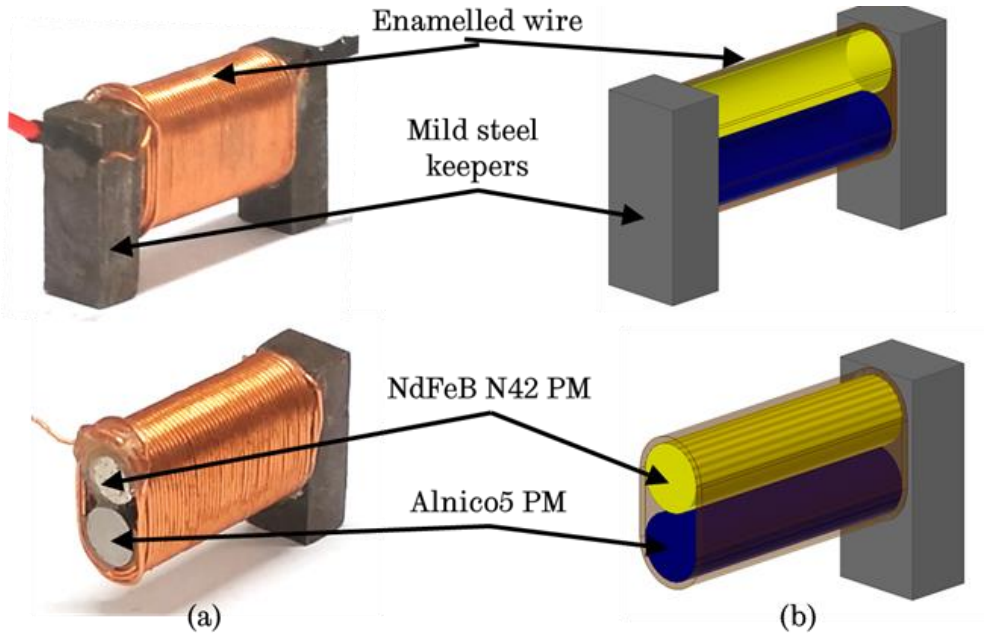

Figure 3.7: Basic EPM device coiled with 132 turns of AWG 26 enamelled wire. (a) Physical model built with off-the-shelf components (NdFeB N42 and Alnico5 PMs, enamelled wire and mild steel keepers), for experiments. (b) CAD model for FEA with equivalent dimensions for simulation purposes.

3.3.2. Equipment and experimental setup

For the case of the experimental validation the following equipment is used for performing the measurements and for controlling the pulse applied to the coil:

Load cell

An "S-Beam" load cell, from Omni instruments[1], is used for measurement of the force produced by the EPM. The model DBBSM-25KG, Figure 3.8, has a bidirectional rated capacity of -25kg to +25kg. These type of load cells are used for tension and compression force measurements.

[1] http://www.appmeas.co.uk/pdf/load-cells/DBBSM.pdf

Figure 3.8: S-Beam bidirectional load cell used to measure the magnetic adhesive force generated by the EPM device. The load cell measures the pull exerted by the attached EPM device.

Motor driver

Due to the high currents needed to produce the external magnetic field in the coil, a dual dc motor driver was selected for performing the switching. The MD30C R2 model from Cytron Technologies[2], shown in Figure 3.9, has the following characteristics:

- Has a bidirectional control, which is essential for the attachment and detachment. A pulse with positive polarity is required for the OFF-ON switching. Conversely, a pulse with negative polarity enables the ON-OFF switching.
- Supports a continuous current of 30amps, with a maximum peak current of 80Amp for one second. The maximum pulse lengths are estimated to be no greater than 50ms (for experimental purposes), thus is safe to use the maximum 80Amp capacity.

[2] http://www.cytron.com.my/p-md30c

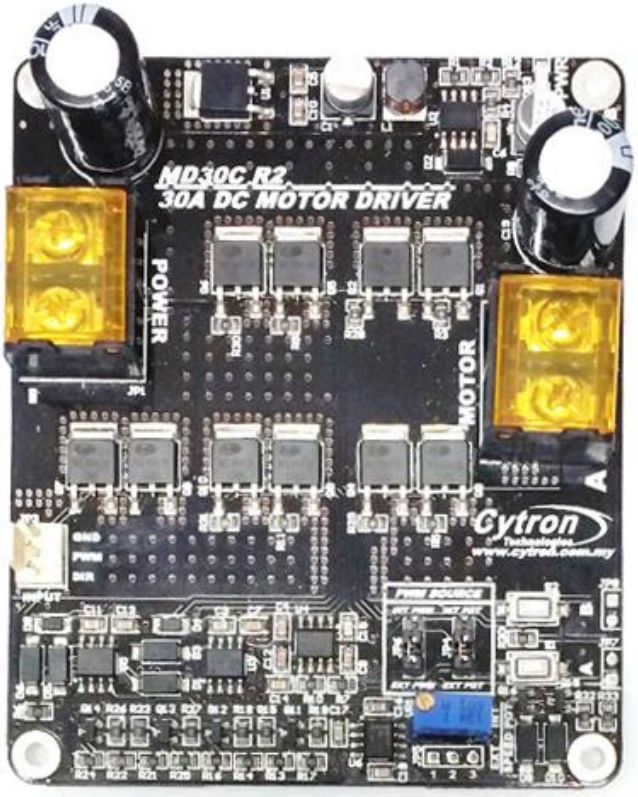

Figure 3.9 Bidirectional motor driver, MD30C R2, used for applying the electrical pulses to the EPM windings. Supports a continuous current of 30amps and a peak current of 80amps for one second.

Data acquisition and control signal generation

For the acquisition of the data, and sending the control signal to the motor driver to perform the switching, a National Instruments NI cDAQ 9178 chassis is employed. For acquiring the force data from the load cell a NI 9201[3] 8 channels module, and for controlling the motor driver the NI 9263[4] 4 channel module are used, Figure 3.10. Both modules have a sampling rate of 100 kS/s and a ±10v input and output range, respectively.

Along with the NI cDAQ chassis and modules, a simple code is programed in LabView[5] to simultaneously apply the electrical pulse to the coil's windings, and acquiring the adhesive force generated by the EPM.

[3] http://www.ni.com/datasheet/pdf/en/ds-184
[4] http://www.ni.com/datasheet/pdf/en/ds-59
[5] http://www.ni.com/labview/

Figure 3.10: Chassis NI cDAQ 9178 with one analogue input module NI 9201 for acquiring load cell data. And one analogue output module NI 9263 for sending the signal to the motor driver for controlling the electrical pulse applied to the solenoid.

Experimental Setup

The experimental setup for the validation of the EPM concept is presented in Figure 3.11. The EPM is attached to the load cell which holds it over a steel plate. The EPM is connected to the motor driver that generates an electric current pulse, whose power is supplied by a LiPo battery. The motor driver is controlled by the NI 9263 output module inserted into the NI cDAQ chassis. The data from the load cell is acquired by the NI 9201 module, also inserted into the NI cDAQ chassis. The chassis is connected to a PC, via USB, that controls the period of the pulse and stores the data from the load cell with the help of a graphical interface programed in LabView.

Experimental protocol

The main objective of the experiments is to validate the working principle of EPMs. For this particular case the independent variable is the length of the electrical pulse, expressed in milliseconds (ms), and the dependent variable is the magnetic force produced by the EPM, expressed in kilograms (Kg).

Once the experimental setup described previously is set, an electrical pulse is applied to the EPM's winding. Using LabView and NI-Daq chassis, the electrical pulse applied and the magnetic force (generated by the EPM) are be recorded for further analysis.

For the OFF-ON transition a 20ms electrical pulse is applied (with the corresponding polarity) in order to set the EPM to its OFF state. Then a set of electrical pulses is applied with lengths that start with 0.1ms with 0.1ms increments. Each length step is repeated 5 times and the final force (after the transient behaviour has settled) is recorded and then averaged. After each pulse is applied and the data recorded an 20ms pulse with inverse polarity is applied in order to reset the EPM to its initial state before the next pulse is applied.

For the ON-OFF transition the same procedure is followed, but previously setting the EPM into its ON state.

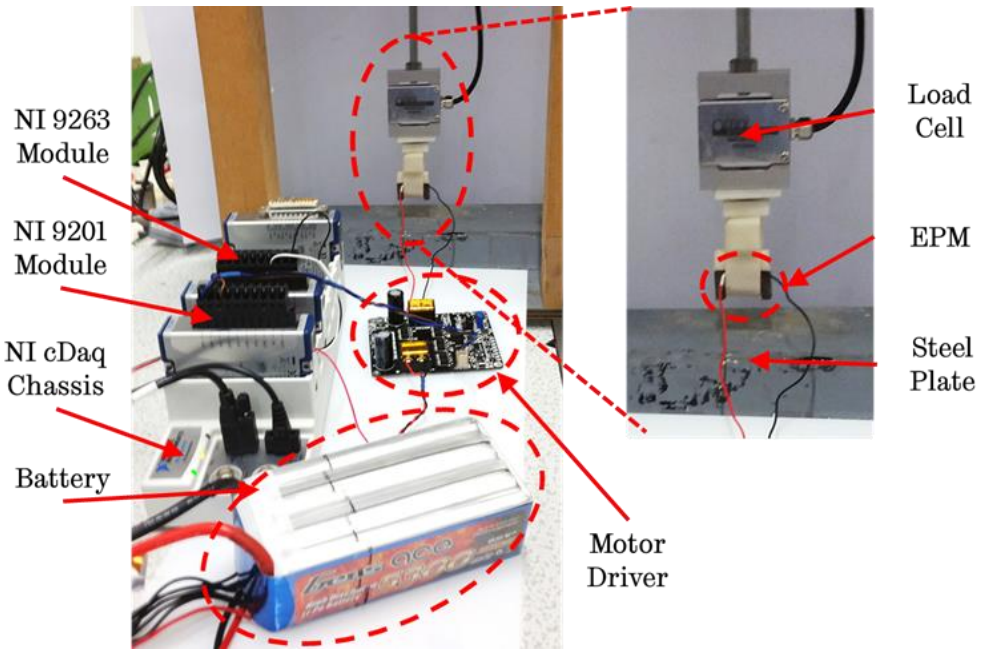

Figure 3.11: Experimental setup for validation the EPM concept. Module NI 9263 sends the control signal to the motor driver, which delivers an electrical current pulse to the EPM. The EPM switches from OFF to ON state and gets attracted the steel plate below it. Load cell measures the force of the pull generated by the EPM and the data is acquired by the NI 9201 module.

Simulation Setup

For the case of the FEA simulations performed for the validation, ANSYS Maxwell 2015.2 software is used. Maxwell software is specifically designed for FEA simulations in the electromagnetics field. It allows to obtain magnetostatic, and transient solutions.

In any FEA simulation setting the appropriate mesh is crucial for obtaining accurate results. One of the advantages of Maxwell is that the software performs the meshing process through adaptive meshing refining. The user only needs to set the desired percentage of accuracy for the final solution, the percentage of mesh refinement after each pass, and the number of passes after which the simulation is stopped if convergence of the desired solution is not reached.

It is possible to decrease the simulation time, if certain mesh refinement operations are performed in areas where the user knows include higher concentrations of the fields. Figure 3.12 shows an example of the adaptive mesh refinement performed by Maxwell software with a setting of 20% refinement per pass and 0.35% percent error as solution target. Solution was achieved in 5 passes and 7 minutes.

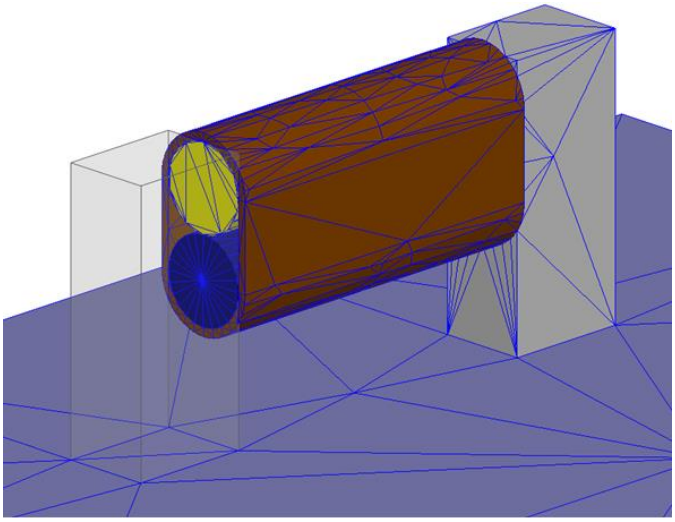

(a) Initial mesh

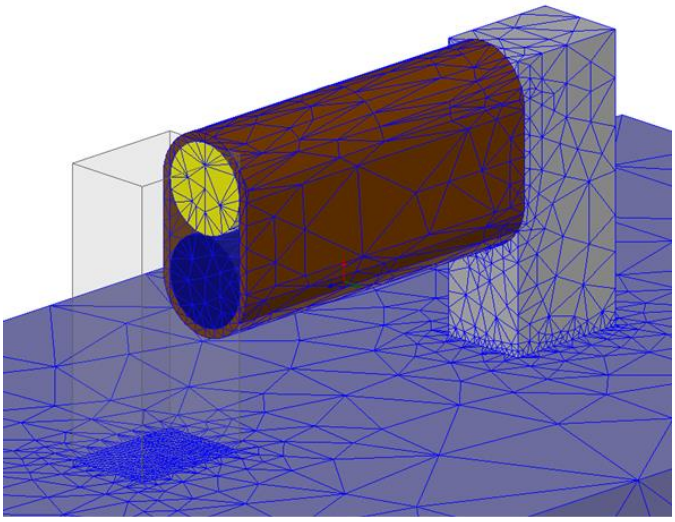

(b) Refined mesh

Figure 3.12: Results from an adaptive mesh refinement in ANSYS Maxwell 2015.2. (a) Initial mesh without any initial mesh operations. (b) Final mesh after 5 passes with a 20% refinement per pass and 0.35% final error as a target solution.

3.3.3. Simulation and experimental results: basic OFF and ON configurations

The two basic configurations (OFF and ON described in Figure 3.4) were explored. Using only the main components, shown in Figure 3.6(a), the FEA simulation in the ANSYS Maxwell software and their corresponding physical experimentation were implemented. Qualitative results are presented showing the behaviour of the EPM, together with quantitative results of the

adhesive force. Both results are shown with the objective of verifying that the physical experimentation correlate to simulations performed with FEA.

Qualitative results

From the FEA simulations, shown Figure 3.13, it is observed that in the case for ON configuration the magnetic flux lines flow through the steel keepers and generate an external magnetic field at the bottom the keepers. This magnetic field will magnetise any ferromagnetic object placed close to the EPM, producing a magnetic adhesive force. For the OFF case the magnetic flux lines are kept in a closed loop inside the EPM, as result no external magnetic field is produced. Consequently, no magnetic adhesive force is generated outside the device.

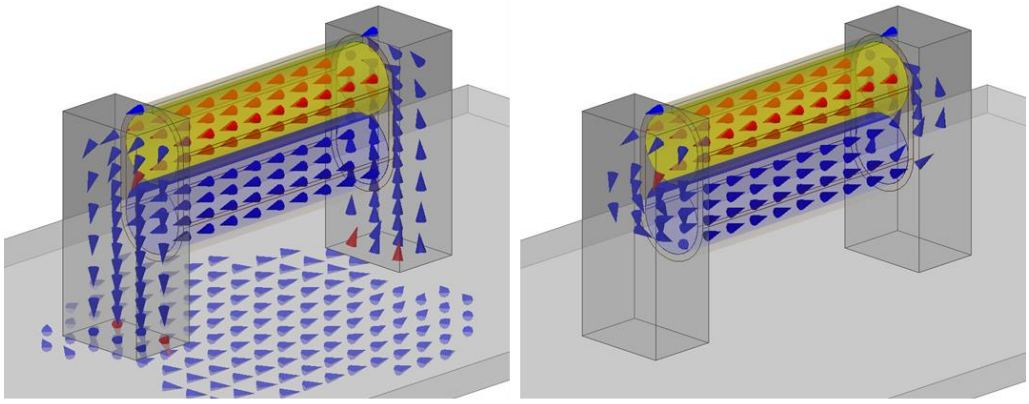

(a) ON State (b) OFF State

Figure 3.13 Qualitative results from quantitative FEA simulation of the EPM two basic states. Arrows represent the magnetic flux lines and the flowing direction. (a) In the ON state both PMs are magnetised in the same axis direction resulting in their magnetic flux lines adding up and flowing through at the steel keepers. This flow is directed to the steel target producing a magnetic attracting force on between the EPM and the target. (b) For the OFF state, the PMs' magnetisation is in opposing directions on the same axis, which results in their magnetic flux lines flowing in a closed loop between the Alnico and NdFeB PMs, inside the EPM. As a result, no magnetic adhesion force is generated.

In Figure 3.14, the physical display of the magnetic field interaction is shown, for the OFF and ON states. When the EPM is in the ON state magnetic flux flows through the keeper and steel piece (placed as target). By placing

the MFVF over the EPM, three main dark areas are shown (left and right keepers, and steel target), indicating the presence of the magnetic field. Similarly, when the MFVF is placed on the EPM in OFF state, only the area where the PMs are present, become dark. This demonstrates that the magnetic field is inside the EPM, flowing in a closed magnetic circuit between the PMs. Additionally, in Figure 3.15 shows in a qualitative way the effect of the adhesive force for both, OFF and ON states, over a group of steel pieces stacked together with a combined weight of 1.268kg.

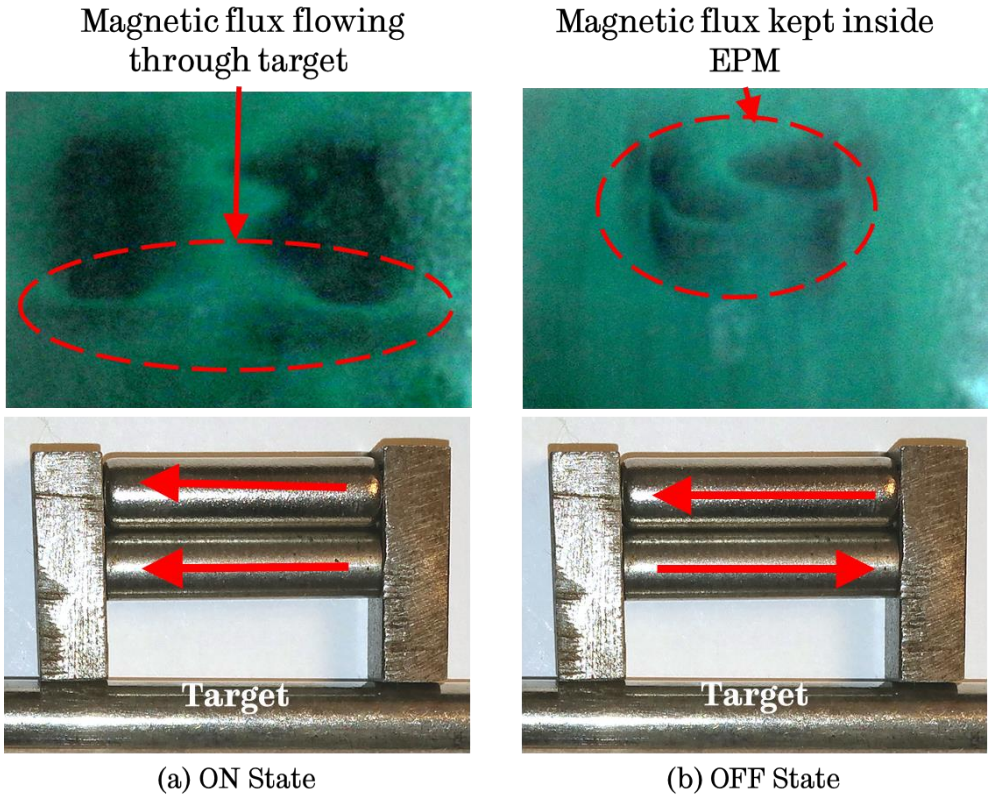

Figure 3.14: Qualitative results from physical validation. Red arrows indicate the direction of magnetic field flux lines, red dashed ovals indicate the interaction of the magnetic field of the Alnico and NdFeB PMs. (a) For the ON state it is observed that the magnetic flux flows through the keepers (dark areas) and then through the steel piece at the bottom. (b) On the other hand, in the OFF state magnetic flux is kept in a closed loop between both PMs.

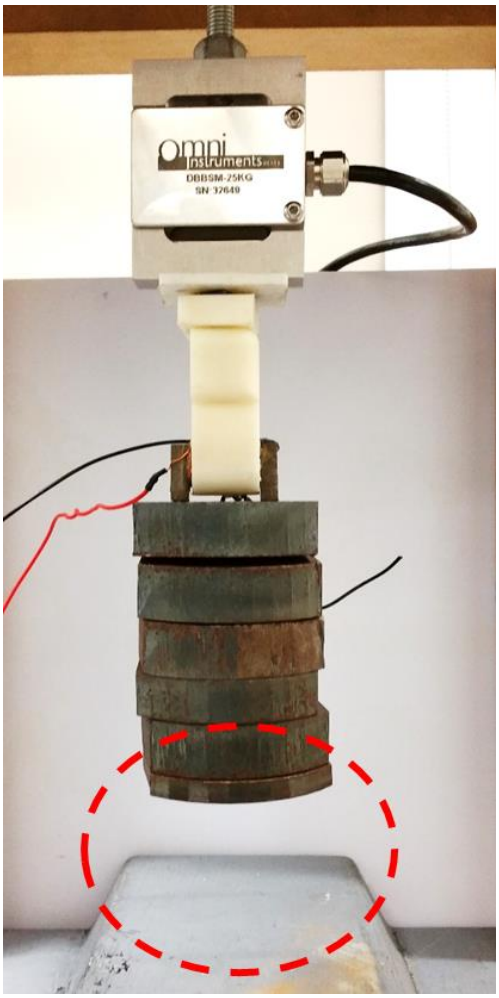

Figure 3.15: Experimental demonstration of the holding magnetic adhesive force. Magnetic field is exerted from the EPM producing a magnetic adhesive force. The EPM can easily hold a 1.268kg pile of steel pieces attached to the device.

Quantitative results

From the same experiments and simulations, actual values for the magnetic adhesive force were also obtained, Table 3.3. The experimental result corresponds to the average value of five independent experiments.

Table 3.3: Comparison of the magnetic adhesive forces obtained through simulations and experiments

State	Simulation	Experimental
ON	1.42 Kg	1.39 kg
OFF	0 Kg	0 Kg

Both, simulation and experimental results demonstrated in a qualitative and quantitative way, the working operation and the interaction of the magnetic fields inside the EPMs. In order to fully validate the concept of EPMs as an adhesion mechanism, its switching behaviour was also corroborated, as described next.

3.3.4. Switching between states and variable magnetic adhesive force

The EPM device and CAD model shown in Figure 3.7 were employed for the validation of the OFF-ON and ON-OFF switching. The setup for the experiments and simulation was the following: voltage applied Vin = 11.84V and pulse width t = 2.5ms. The electrical circuit is shown in Figure 3.16. The value of the resistance R depends on the gauge of the magnet wire and its length. For this particular case, a 26AWG magnet cable was employed with a length of 7.59mts and 132 turns. The resistance measured was R = 0.57 ohms.

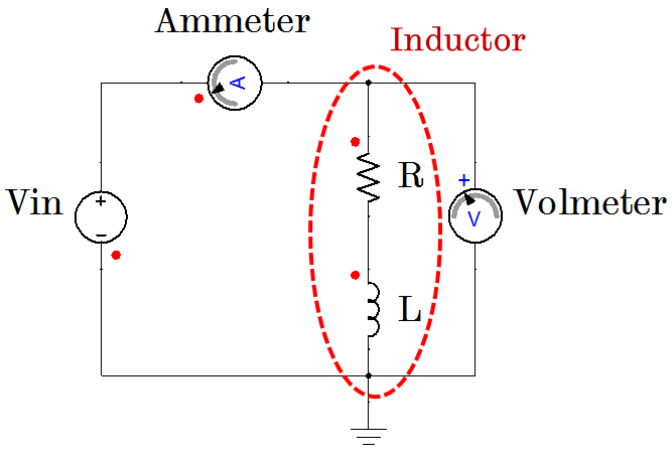

Figure 3.16: Electrical diagram for both experiment and simulations. R and L are the same component, coil or winding, it was split into its resistance and inductance parts due to software requirements to perform the simulation.

In the case of the physical experiments a LiPo battery was employed as source of power to minimise the noise in the measurements. It was found that the DC power supply used initially introduced the frequency of the electrical mains, and incremented the level of noise in the measurements.

OFF-ON switching

Simulations results, Figure 3.17 (b) red dashed line, show that for this design, saturation is reached in approximately 1ms. Applying longer pulses does not add extra adhesive force to the device. Once the EPM has reached saturation, 1ms for this case, the remaining time the adhesive force keeps constant until the pulse is removed, at 2.5ms.

The magnetic adhesive force switched from 0Kg to 1.42Kg by applying just a 2.5ms electrical pulse, with a power consumption of 0.187mWh. In the same way, results from the experiment showed a final magnetic adhesive force of 1.39Kg after switching from OFF to ON.

The blue line in Figure 3.17 (b), represents the experimental result, it can be observed that there exists a discrepancy in the transient switching between simulation and real experiment. There exists a 0.6ms delay in the measured force after the external pulse is applied. The reason for this delay is the type of sensor that was employed to measure the force an S-Beam load cell. The "S" shape of the sensor causes it to behave like a spring, when the load receives an impulse excitation. Therefore, explaining the delay at the beginning of the measurement and the oscillations after the excitation is removed, Figure 3.17(a) blue signal.

Transient behaviour of the EPM

The characteristic transient behaviour of an EPM whilst the electric pulse is applied is presented in Figure 3.17(b). The black dashed line represents the electric pulse applied to the windings, which has a 2.5ms width for this example. The red dashed line represents the magnetic adhesive force produced by the EPM. When the pulse is applied, the adhesive force starts increasing until the maximum peak force is reached. The magnitude of this peak force is determined by external magnetic field produced by the solenoid, which always is bigger than the internal magnetic field of the PMs combined. The slope is determined by the charging time constant of the solenoid, τ, which depends on the internal resistance and

self-inductance, as mentioned in Section 3.1.1. For this example, the maximum current magnitude is reached in approximately 1ms. Once the current gets to its maximum value the adhesive force remains constant until the electric pulse is removed. After which, the magnetic adhesive force exerted by the EPM decreases to the steady state magnitude that depends exclusively on the internal magnetic field of the PMs.

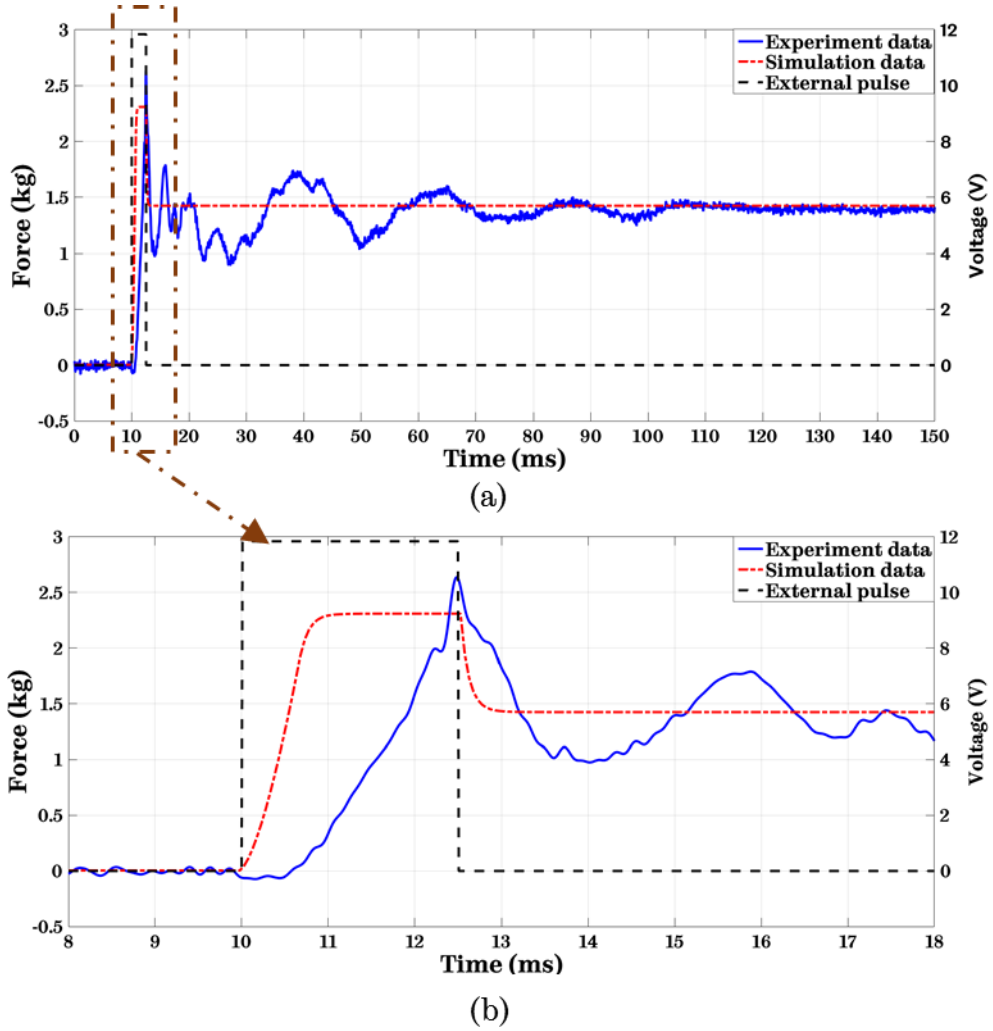

Figure 3.17: Comparison of experiments vs simulation results. Black dashed signal: external pulse with a 2.5ms width. Blue signal: magnetic force measured from experiment. Red dashed signal: magnetic force obtained through FEA simulation. (a) Switching from OFF to ON state after applying a 2.5ms pulse with amplitude 11.84V. During the pulse the amplitude of the magnetic force peaks at 2.31Kg for the simulation case and 2.63Kg for the experiment. After applying the pulse the magnetic force decreases to 1.42Kg for the simulation and 1.39Kg for the experiment case. (b) Zoom of the pulse for a better appreciation of the OFF-ON transition.

For the case of the experimental result, the blue line, this behaviour gets distorted by external factors that are not considered by the FEA simulation, because of their computational and simulation time cost compared to the final contribution. These are the transient behaviour of the S-Beam load cell, which introduces an initial delay and a spring oscillation behaviour after the initial pull. The latter is produced when the external magnetic field of the pulse is removed. Additionally, the rigidity of the test bench, which too introduces transient oscillations to the system is omitted.

Variable magnetic adhesive force

The capability of EPMs to vary their adhesive force to a specific value, between the minimum and maximum outputs, was explained in Section 3.2. The most intuitive way of varying the magnetic adhesive force in EPMs, which directly depends on the electric current flowing through the solenoid, is to vary the input voltage. Therefore, varying the current flowing through the windings. This current along with the number of turns in the coil produces the external magnetic field needed to modify the magnetisation of the Alnico PM, hence its adhesive force.

However, since the EPM is an inductor in electrical terms, it is possible to take advantage of its electric current charging behaviour when a voltage is applied to its terminals. If the input voltage is a fixed value, 11.84V in this case, and the length of the pulse is varied the same result, compared to varying the input voltage, can be achieved.

Previously it was determined that the EPM reached saturation in less than 1.0ms. This is the length a pulse must have in order to reach the maximum possible adhesive force for this particular EPM. Any pulse longer than 1.0ms does not increase the adhesive force, but wastes energy via heat through the windings. For the particular case of this research a PWM controller is used for controlling the length of the pulse. Pulses lengths of 0.3, 0.5, 0.8, 1.0, 1.5, 2.0 and 2.5ms were applied. All other variables were set as previously stated in the ON-OFF switching case.

Results from FEA simulations from the design proposed in Figure 3.7 are presented in Figure 3.18. It is observed that by applying an electric pulse with increasing length, between zero and 2.5ms, it is possible to achieve a specific adhesive force. Also, it is established that any excitation beyond the point the system reaches saturation, 0.8ms for this design, does not contribute any changes to the adhesive force.

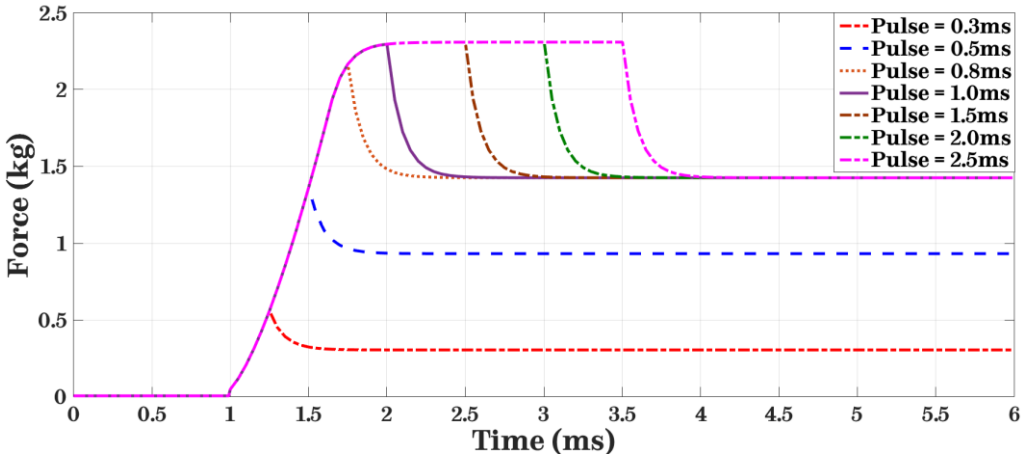

Figure 3.18: Magnetic adhesive force as result of different pulses lengths 0.3, 0.5, 0.8, 1.0, 1.5, 2.0 and 2.5ms. It is showed, through pulses 1.5, 2.0 and 2.5ms, that after 1.0ms the system does not increase its final adhesive force.

In order to corroborate the results obtained in the simulations, their corresponding physical experiments were performed and the results presented in Figure 3.19. Similarly to the OFF-ON switching experiment, results are presented in a 150ms window to allow the transient effect of the load cell to settle down. The results correspond to the OFF-ON switching with pulse lengths: 0.3, 0.5, 0.8, 1.0, 1.5, 2.0 and 2.5ms. Although the performance is similar to the simulations, in the experiments it takes 2.0ms to reach the maximum value of the final adhesive force. Again, this can be explained by the transient behaviour of the load cell employed in the measurements. Which, as mentioned before, is also responsible for the oscillations observed after the pulse is applied.

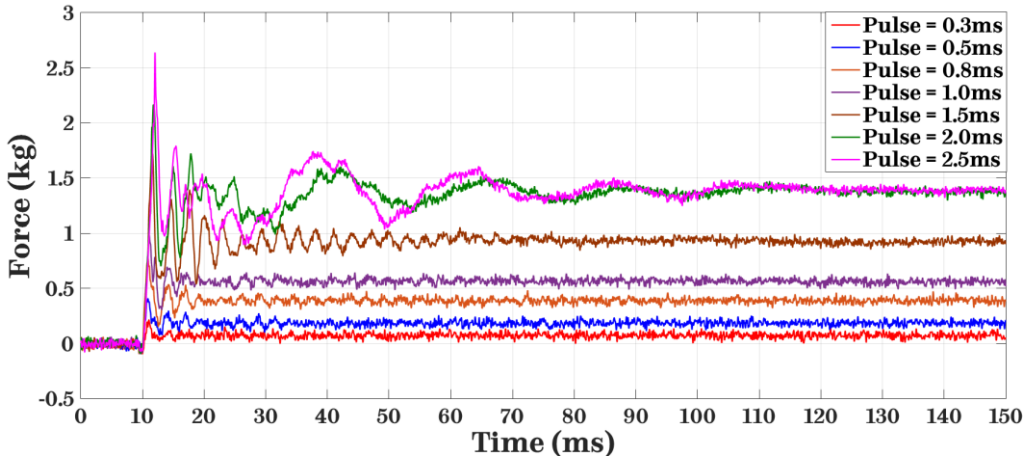

Figure 3.19: Experiment measurements for the OFF-ON switching. Pulses with lengths 0.3, 0.5, 0.8, 1.0, 1.5, 2.0 and 2.5ms were applied. It is observed that increasing the length of the pulse increments the final adhesive force. Once EPM reaches saturation longer pulses do not add higher adhesive force. In this case, a greater period of time (150ms) to allow the transient effect of the S-shape load cell to settle down is shown.

In the same way, Figure 3.20 presents the results for the ON-OFF transition. For this case the pulse lengths were from 0.2 to 1.0ms with 0.1ms increments. Results show that the time required to perform the transition from ON to OFF state is 0.8ms, which translates into energy savings.

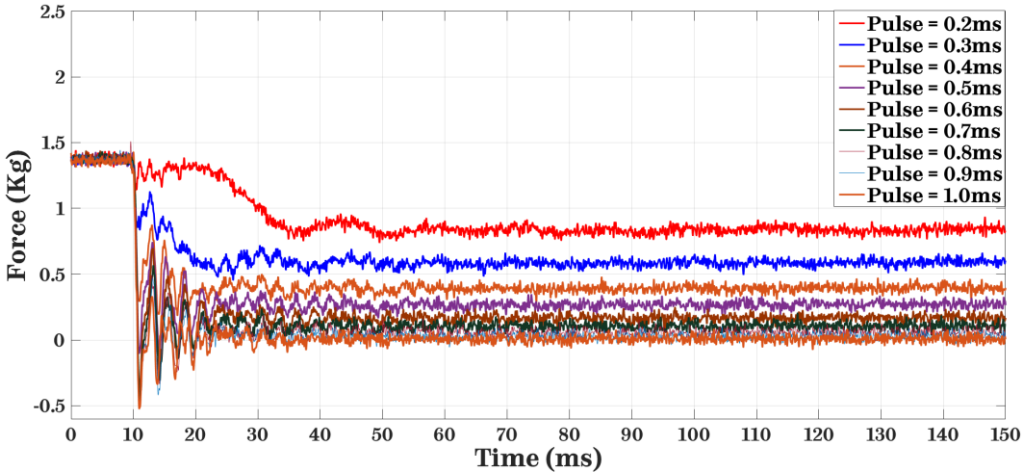

Figure 3.20: Experiment measurements for the ON-OFF switching. Pulses with lengths from 0.2 to 1.0ms with increments of 0.1ms were applied. Increasing the length of the pulse results in a bigger decrease in the adhesive force. In this case a greater period of time (150ms) to allow the transient effect of the S-shape load cell to settle down is shown.

In the case of the transition ON-OFF, in Figure 3.20 appears a negative force between 10ms and 20ms, which is due to a transient oscillation effect that is introduced by the load cell. This negative force does not represent a push-force but the spring effect due to shape of the load cell and the holding mechanism used to fix the EPM.

3.4. Concluding remarks

EPMs working principle has been presented. Different FEA simulations, and their corresponding physical experiments were performed in order to validate its feasibility as an adhesion mechanism for WCMR in ferric structures. Results obtained from simulations were validated by their matching experiments. Results corroborated the EPMs ability to be switched OFF and ON, and determined the maximum adhesive force and switching periods, for a particular EPM size and design.

Furthermore, the possibility to vary the adhesive force between the minimum and maximum values (0 – 1.39Kg for the case of the present work) was demonstrated. This characteristic is a major improvement over conventional magnetic adhesion mechanisms. And its implementation in WCMRs can increase their ability to explore unstructured environments as well as overcome complex obstacles.

Now that EPMs feasibility as an adhesion mechanism for WCMRs has been proven, its implementation along with a suitable locomotion mechanism is explored.

The following chapter explores the locomotion mechanisms in which EPM can be integrated as the main adhesion mechanism, and the optimal combination is selected.

Chapter 4

Locomotion Mechanism and EPM Adhesion Mechanism Integration

Locomotion and adhesion mechanisms are the crucial components in the design of a Wall Climbing Mobile Robot (WCMR). Whilst the first enables the movement in a particular scenario, the second allows the MR to adhere to the surface in the presence of a slope, or when the MR is in an upside down position. In Chapter 3, EPMs were proposed as a novel adhesion mechanism, and their working principle and characteristics were presented and corroborated. Furthermore, their use as a potential adhesion mechanism for ferric structures was demonstrated.

In the present chapter, the combination of the EPM Adhesion Mechanism (EPMAM), and the most suitable locomotion mechanism, legged, tracked or wheeled, is explored. The main objective being its implementation in a WCAMR, for inspection of ferric structures. In Section 4.1, a detailed evaluation of the main locomotion mechanisms is given. Based on this, the most suitable to be implemented in a WCMR for ferric structures is selected. In Section 4.2, different solutions for the integration of an EPMAM and the selected locomotion mechanism are presented, the most promising is selected. Finally, in Section 4.3 presents simulations and their corresponding experiments to verify that the proposed EPMAM and locomotion mechanism configuration comply with the intended OFF-ON

and ON-OFF switching adhesion, as well as the selection of a specific adhesive force.

4.1. Locomotion mechanism selection

Each locomotion mechanism provides MRs with particular mobility capabilities. These can be an advantage or disadvantage, depending on the scenario where the MR is going to be implemented in addition to the task that is to be performed (Bruzzone & Quaglia 2012; Nie et al. 2013). When selecting the most appropriate locomotion mechanism for a WCMR, certain requirements have to be defined. The most important are:

- The type of scenario where the WCMR is going to perform: including the dimensions of the area that the MR has to cover, whether there are flat or uneven surfaces, and if it will operate on rigid or flexible structures.
- The complexity of the structure being inspected as well as the type of the obstacles that could be present.
- Speed required to move through the structure whilst performing the inspection or maintenance tasks.
- Power consumption of the adhesion mechanism.

The number of existing ferric structures is immense, and these have a great diversity of shapes, sizes and complexities. These factors make it extremely difficult to design a generic WCMR for their inspection. For this reason, most of the MR used for inspection of steel structures are designed for a specific scenario and task (Balaguer et al. 2005).

For the case of the present research, the proposed integration of the locomotion mechanism and EPMAM, is intended to be implemented in a WCMR for inspection of ferric structures with the following requirements:

- To move around in structures that have large flat areas, with uneven sections in between.

- To perform on structures that are both relatively simple, such as oil storage tanks, and complex with transitions and connecting parts, such as steel bridges.
- To be able to move at relatively high speeds (>0.5 $\frac{m}{s}$) in order to cover large distances in short periods of time.
- To have a low power consumption due to the limited life of batteries used to power them.

Having set the requirements for the WCMR in terms of the locomotion needs, the four main locomotion mechanisms that can be implemented in a MR for inspection of steel structures are presented in Figure 4.1. Each mechanism can be implemented in a WCMR, depending on the task that has to be performed. The advantages and disadvantages of each locomotion mechanism are given next.

Legged locomotion mechanism

Legged WCMR can be either bipedal, Figure 4.1 (a), or multi-legged, Figure 4.1 (b). This type of locomotion provides WCMR with several degrees of freedom allowing a broad mobility. This makes the MR suitable for implementation in unstructured environments, steep and uneven surfaces (Bovim 2014).

The simplest mechanism is bipedal, however this design is highly unstable, which increases the complexity of the control and stability systems. By increasing the number of leg-pairs the instability is eliminated, however, the number of degrees of freedom is increased. This increments the complexity of the design and the related control systems, along with an increase in the power consumption. Another drawback is the walking speed, which is slow compared with other locomotion mechanisms.

Based on these characteristics and the requirements, legged locomotion mechanisms, are not suitable to be implemented in a WCMR

used for inspection of large ferric structures. Although they can be employed for alternative situations.

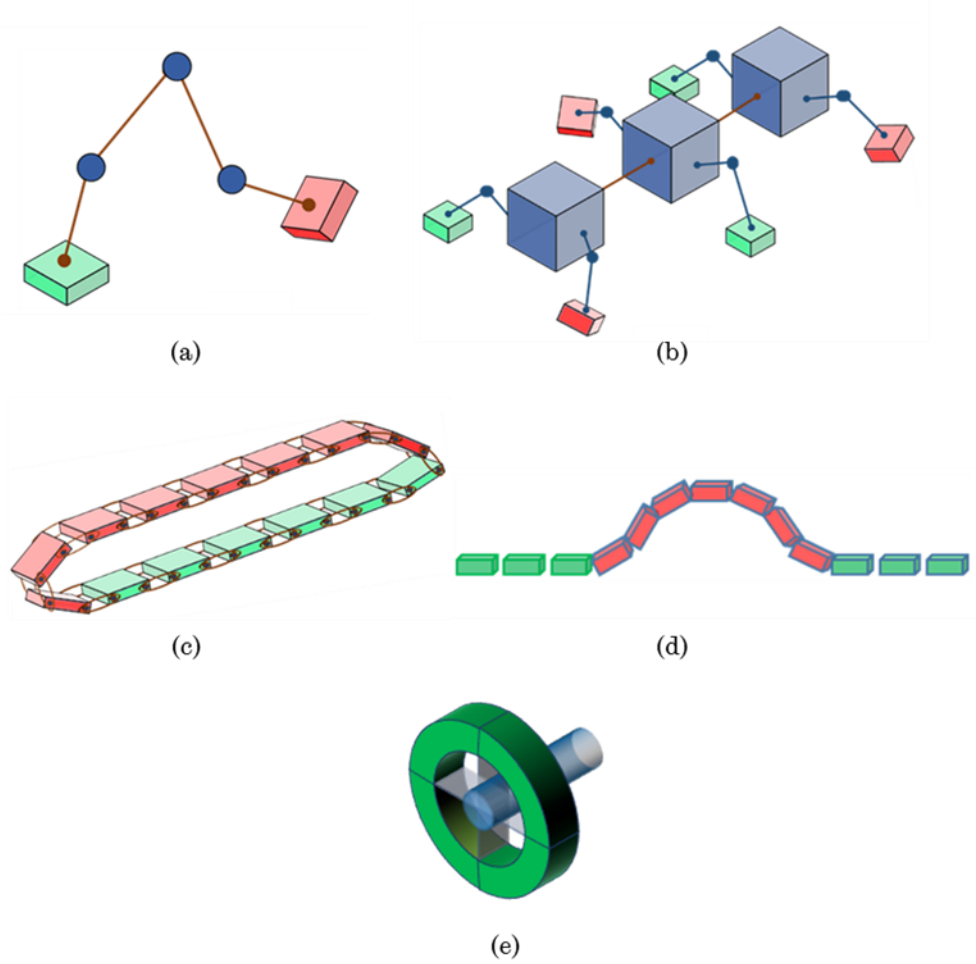

Figure 4.1: Main locomotion mechanisms that can be implementation in a WCMR for inspection of ferric structures. (a) Bipedal mechanism. (b) Multi-legged mechanism. (c) Tracked mechanism. (d) Snake mechanism. (e) Wheeled mechanism. Green blocks indicate adhesion mechanism switched ON, red blocks indicate the adhesion mechanism is switched OFF.

Snake locomotion mechanism

Mobile robots with this particular type of locomotion consist of long bodies divided into modules, Figure 4.1 (d). They move around by a continuous sliding locomotion or by an extension-compression movement. The modules are connected by actuators which allow the MR to have sliding movements like a snake or by extending and contracting like a caterpillar.

Snake locomotion mechanisms are mostly implemented in modular MR, used in very constricted environments such as thin tubes or through debris from collapsed structures. The operation range is limited to small areas mainly due to the slow speed at which they move. This can lead to high energy consumption when large distances need to be covered (Ting Wang et al. 2005). Therefore, they are not suitable for inspection of large steel structures.

Tracked locomotion mechanism

Tracked MR, Figure 4.1 (c), are especially suitable to move on uneven and soft terrain overcoming complex obstacles. They have faster speeds than legged or snake MR, and their energy consumption per distance travelled is lower (Jahanian & Karimi 2006).

The mechanical nature of the tracked systems produce considerable vibrations which can be a problem in some structures where they are implemented. Also, the efficiency and speed are effected by vibrations (Bruzzone & Quaglia 2012; Jahanian & Karimi 2006).

This type of locomotion is suitable for MR use in the inspection of ferric structures thanks to their ability to overcome obstacles. However, they are limited to constructions where vibrations introduced by this mechanism is not a major problem.

Wheeled locomotion mechanism

Wheeled WCMR, Figure 4.1 (e), have the highest speed rates with a low power consumption per distance travelled. Configurations for the majority of this type of MR go from two, three, up to six wheels, depending on the task and the scenario. The mechanical complexity is relatively simple, as well as the control. The technologies used for this type of locomotion mechanism are in a mature state, since they have been employed in different fields for a few decades.

The obstacle overcoming capability is limited to small obstacles. Nonetheless, by implementing an independent and articulated suspension mechanism to the frame, the ability to overcome obstacles is substantially enhanced. Also, the manoeuvrability is benefited by this type of implementation.

Discussion

The main locomotion mechanism characteristics were presented and their feasibility to be integrated in a WCMR for ferric structures were explored. Based on a pre-established criteria, advantages and drawbacks of each locomotion mechanism were examined and the best options for implementation in a WCMR for inspection of large steel structures are: 1. Tracked locomotion mechanisms in the case that obstacles are a big concern; and 2. Wheeled locomotion mechanisms for scenarios where obstacles are not an big issue and the range of operation, speed and power consumption are of greater importance. The effect of using an EPMAM with each of the two locomotion approaches is now evaluated.

4.1.1. Selection of the locomotion mechanism and EPMAM integration

Another consideration that is important to account, in the design of a WCMR for ferric structures, is the effect of integrating a magnetic adhesion mechanism with the two selected locomotion mechanisms. As discussed in Section 2.2.2, conventional magnetic adhesion mechanisms use PMs as the source of the adhesive force result in a fixed magnetic adhesion. Furthermore, the adhesive force needed to keep the WCMR, along with the payload, attached to the structures often limits the manoeuvrability and performance of the WCMR.

However, as demonstrated in Chapter 3, EPMs have the capability to switch between OFF and ON states, and to vary their magnetic adhesive force to a desired magnitude. This characteristic makes EPM suitable to be

implemented along with most locomotion mechanisms, but specifically with wheeled and tracked locomotion mechanisms.

For all the locomotion mechanisms presented, switching depends on the speed of the MR and the amount of independent EPAMAM that are implemented in each configuration. The main considerations to be taken into account in the implementation of an EPMAM due to the switching frequency are:

- Adhesive force: is the produced magnetic adhesive force enough to adhere to the structure.
- Manoeuvrability: is the adhesive force so strong that it limits the performance of the WCMR.
- Controllability: does the amount of EPMs integrated to the locomotion mechanism impact the complexity of the control of both, the adhesion and locomotion mechanism.
- Power consumption: does continuous and prolonged switching derive in a high power consumption.
- Temperature rise: another side effect of a continuous and prolonged switching is a high temperature rise produced by the solenoid.

Tracked locomotion mechanism

For the case of tracked locomotion mechanism, Figure 4.1 (c), the adhesion mechanism is divided into a series of sequential independent EPMAMs. To allow the movement of the WCMR the bottom EPMAMs are turned ON whilst the top EPMAMs are being turned OFF. Whilst the MR is moving, the upper EPMAMs are kept OFF until they reach the front of the track. While the bottom EPMAMs are kept ON until they reach the back of the track.

With this type of locomotion the switching frequency of each independent EPMAM is not a problem. The individual switching of each module happens once it reaches the front of the track (OFF switching) and

the back of track (ON switching). In this case the heat rise is eliminated due to the relatively long periods between switching of each EPMAM. Even though the individual switching of the EPMAM modules is not an issue, their sequential switching becomes a problem in terms of power consumption. Whilst the MR is moving, a continuous and sequential set of electrical pulses are needed to activate the EPMAM that make the transition from the top to the bottom. At the same time as deactivating the modules transitioning from the bottom to the top of the track. Furthermore, as a result of using several EPMAM modules, the complexity of the control for the adhesion mechanism increases, along with a decrease in manoeuvrability. Based on the mentioned drawbacks the implementation of a tracked locomotion mechanism with EPMAM is dismissed.

Wheeled locomotion mechanism

Wheeled locomotion mechanisms, as mentioned in Section 4.1, has better capabilities in terms of mobility, range of operation and power consumption compared to tracked locomotion mechanism. In addition, combining an EPMAM with a wheeled locomotion mechanism results in a WCMR that meets the requirements established in Section 4.1. A wheeled WCMR with an EPMAM has the following characteristics:

- It is able to move over large flat structures with uneven areas and small obstacles.
- It can move at high speeds around structures covering large distances in short periods of time.
- It has a low power consumption for both, motion and adhesive mechanism control.
- The complexity of the control for the adhesive mechanism is simple compared with the tracked mechanism.

Based on the mentioned characteristics, the wheeled mechanism and EPMAM is the most feasible combination in order to meet the requirements

set in Section 4.1. Hence, for the particular case of a WCMR for inspection of large ferric structures, wheeled locomotion mechanism is the most suitable choice, up to now. The next stage is to explore the main possible designs for integrating both mechanisms. The next section presents some of the possible configurations of an EPMAM, and a wheeled locomotion mechanism, and the best option is selected.

4.2. EPMAM Implementation in the wheeled locomotion mechanism

For the case of implementing EPMAM in a WCMR with wheeled locomotion mechanisms, a number of possible configurations are possible, some of these configurations are presented in Figure 4.2 and are described and analysed next.

Segmented wheel

The first approach was to divide the wheel into a number of segments Figure 4.2 (a). Each segment being an independent EPMAM. This design has similar disadvantages to the tracked locomotion. This mainly due to the high switching frequency required whilst locomotion is performed, which results in a high temperature rise and increase in the power consumption.

EPMAM integrated in the main body

A different approach is to place the EPMAM in the main frame at the bottom of the WCMR body, Figure 4.2 (b). With this configuration, the switching is reduced to a minimum, needed just for attachment or detachment, and for adjustments of the adhesive force. The downside of this particular approach is that the WCMR can only be employed on a flat surface with no obstacles. If the distance between the EPMAM and the structure surface is increased for any reason (e.g. an uneven surface below the MR or overcoming a small obstacle) the adhesive force will decrease exponentially causing the MR to lose adherence.

External EPMAM (outside the wheel)

An alternative configuration is the implementation of the EPMAM independent from the wheel rotation, by fixing the adhesion mechanism either at the sides of the wheel Figure 4.2 (c) or around the wheel Figure 4.2 (d). With this approach, the main drawbacks (continuous switching and separation from the structure's surface) from the two previous configurations are eliminated. The only disadvantage is that the size of the wheel is increased significantly, which makes the wheel bulky and not suitable for certain WCMR.

EPMAM integrated in the wheel shaft

Another possible configuration is to implement the EPMAM in the shaft of the locomotion mechanism and letting the wheels, at each side of the shaft be the keepers for the EPM Figure 4.2(e). With this design the magnetic field produced by the EPM becomes a major concern. As the EPMAM is integrated to the shaft, which crosses the body of the WCMR, the magnetic fields produced will be too close to the circuitry of the MR. This may lead to malfunctioning or even damage the circuitry components by the strong and varying magnetic field produced by switching of the EPM.

Internal EPMAM (inside the wheel)

One more configuration is presented in Figure 4.2 (f), in which the EPMAM is integrated into the wheel, as a whole. In other words, the wheel consists of only one EPMAM, which is the wheel itself. With this approach the locomotion and the adhesion mechanism are independent from each other. Hence, the frequent switching is eliminated. Once the attachment to the surface has been achieved, the WCMR can move around maintaining the adhesion. The next switching is performed only if detachment or an increase/decrease in the adhesive force is required. Two possible variants for the design are presented: 1. with both PMs, of the EPM, in a concentric configuration (one inside the other); and 2. Both PMs placed parallel to each

other. With this approach the size of the wheel is reduced, compared to design with the EPMAM integrated at the sides or around of the wheel. Moreover, the magnetic fields are kept relatively far from the circuitry in order to avoid interferences or damages.

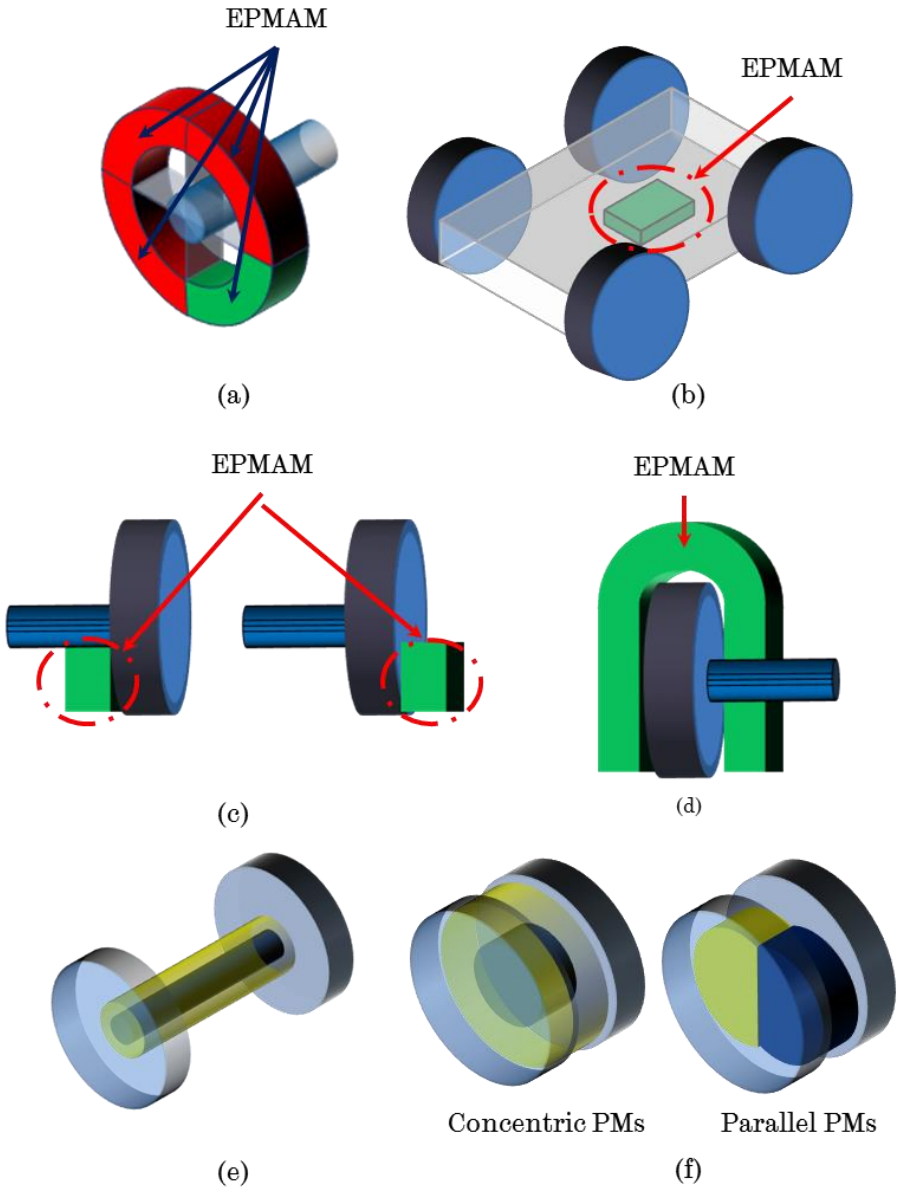

Figure 4.2: Possible wheeled locomotion mechanisms and EPMAM configurations. (a) Radially segmented wheel, each segment is an independent EPMAM module. (b) EPMAM integrated to the bottom of the WCMR body. (c) EPMAM placed at either side (left or right) of the wheel. (d) EPMAM integrated around the wheel. (e) EPMAM integrated in the shaft, with the wheels at each side acting as the keepers of the EPM. (f) EPMAM integrated inside of the wheel, with the PMs in a concentric and parallel array.

Discussion

Taking into account the advantages and disadvantages of each combination of locomotion and adhesion mechanism, it can be stated that there does not exist a superior configuration. The selection of the most appropriate combination depends on the scenario and tasks that the WCMR is intended to perform.

In terms of the present research, based in the advantages and disadvantages for the 5 possible configurations presented, the proposed design "4.2 Internal EPMAM" is selected as the most promising design for wheeled WCMR with EPMAM integrated. Figure 4.3 shows a chart with the proposed designs and in blue is highlighted the most promising design for a WCMR for ferric structures.

In order to verify that the viability of these alternative designs preliminary FEA simulations are perform for the cases 4.1.1, 4.1.2, 4.2.1 and 4.2.2 designs from chart in Figure 4.3.

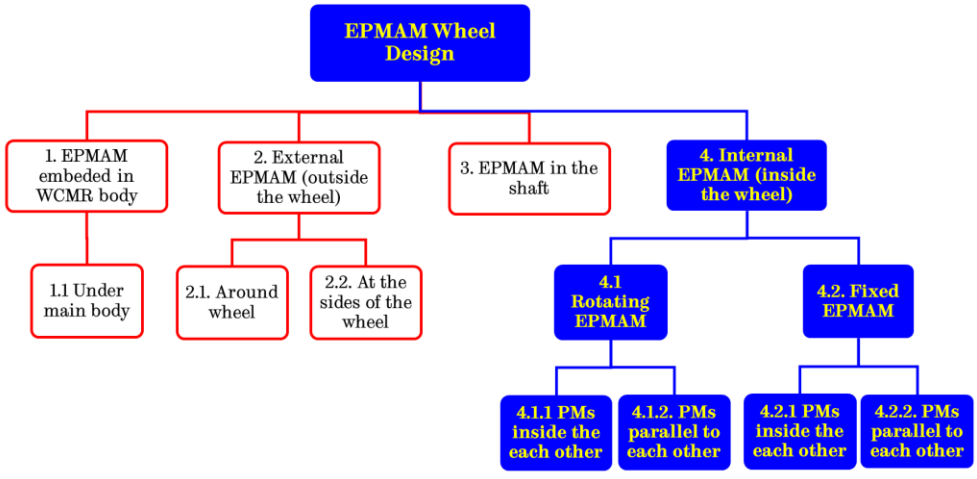

Figure 4.3: EPMAM wheel design selection chart. Some of the possible configurations of a wheeled locomotion mechanism with an EPMAM are presented. Blue colour shows the path followed in the selection of the final EPMAM to be integrated in a wheeled locomotion mechanism.

4.2.1. Preliminary simulations of the wheeled EPMAM design

Two main approaches can be used in this particular design: 1. PMs placed side by side, Figure 4.4(a); and 2. PMs placed inside the other Figure 4.4(b). In both cases, the main constraint is that the area of the magnetic poles of both magnets has to equivalent, as stated in Section 3.1.

In order to verify that the magnetic adhesion is not affected by the rotation of the proposed EPMAMs, simulations were performed of each of the two proposed designs. In addition, the effect of different sizes of the length of the PMs in the adhesion force is evaluated.

The dimensions and properties of components for each of the two proposed designs are:

- Both PMs (Alnico and NdFeB) are a half cylinder of 10mm diameter x 20mm thick and the steel disc keepers were 20mm diameter x 5mm thick.
- The NdFeB PM is a cylinder of 7mm diameter x 20mm thick; the Alnico PM a hollowed cylinder with 7mm inner diameter and 10mm outer diameter x 20mm thick; the steel disc keepers were 20mm diameter x 5mm thick.

In both cases the PMs used were Alnico5 and NdFeB 42, and the keepers made of mild steel. Simulations consisted of a complete revolution along the rotation axis of the wheel, with steps of 10 degrees. The “PercentError” setup for the convergence of the solver is set to one percent with 15% increments in the mesh refinement after each pass.

Results are shown in Figure 4.5, in the OFF and ON states for both designs. In the OFF state the adhesion force remains at 0kg for the full revolution. In the case of the ON state it is observed that for both proposed designs the fluctuation in the magnetic adhesion force is small, compared to the overall force, whilst the EPMAM is rotated. Hence, once the adhesion mechanism is on either ON or OFF state, it maintains its adhesive force

independently from the movement of the WCMR, until a different state or adhesive force is selected.

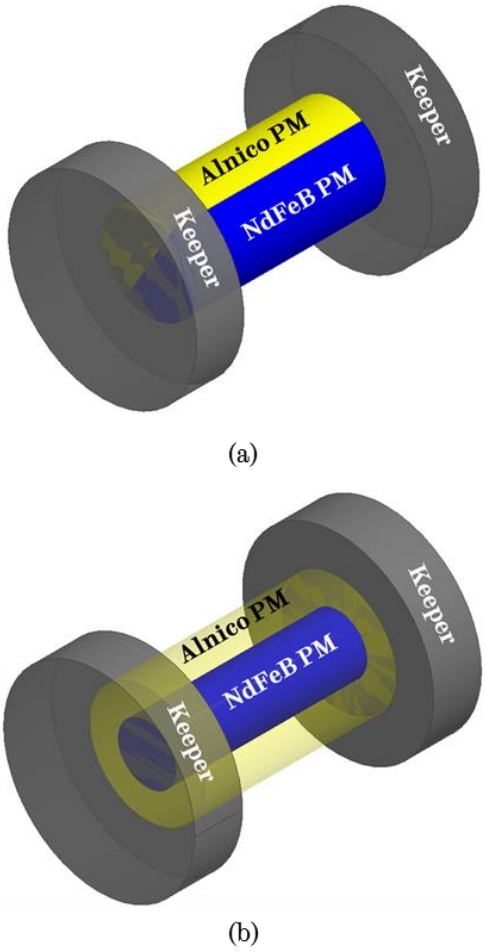

Figure 4.4: Proposed basic concept for an EPMAM for a wheeled locomotion mechanism. (a) Both half cylinder PMs are placed parallel to each other and capped at their magnetic poles with two steel discs as keepers. (b) The NdFeB PM is place inside the Alnico PM and capped with two steel discs at the magnetic pols of the PM. In both cases the PMs are magnetized along their length.

The second characteristic that is important to validate before further designs are explored is the effect of the length of PMs used in the EPMAM whilst the PMs' poles areas are kept unchanged. As mentioned in Section 3.2.3, in an EPM design the adhesive force can be maintained fixed as long as the area of the PM's poles remains unchanged. This means the length of the proposed design can be increased or decreased without affecting the final adhesive force.

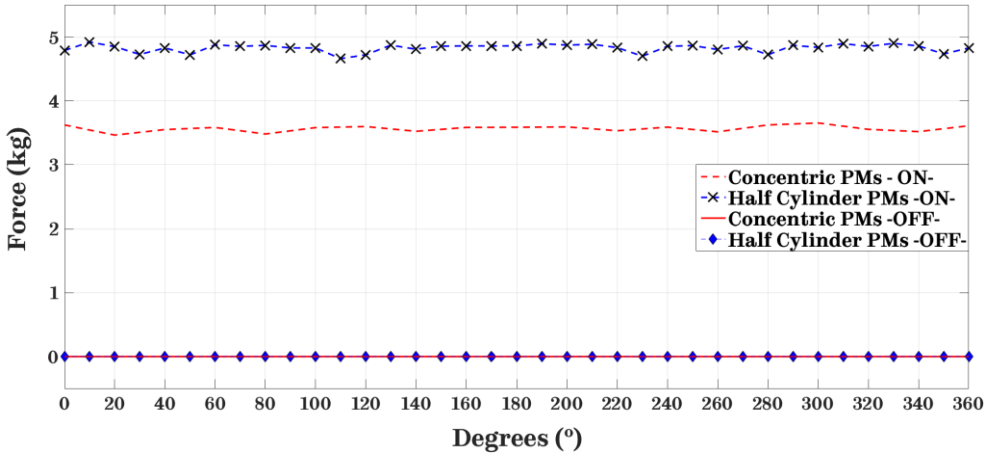

Figure 4.5: Magnetic adhesion force simulation results corresponding to the designs proposed in Figure 4.4. The graphs correspond to a full revolution from: half cylinder PMs design, blue graph; concentric PMs design, red graph. The variation in the adhesive force whilst the EPM is rotated can be considered small.

With the purpose of verifying whether this characteristic is true, a set of simulations are performed for different lengths of the initial design, proposed in Figure 4.4. The sizes of the EPMAM length ranges from 10mm to 30mm with increments of 2mm. The results are presented in Figure 4.6.

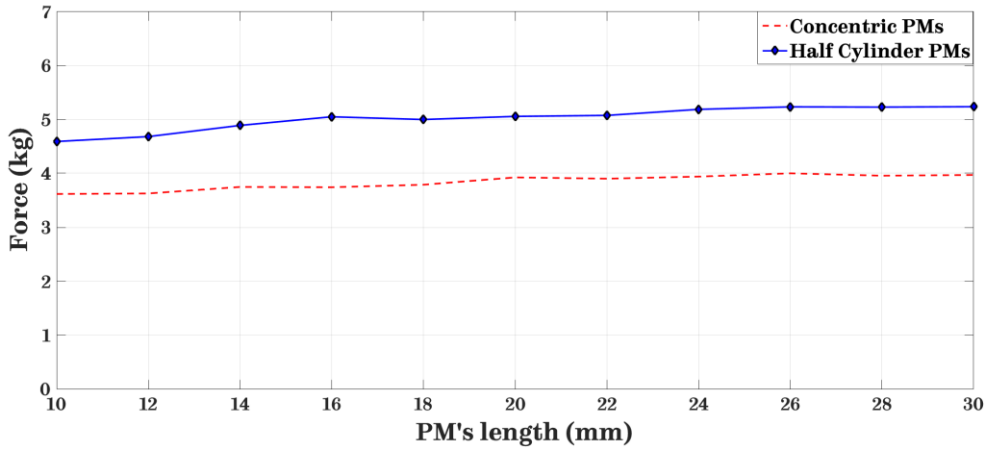

Figure 4.6: Effect on the adhesive force of different lengths of the EPMAM designs proposed in Figure 4.4. In both designs the influence of increasing or decreasing the length of the PMs can be considered relatively small, when compared to the maximum adhesive force.

From the simulation results presented, it was shown that the rotation of a wheel has small fluctuations in the adhesive force, but these variations

do not have a significant impact on the overall adhesive force. Also, it was shown that if the length of the PM varied from 10mm to 30mm (200%) the maximum adhesive force varies approximately 20%. This variation in the force, compared with variation in length, implies that it is possible to reduce the size of the wheel without considerably affecting the adhesive force by maintaining the area of the PM's poles unchanged.

Based on these results it is determined that the proposed EPMAM for a wheeled locomotion mechanism is a feasible approach, and gives confidence for further designs and real experimentation.

In order to corroborate that a wheeled locomotion mechanism with an integrated EPMAM is a practical solution for a WCMR for ferric structures, a device is constructed using the same off-the-shelf components employed in Section 3.3. In the next section the device is presented and validated by FEA simulations and corresponding experiments.

4.3. Validation of the proposed wheeled locomotion mechanism with EPMAM

With the purpose of fully validating the feasibility of the proposed wheeled locomotion mechanism, a physical model is assembled employing off-the-shelf components. The corresponding CAD model is also generated in order to be employed in the FEM simulations, Figure 4.7. The model consists of five pieces of 5mm diameter x 20mm thick Alnico5 PMs, 5 pieces of 5mm diameter x 20mm thick NdFeB N42 PMs, two 20mm diameter x 5mm thick mild steel discs and 176 turns of AWG 26 enamelled wire. The 176 turns correspond to 4 layers of 44 turns each, which are the turns of enamelled wire (0.454mm diameter) that fit in the length of the PMs.

$$Turns\ per\ layer = \frac{PM\ lenght}{wire\ diamenter} = \frac{20mm}{0.454mm} \approx 44$$

$$Total\ turns = (Turns\ per\ layer)(Number\ of\ layers) = (44)(4) = 176$$

By using the data provided in Table 3.2 for the AWG 26 wire the total resistance for coil can be determined:

$$R_{coil} = \pi N d \rho = \pi(176)(0.02m)\left(0.133\frac{\Omega}{m}\right) = 1.47\Omega$$

The equipment used for the experimental measurement of the forces, and applying the excitation to the windings is the same described in Section 3.3.2. ANSYS Maxwell 2015.2 is the software used for performing the FEA simulations.

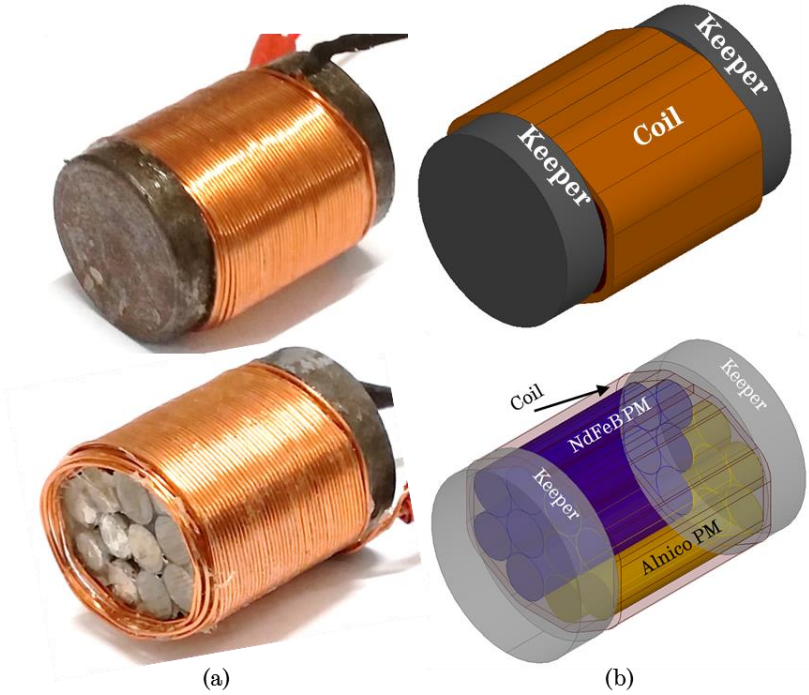

Figure 4.7: Proposed EPMAM for a wheeled locomotion mechanism composed of 5 Alnico5 PMs, 5 NdFeB N42 PMs, both coiled together with 176 turns of AWG 26 enamelled wire and topped with a 20mm diameter x 5mm thick mild steel disc at each of the PMs poles. (a) Physical design assembled with off-the-shelf components, for experimental purposes. (b) Matching CAD model for FEA simulations.

4.3.1. OFF and ON states validation

Similarly to Section 3.3, the OFF and ON states of the proposed design are explored to verify the EPMAM wheel behaves as expected. The OFF and ON state configuration setup has the same principles used in Section 3.3.3. Qualitative results from quantitative simulations for OFF and ON states are presented in Figure 4.8. The quantitative results from both, simulations and

experiments, are presented in Table 4.1. The experiments were repeated five times and the results averaged.

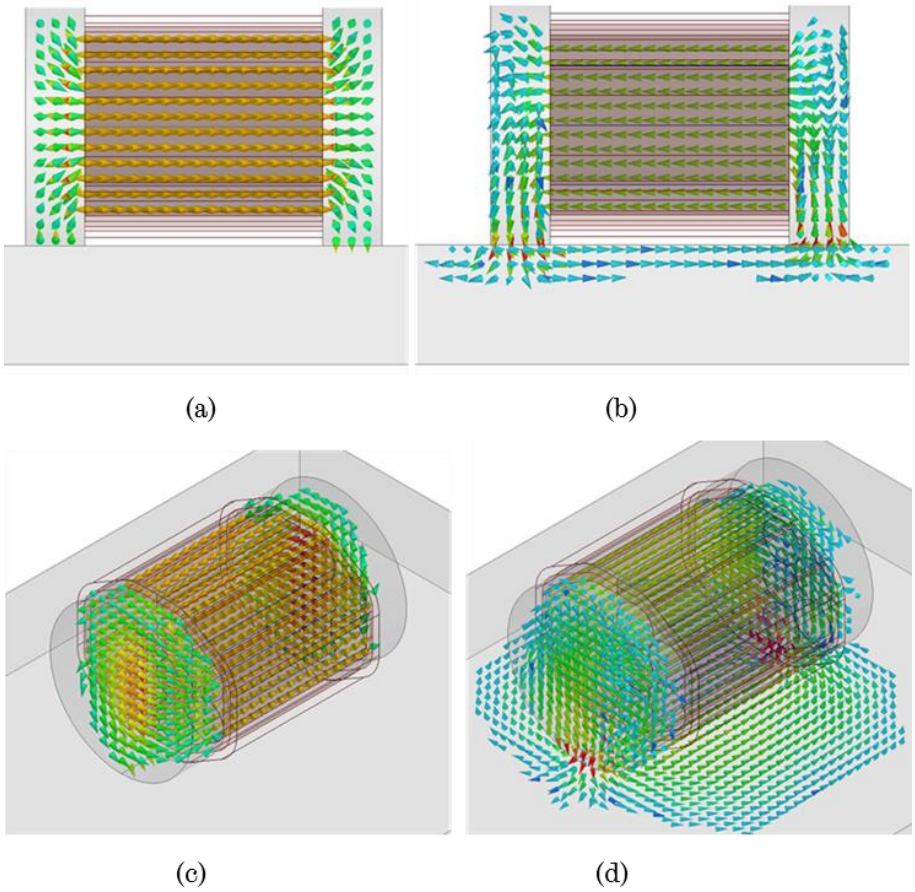

Figure 4.8: Simulation results from OFF and ON states: (a) OFF state, front view. (b) ON state, front view. (c) OFF state, isometric view. (d) ON state, isometric view. Arrows indicate flux lines flowing in a closed loop inside the EPMAM for the OFF state. For the ON state, magnetic flux lines are exerted from the poles to the target, producing the magnetic adhesion force.

For the OFF state, although the difference between experimental and simulation results is 251%, the overall magnitude is just 1g. For the ON state, percentage difference between experimental and simulation results is 5%, with maximum adhesive force of 4.26kg for the experimental results. This variation can be explained because of the factors that where not considered in the simulation, such as: temperature; rigidity of the load cell; and hysteresis loss in the PMs and keepers. The contribution of these factors, to the final result, is considered negligible compared to the increase in

computational power and simulation time required if they are considered in the initial setup.

Table 4.1: Comparison of the magnetic adhesive forces obtain through simulations and experiments for the proposed wheeled locomotion mechanism.

State	Simulation	Experimental	Difference	|%|
OFF	0.00037 kg	0.0013 kg	-0.00093 kg	251
ON	4.4845 kg	4.2602 kg	0.2243 kg	5

The total weight of the EPMAM wheel is 112g, which compared to the 4.26kg of adhesive force produced, demonstrates the potential of this novel adhesion mechanism.

4.3.2. Validation of the OFF-ON and ON-OFF switching, and variable magnetic adhesion

In order to verify the switching performance for the OFF-ON and ON-OFF as well as the specific adhesive for selection, similar procedures as in Section 3.3.4 are stablished and presented next.

For the case of the transition between states a 23V pulse is applied to the windings in order to generate the electric current needed to produce the magnetic field in the solenoid. From eq. 3.7 is possible to determine the current needed to produce the magnetic field intensity for demagnetizing the Alnico 5 PM:

$$I = \frac{H_c \boldsymbol{\ell}}{\boldsymbol{N}} = \frac{(48\frac{kA}{m})(0.02m)}{176} = 5.45A$$

In order to ensure the demagnetisation of the Alnico 5 PM recommended to apply magnetic field intensity three times bigger, hence the maximum current needed is 16A.

If the total resistance of the solenoid is 1.47Ω, by using the ohms law the voltage can be depicted:

$$V = IR = (16A)(1.47\Omega) = 23.52V$$

An incremental electric pulse is applied starting from 0.3ms until saturation of the Alnico 5 PM is reached. Once the Alnico5 PM reaches saturation no more final adhesive force, for the ON state, will be obtained. Similarly, for the OFF state, once Alnico5 PM reach saturation the final adhesive force is zero.

Results from simulations are presented in Figure 4.9(a) where it is observed that by increasing the length of the pulse the final adhesive force increases in a monotonic way. After the system reaches saturation, 2.0ms in this case, no increase in the magnetic force is generated. The maximum adhesive force for this design is 4.4845kg.

Correspondingly, the experimental results in Figure 4.9(b) have a comparable increasing behaviour, in a qualitative way, compared with the simulations. As it was mentioned in Section 3.3.4, several factors are involved in the experiments that were not considered in the simulations, to reduce computational and simulation time. These factors are: the spring behaviour of the load cell; the rigidity of the test bench (which also introduces transient oscillation when a pull is produced by the EPM on the load cell); and, temperature.

These factors introduce transient effects in the response behaviour of the experiments, which are present as oscillations in the measured data. In other to show the final state of the measurement after the transient effects have settle, a longer period of time (100ms) is presented in Figure 4.9(c).

From simulation results it is observed that for this particular design saturation is reached with an electric pulse of 2.0ms, Figure 4.9(a). As discussed in Section 3.3.4, longer pulses do not generate bigger final adhesive forces. On the contrary, pulses longer than 2.0ms only produce bigger peak adhesive force, whilst applied, and generate a temperature rise in the EPM due to the extra magnetic field generated. In the case of the experimental results it is observed that saturation is reach with a 4.5ms pulse, Figure 4.9(b) and (c).

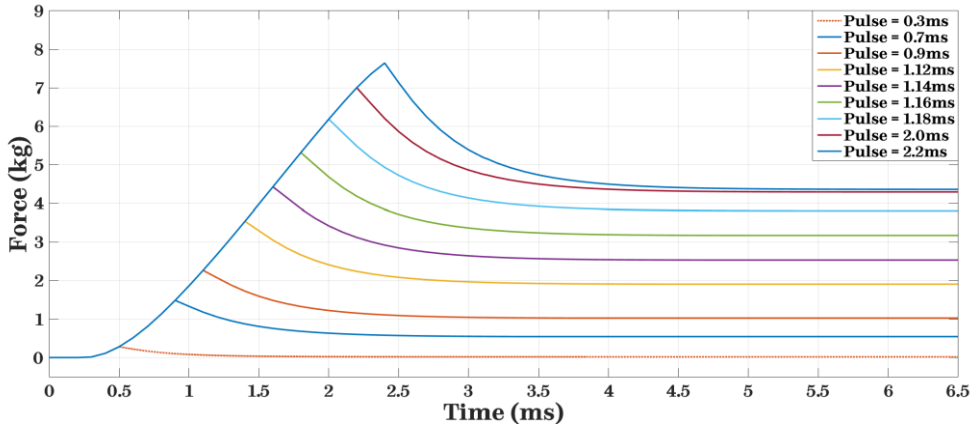

(a)

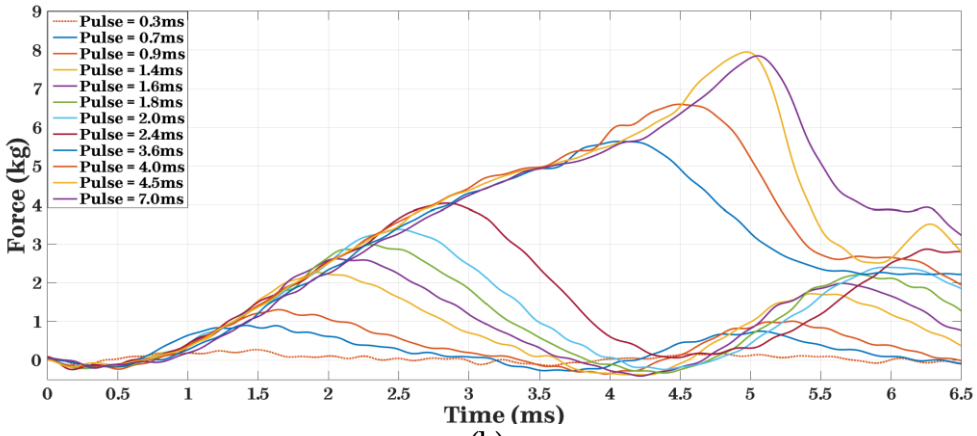

(b)

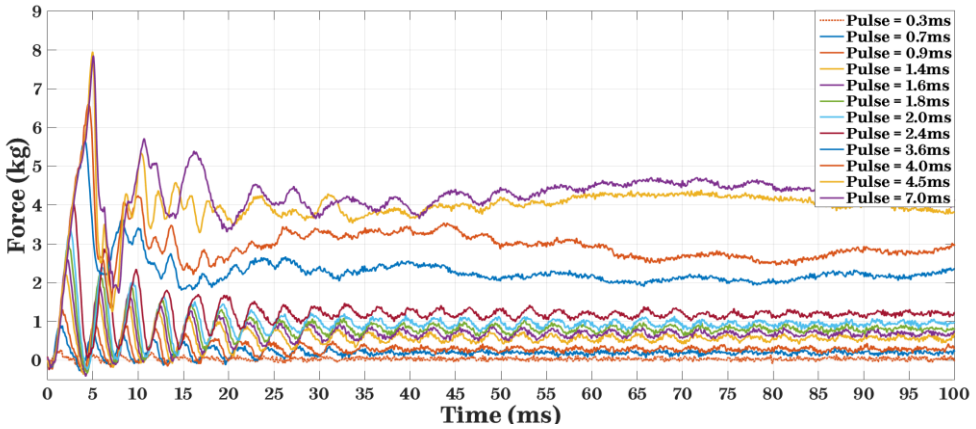

(c)

Figure 4.9: Final adhesive force vs increasing pulse lengths. (a) Simulation results, saturation is reached with 2.0ms pulse width. (b) Experiment results, saturation reached with a 4.5ms pulse width. (c) Experimental results presented for an extended period of time to show final magnetic force values after the transient effects of the load cell, test bench and holding components have settle down.

By comparing the simulation and experimental results, it is observed that the time to achieve the saturation in the experiment is approximately twice that for simulations. The reasons for this discrepancy are the factors not included in the simulations due to computational and simulation times. These factors have an impact in the final magnitude of the solenoid inductance, which determines how fast the current flowing through the windings reaches the maximum value.

To better appreciate how the force increases with the length of the pulse applied to the windings for the OFF-ON switching, in Figure 4.10 a comparison of the simulation and experimental data is presented.

The force values plotted correspond to the final value of the adhesive force, long after all the transient effects have settled. This final adhesive force value is obtained by taking the mean of the final 1.0ms for the case of the simulations data. For the case of the experimental measurements, the final 20ms from the data are taken and the mean is obtained, for minimizing the impact of the noise present in the measurements.

From the results obtained from both, experiments and simulations, a big discrepancy is observed regarding the length of the electrical pulse needed to reach maximum final adhesive force ($\approx 100\%$). This percent error may be enough to dismiss the EPM switching behaviour in a quantitative way. However, from the qualitative point of view both, experimental and simulation results present similar behaviours, they increase proportionally to the length of the electrical pulse applied, both reach comparable maximum adhesive force once the PM are driven to saturation. Furthermore, taking into account the time scale (ms), experimental results prove the viability of the EPMAM, because it only takes a few milliseconds to perform the switching.

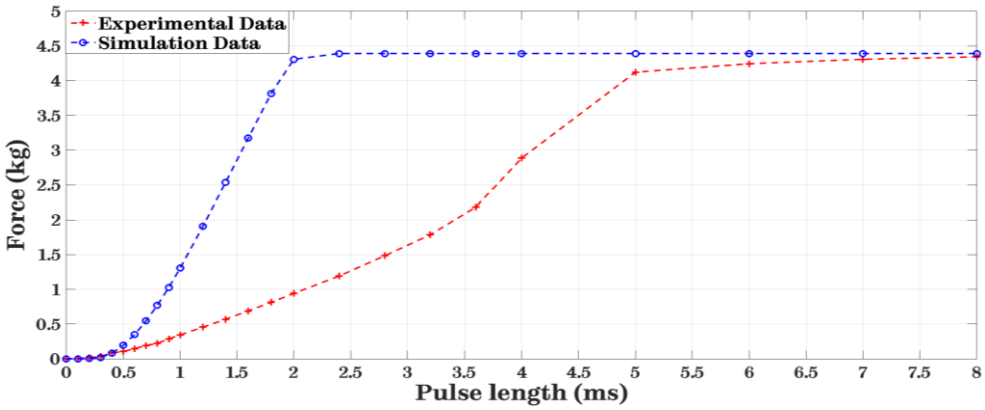

Figure 4.10: Comparison of magnetic force from experiments and simulation for increasing pulse lengths. Blue line represents the simulation results and red line the corresponding experimental results. The time for reaching the maximum force in the experiments is approximately three times the time obtained in simulations. This difference is due to factors that were not taken into account in the simulations, which have an effect in the inductance of the solenoid.

However, if the length of pulse needed to reach the maximum adhesive force, for a specific design, turns out to be significantly long, there ways exist to reduce this time:

- **Increasing the voltage applied to the windings.** As discussed in Section 3.1.1, a coil with a fixed number of turns has a defined resistance, if the voltage applied to the coil is increased the current flowing through the coil increases proportionally. However, increasing the magnitude of voltage is limited by the maximum voltage supported by the circuitry needed to control this voltage, as well as the capacity of the batteries. In both cases a high voltage reduces the time of the switching, however, the cost of the related circuitry and batteries can make it unpractical.

- **Reducing the resistance of the coil:** By reducing the resistance of the coil, the maximum current due to a fixed voltage is increased. One way to reduce the resistance of a solenoid is by increasing the diameter of the enamelled wire used in the solenoid and keeping the magnitude of the applied voltage fixed. The only constraint in this case is the size of the final EPM.

- **Reducing the coil inductance:** Another way is reducing the self-inductance the coil. By dividing a single coil into several different ones, while keeping the original number of turns among the coils, and connecting those coils in parallel, it is possible to reduce the total self-inductance. If two or more inductors are connected in parallel the equivalent inductance is less than any of the inductors connected in parallel, Eq. 4.1.

$$L_T = \frac{1}{\frac{1}{L_1}+\frac{1}{L_2}+\cdots\frac{1}{L_n}} \tag{4.1}$$

For this particular case, the motor driver used for controlling the switching has a maximum input voltage of 30V. Also, the available enamelled wire at that moment was an AWG 26 wire with 0.454mm diameter. For these reasons, it was chosen to split the coil in order to verify that it is possible to reduce the time to reach the maximum adhesive force by dividing the original coil, into two coils and connecting them in parallel. Experimental results are presented in Figure 4.11.

The experimental results show that, by splitting the original coil into two or more coils, it is possible to reduce the time for reaching the maximum final adhesive force without changing the input voltage, or gauge of the enamelled wired. The only condition is to keep the number turns of the original coil.

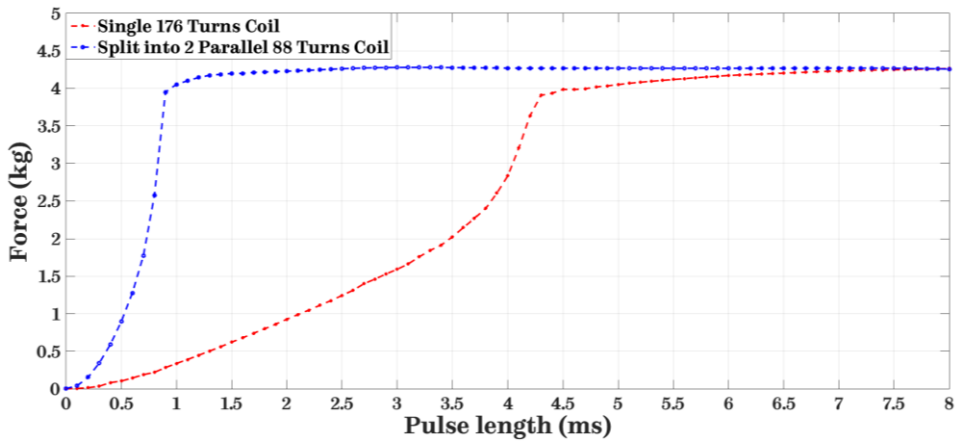

Figure 4.11: Comparison of the experimental results from the EPMAM wheel for both cases: 1. a single 176 turns coil, blue graph; and 2. coil split in two parallel coils of 88 turns each, red graph. By dividing the coil of the

EPM into two branches the time to reach the maximum adhesive force is reduced approximately four times.

Experimental and simulation results, performed with the initial wheel design with an EPMAM, have shown that such adhesion mechanism is feasible and has potential in the field of climbing robots for ferric structures.

A particular condition that must be taken into account in the design of any magnetic adhesion mechanism is the effect of air gaps or any non-ferric material between the EPMAM and the steel structure. Magnetic force decays in an exponential way, which means that in the presence of a small non-ferric obstacle, a thick coating or even corrosion, the adhesive force can be adversely impacted.

With the purpose of defining how the presence of an air gap or a non-ferric object impacts the adhesive force, the preliminary EPMAM wheel design is used in a set of FEA simulations and experiments. These consist on setting different air gaps (from 0.1mm to 3mm, with 0.1mm increments). Results from both, experiments and simulations, are presented in Figure 4.12.

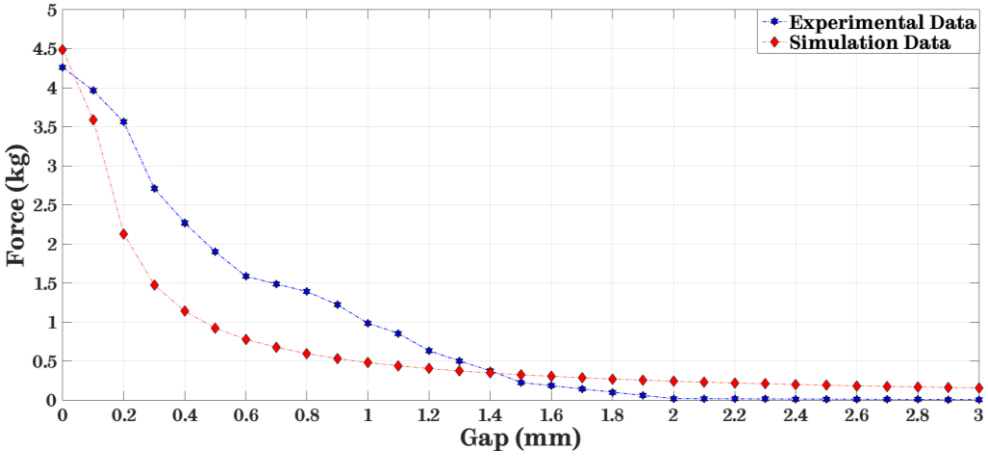

Figure 4.12: Adhesive force vs increasing gap, between EPMAM device and ferric surface. Red line corresponds to simulation data and blue line to experimental data. For both cases the magnetic adhesive force is reduced by 75% after 1.5mm.

For the particular case of the device proposed in Figure 4.7, simulation and experimental results show that the magnetic adhesive force decreases to approximately 75% with a 1.5mm gap. Although this side effect is the same for all magnetic adhesive mechanism, the particular capability of the EPMs of varying their adhesive force allows to design a stronger EPMAM to overcome this limitation, up to some degree.

4.4. Concluding remarks

In the present chapter, the main potential locomotion mechanisms were presented and the feasibility of being implemented in a WCMR was explored. A set of specific requirements, for the final WCMR, were established in order to allow the performance of certain tasks for a specific scenario. Based on the requirements, the wheeled locomotion mechanism was selected as the most appropriate for the inspection of large ferric structures. Next, possible configurations of the selected wheeled locomotion mechanism and the EPMAM were investigated, and the most suitable was chosen. Having selected the most suitable wheel-EPMAM combination a preliminary design was built, using off-the-shelf components. Correspondingly, a CAD model was drawn (for simulation purposes) with the aim to validate the viability of the design.

The validation of the design consisted of simulations and experiments for the OFF and ON states, the specific selection on a particular adhesive force value, and the impact of the presence of an air gap. Additionally, the possibility of reducing the total self-inductance of coil was proposed. It was suggested that by splitting the in two or more coil branches, without modifying the original number of turns, it was possible to reduce the time for reaching the maximum adhesive force. Results from the corresponding experiment demonstrated that it is a viable strategy.

The results obtained from the validation of the wheel-EPMAM design confirmed its feasibility and the potential for its use as a novel adhesion mechanism to be implemented in WCMR for ferric structures.

Starting from the results obtained in the present chapter, a more detailed analysis of the initial wheel-EPMAM design is presented in the next chapter and the most critical factors for the performance of adhesion mechanism are explored in detail.

Chapter 5

EPM Wheel Design

In Chapter 4 the most suitable locomotion mechanism, to be implemented in a WCMR for ferromagnetic structures, was explored. From the main locomotion mechanisms, wheeled locomotion was elected as the best option based on the predefined requisites. Next, different potential configurations for the integration of the locomotion mechanism and EPMAM were presented. Based on the advantages and disadvantages, for the specific scenario of performing over large ferromagnetic structures, each of the suggested configurations were examined and the most promising configuration was selected. In order to validate the chosen configuration a wheel EPM device was constructed, using off-the-shelf components. Additionally, a set of experiments and FEA simulations were presented. Finally, results from simulations and experiments showed that the proposed wheeled-EPMAM configuration is feasible.

In the present chapter the proposed wheeled-EPMAM configuration is examined in more detail using customised components in order to determine their impact on the performance of the EPMAM. The relevant parameters of each component is determined and varied to determine its influence in the final adhesive force. The final EPMAM wheel is intend to be implemented in an existing MR, which uses wheels with a diameter of 7cm.

Section 5.1 explores the influence of different magnitudes for the thickness of the steel keepers, the gauge of the enamelled wire and the presence of an air gap, and the most suitable is selected. Next, in Section 5.2 two configurations for the implementation of the EPMAM in an actual wheel are explored and the best is selected. In Section 5.3 a wheel design, using the customised selected components is proposed based on the cost and the manufacturability the components. Section 5.4 presents the final EPMAM device built with the customised components selected in the previous section and a set of simulations and experiments are presented in order to validate performance of the EPMAM. Finally, Section 5.6 presents the concluding remarks of the chapter.

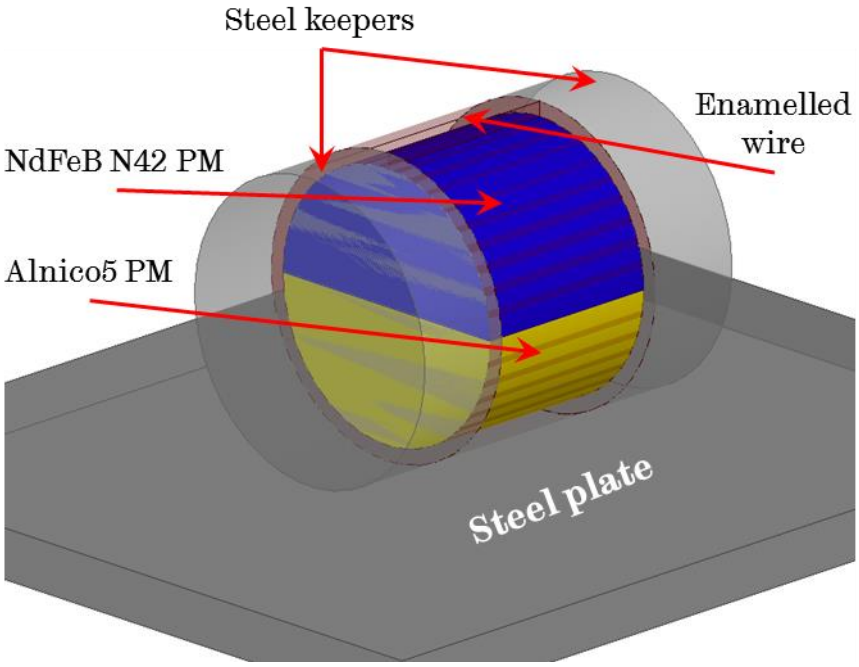

Figure 5.1: EPM wheel design using customised components. The design consists of two parallel PMs both coiled with enamelled wire and capped with two steel keepers.

5.1. Influence of the individual design components in the final adhesive force

In an EPM wheel, each component is contributes, to the optimum performance of the final device. With the purpose of determining the

influence of the main components, in addition to define the most appropriate size for a specific design, they are individually examined in the next sections. An initial design using customised components, that are feasible to be manufactured, is explored, Figure 5.1. The design consist of two parallel PMs (Alnico5 and NdFeB N48) both coiled with enamelled wire and caped with two steel keepers, with the same configuration of the design examined in Section 4.3.

In order to determine the impact of each of the components, FEA simulations are performed using different values of characteristic parameters, such as diameters and wire gauge, whilst keeping the rest unchanged. The setup for each simulation and the corresponding results are presented below. Section 5.1.1 examines the influence of the steel keepers' size on the magnetic adhesive force. In Section 5.1.2, the effect of different enamelled wire gauges, in the EPM wheel adhesion performance, is explored. Finally, Section 5.1.3 explores the impact of an air gap, or any non-ferric material, between the EPM wheel and the surface on which it is adhered.

5.1.1. Steel keepers

The size of the steel keepers is important, since they are the path to redirect and focus the magnetic flux lines to a specific target. Small keepers saturate with low magnetic field densities, thus the just a small part of the magnetic field lines is focused to the specific area where the magnetic attraction is needed. On the other hand, although big keepers, are capable of taking the magnetic flux lines without saturation, might become too heavy. Thus, reducing the maximum net adhesive force.

Keeper thickness

With the aim of defining how the maximum adhesive force is affected by the thickness of the steel keepers, FEA simulations are performed for different thicknesses. From the design shown in Figure 5.1, the thickness, along the rotation axis, is increased in the range from 2.5mm to 20mm, with

1mm increments. In Figure 5.2 the initial (2.5mm), intermediate (10mm) and final (20mm) models are presented.

Results from the FEA simulations for the different steel keepers' thicknesses are presented in Figure 5.3. It can be observed that increasing the thickness of the keepers increases the maximum adhesive force. This is due to the increasing volume that can contain more magnetic flux lines.

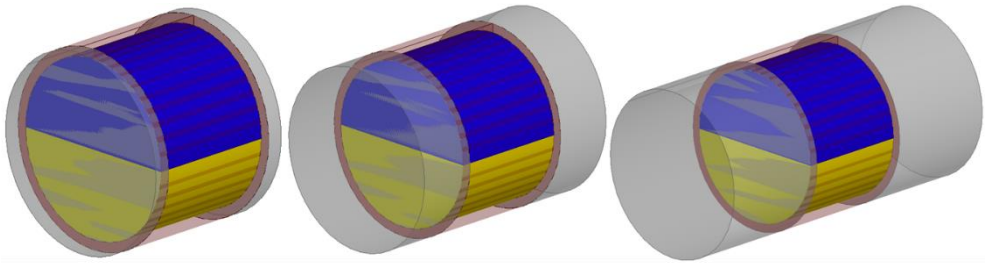

Figure 5.2: EPM wheel designs for different steel keepers' thickness. (a) Initial 2.5mm thickness. (b) Intermediate 10mm thickness. (c) Maximum 20mm thickness.

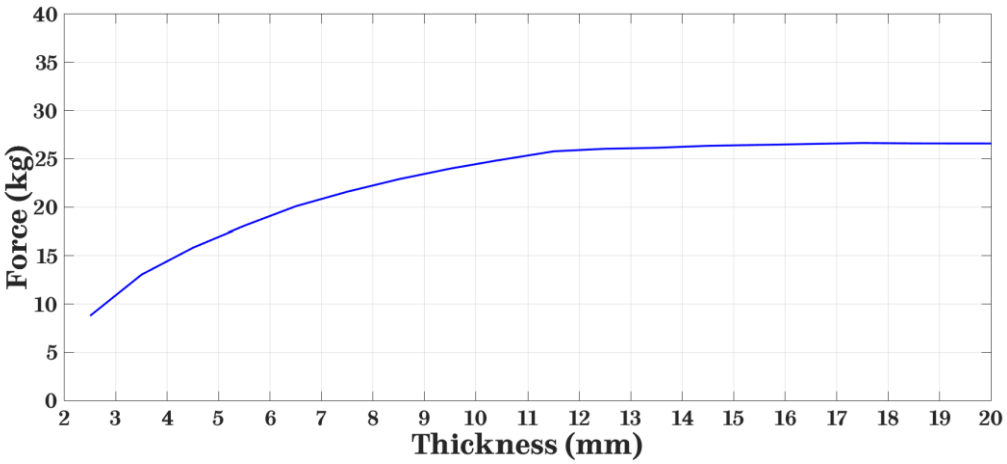

Figure 5.3: Force vs steel keepers' thickness. The adhesive force is increased with increasing keepers' thickness.

In order to select the most suitable keeper other factors must be considered, such as the final size of the wheel and weight. For the specific design of a wheel with a diameter of 70mm and ≈70mm in thickness, the 10mm keeper is selected. A thicker keeper, increases the final wheel size and weight beyond acceptable limits. For instance, a 15mm thick keeper

increases in 50% its size and weight, however its maximum possible adhesive force is increased by only 12.76%.

5.1.2. Enamelled wire gauge

A crucial part in the design of an EPM is the appropriate selection of the enamelled wire gauge. As mentioned in Section 3.3.1, diameter, resistance and weight depend on the wire gauge. A small wire gauge number indicates a low resistance, and a large diameter, inversely, bigger wire gauges refer to a wire with higher resistance, and smaller diameter. Table 3.2 shows the seven wire gauges considered for the proposed EPM wheel design.

With the purpose of exploring the influence of each wire gauge, the design presented in Figure 5.1 is simulated for each of the wire gauge of Table 3.2. Simulations are performed for a 0 - 60v range for each of the wire gauges in order to determine the how the final adhesive force is influenced. Results are presented in Figure 5.4.

Results show that, in order to achieve the maximum possible adhesive force, bigger voltages are needed for enamelled wires with smaller resistance. In order to select the most suitable wire gauge the three main factors, presented in Table 3.2, must be considered. Bigger wire gauges have smaller diameters and are lighter. However, their resistance increases, which means that only smaller electric currents are allowed to flow through the wire. Consequently, the external magnetic field generated by the solenoid will not have the sufficient strength to fully magnetise and demagnetise the Alnico PM.

On the other hand, smaller wire gauges have lower resistances that allow bigger electric currents. Hence, bigger magnetic fields can be produced when used in a solenoid. However, as seen in Table 3.2, the size and weight increases considerably, which means a bigger and heavier solenoid. Based on the FEA simulation results, from the seven proposed enamelled wire gauges. Additionally taking into account the maximum voltage allowed by the motor

driver (30v), which is going to control the direction and length of the electric pulse, AWG 26 is selected as the most feasible.

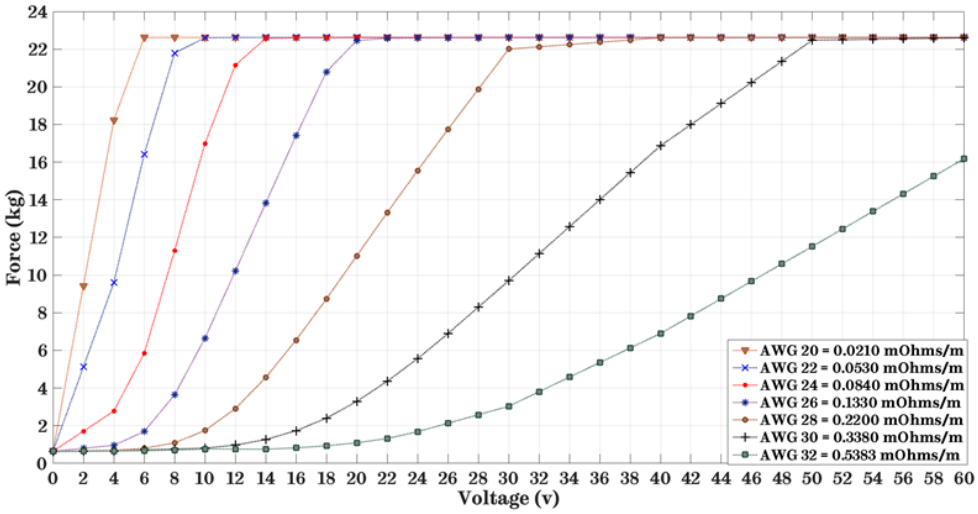

(a)

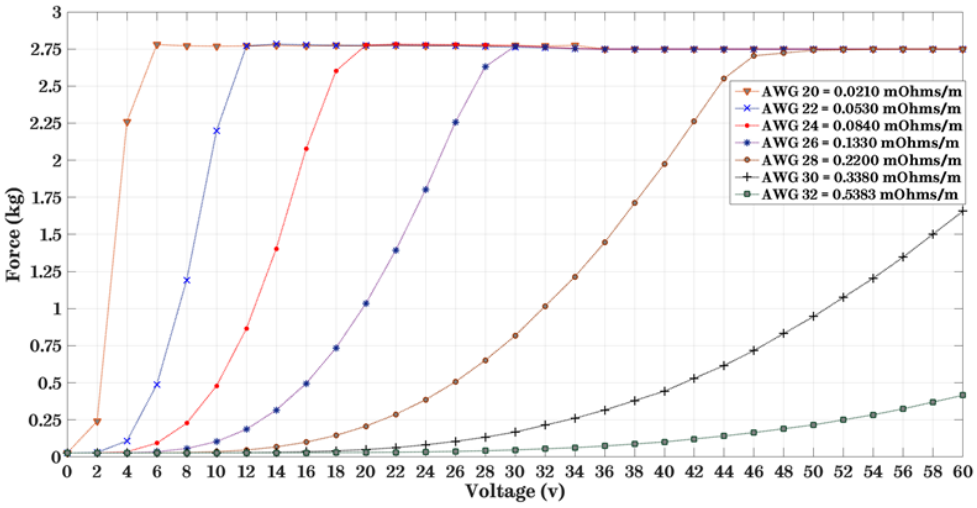

(b)

Figure 5.4: Force vs voltage for each of the enamelled wire gauges presented in Table 3.2. (a) No gap between EPM wheel and target steel plate. (b) 2.5mm gap between EPM wheel and target plate. It is observed that as the resistance of the wire increases, the voltage needed to achieve the maximum possible adhesive force increases.

5.1.3. Gap between EPM device and adhesion surface

Another crucial part in the design of any magnetic adhesion mechanism is the impact of an air gap, or any non-ferric material, between

the adhesion mechanism and the surface where it is adhered. Gaps must be considered, because in most of the situations there are factors that will not allow direct contact between the device and the surface. Things like corrosion, steel coatings, grease or dirt are some of the most common factors that do not allow a direct contact. Therefore, the maximum possible adhesive force is not achieved in most of the cases.

With the purpose of examining this effect, an increasing air gap between the proposed design and the target steel plate gas simulated, Figure 5.5. The initial magnitude of the gap is 0mm, and is increased in 0.01mm intervals, up to 5.0mm. Results from the corresponding FEA simulation are presented in Figure 5.6.

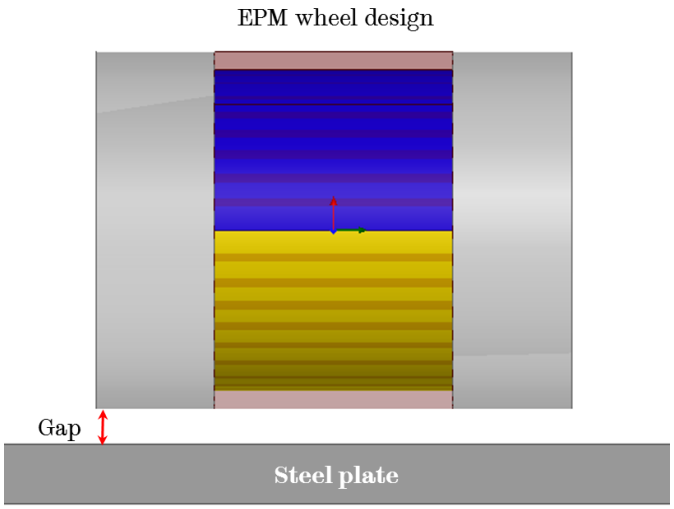

Figure 5.5: Gap between EPM wheel device and target steel plate.

FEA simulations results show that the magnetic adhesive force decreases dramatically with small gaps. For this design, although the initial magnetic adhesion can be considered high (24.58kg), it decreases in 90%, to 3.12kg with a 1.0mm air gap between the EPM wheel and the target (steel plate).

Furthermore, in order to get a better understanding of the influence of an air gap, a set of simulations are presented in Figure 5.7. In these FEA simulations, the presence of different gaps for each of the keeper's thickness, examined in Section 5.1.1, are explored in Figure 5.7.

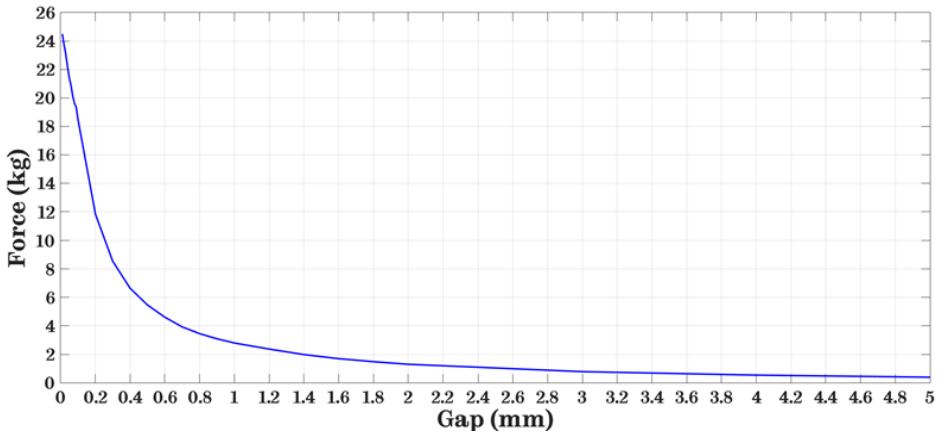

Figure 5.6: Force vs increasing gap between the EPM wheel device and the target steel plate.

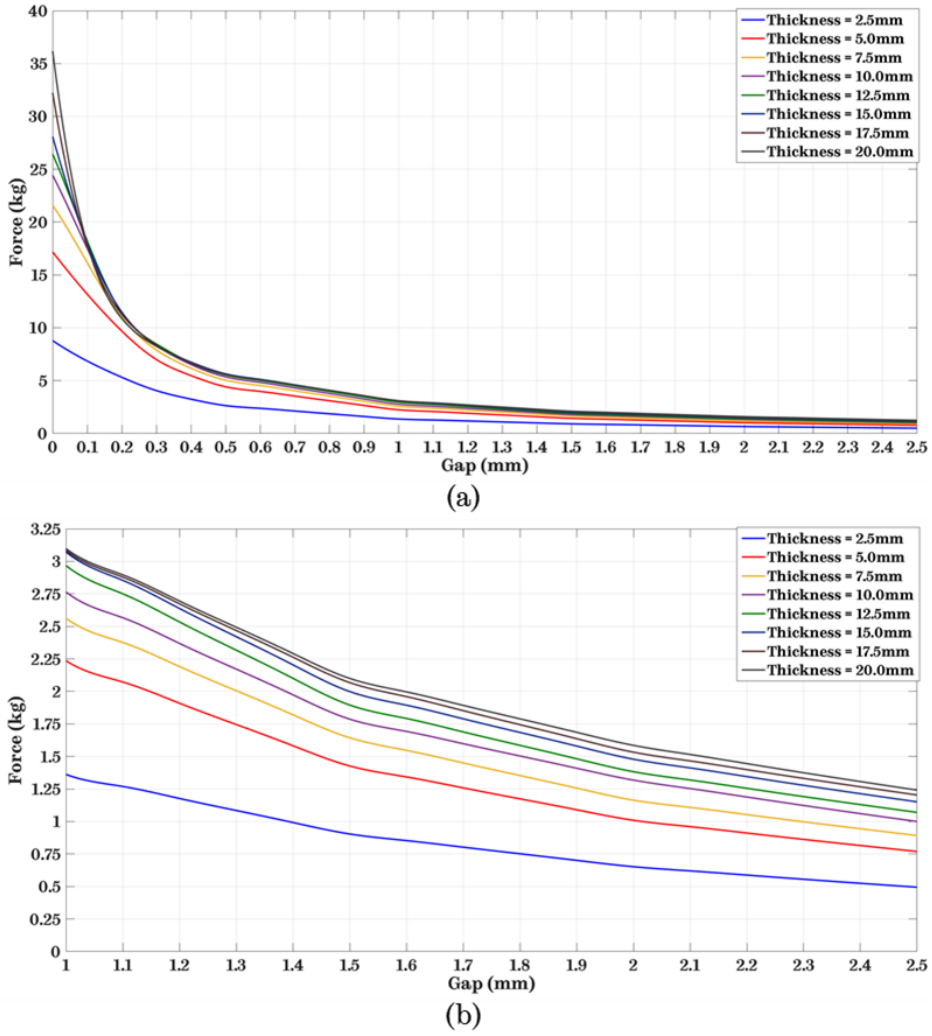

Figure 5.7: Force vs gaps for different steel keepers' thickness. Steel keepers' thickness ranges from 2.5mm to 20mm with 2.5mm increments. (a) Results from gaps ranging from 0mm to 2.5mm. (b) Gaps range from 1mm to 2.5mm.

Additionally, FEA simulations are performed exploring the influence of the keepers' thickness for different air gaps. Results are presented in Figure 5.8. It can be observed that the main factor that impacts the final adhesive force, is the length of the gap for keepers with thickness greater than 10mm. From this results, also it is verified that a 10mm thick keeper is the most appropriate for the case of the present design.

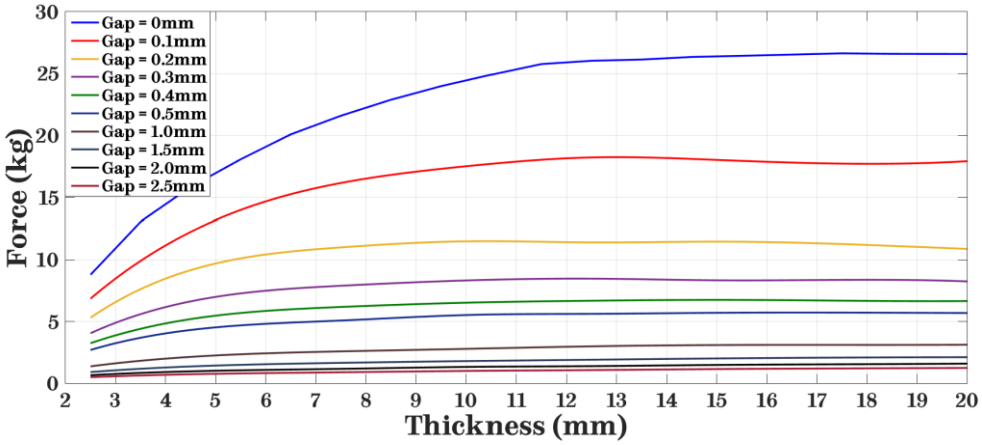

Figure 5.8: Force vs thickness for air gaps, ranging from 0mm to 2.5mm. These results confirm that the 10mm thick keeper is the appropriate selection for the proposed design.

5.2. Configuration of the EPMAM into the wheel

An important consideration on the integration of the EPMAM and the wheel design is how the electric pulse is going to be supplied to the EPMAM as the wheel rotates. Two possible solutions for this configuration are discussed next, in order to select the most appropriate method of supplying the power energy to the solenoid windings.

5.2.1. Rotating EPMAM

On possible solution is to fully integrate the EPMAM with the wheel, or let the EPMAM be the wheel itself. For this configuration the electric pulse needs to be supplied, from the static MR frame to the rotating wheel, with the help of carbon brushes. However, carbon brushes have several disadvantages when employed in small devices:

- Contact resistance is high.
- Considerable voltage drop.
- Production of sparks, which can be potentially dangerous in some scenarios.
- Brush holders and commutators are needed, resulting in a bigger wheel size.
- Required to be replaced once the useful life is reached, or get damaged.

5.2.2. Static EPMAM

An alternative solution is to maintain the EPMAM fixed, with respect to the MR frame, and using gears and bearings to allow the rotation of the wheel. The main advantage of this approach is that the can be connected directly to the power source. Additionally, by maintaining the EPMAM fixed the volume of the keepers can be reduced. Considering results from FEA simulations, shown in Figure 5.9, it can be observed that the upper part and outer region of the keeps, do not contribute to concentring the magnetic flux lines. On the contrary, these areas disperse the magnetic flux and add dead weight to the final device. Eliminating these portions of the keepers' results in the design shown in Figure 5.10.

Results from the corresponding FEA simulations for the optimized design, Figure 5.10, are presented in Figure 5.11. It is observed that magnetic flux is more evenly distributed throughout the keepers' volume. Furthermore, the quantitative results show that the maximum possible adhesive force is increased in by 55% from 25.1kg to 38.76kg. The reason for the increase in the adhesive force is that the magnetic flux lines, which were dispersed in the first design, are now concentrated and focused to the target plate by the optimized shape of the keepers. This denser and concentrated magnetic flux produces a stronger magnetic adhesive force.

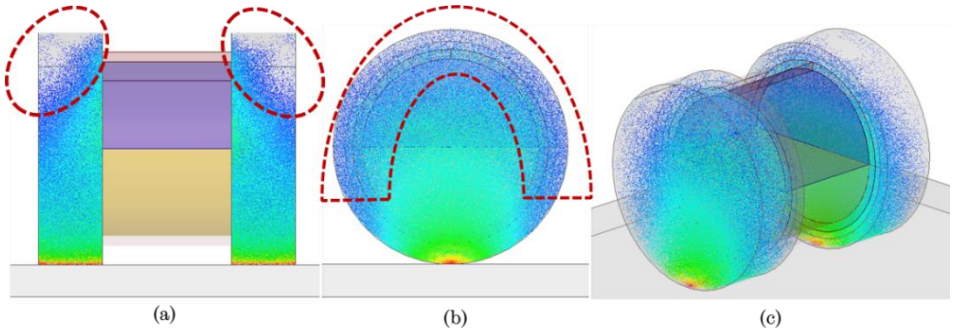

Figure 5.9: Concentration of the magnetic flux inside of the keepers, for the case of a rotating EPMAM design. Areas within the red dashed lines show the portions of the keepers that reduce the efficiency of the EPAM by dispersing the magnetic flux and adding dead weight. (a) Front view. (b) Side view. (c) Isometric view.

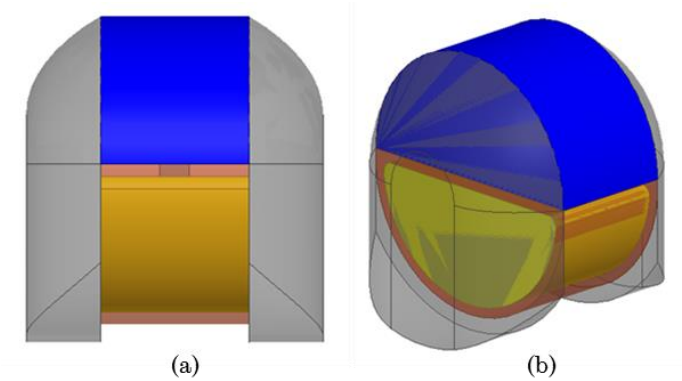

Figure 5.10: EPMAM with optimized steel keepers for the case of a fixed EPMAM – wheel configuration. The portions that reduce the efficiency of the EPMAM from the previous design, Figure 5.9, are removed. (a) Front view. (b) Isometric view.

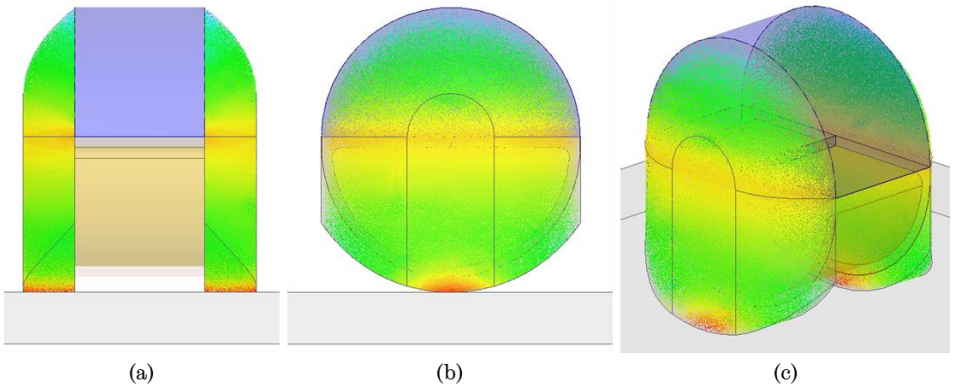

Figure 5.11: Concentration of the magnetic flux inside of the keepers, for the case of the improved EPMAM design. By removing the portions of the original design, which dispersed the magnetic flux, a denser and focused magnetic field is generated. (a) Front view. (b) Side view. (c) Isometric view.

5.3. Customised EPMAM design for manufacturing purposes

Based on the advantages and disadvantages of the both, rotating and static approaches, and taking into account the results from the FEA simulations, the static EPMAM configurations is selected. The assembly for the EPM wheel with EPMAM is presented in Figure 5.12. The fixed EPMAM and the rotating outer part of the wheel are connected using bearings.

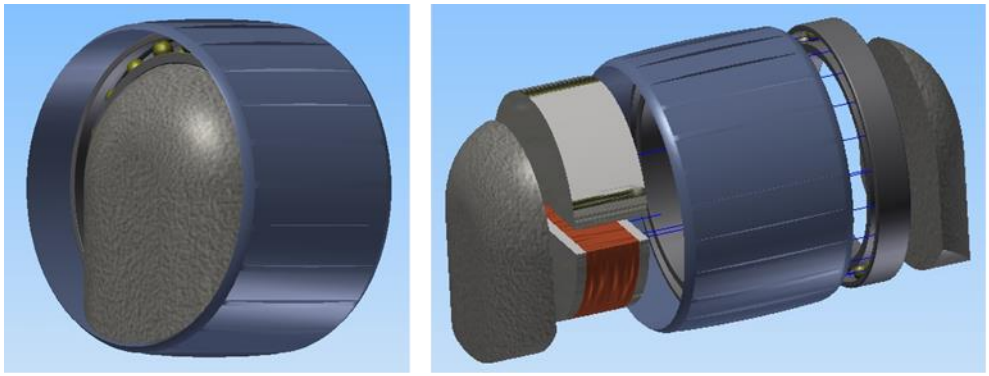

Figure 5.12: Wheel design with a static EPMAM for manufacturing purposes. (a) Isometric view. (b) Exploded view, for showing the internal components of the EPMAM.

5.3.1. Manufacturability of the EPMAM components

In order to build the customised EPM wheel different companies have been consulted, to assess whether the manufacturing of the components is feasible, in addition to the costs. All of them agree that the manufacturability of the internal EPMAM components is feasible, however the costs are increased by the presence of round elements and chamfer cuts manufacturing times are also heightened.

In the case of the PMs, the simplest design a half cylinder shape, with magnetisation along the thickness is chosen. Although, initially different shapes and magnetisations were considered, the manufacturing cost of the quantities need was out of the current budget. For this reason, the initial design was chosen to be manufactured.

For the case of the steel keepers the cost for manufacturing the design presented in Figure 5.10 and Figure 5.11, was also out of budget. For this reason a simplified design is used for the keepers shape, Figure 5.13.

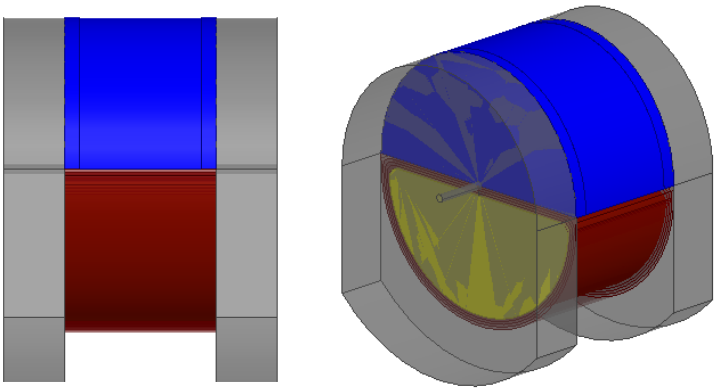

Figure 5.13: Final EPMAM customised components including a simplified keepers' design.

In the case of the windings around the Alnico5 PM, the 480 turns are distributed in eight layers of 60 turns each. As shown in Table 3.2, AWG 26 enamelled wire has a resistance of 0.133mΩ/m, which results in 3.9Ω for the 480 turns around the Alnico PM. The magnitude of the resulting resistance along with the 23V supplied by the LiPo battery only produced a 5.89A current. This current was not enough to re-magnetise the Alnico5 PM. However, as discussed in Section 4.3.2, it is possible to reduce the total inductance and resistance of a fixed number of turns in a coil by splitting the number turns into branches. For this particular case, the 480 turns, are split into 4 branches of two layers of 60 turns, in each layer. By doing this, the total resistance is reduced to 0.256Ω.

With the purpose of verifying the performance of the EPMAM shown in Figure 5.13, FEA simulations are performed. Results are presented in Figure 5.14 for two scenarios: 1. Gap=0mm; and 2. Gap=2.5mm.

From the results, it is observed that the maximum possible adhesive force is reached with a 50A current. Additionally, it is observed that the maximum adhesive force is 21.72kg and 7.22kg for the 0mm and 2.5mm gaps,

respectively. The later, although decreased considerably, is an acceptable adhesive force for small WCMR, which normally weigh less than 4kg.

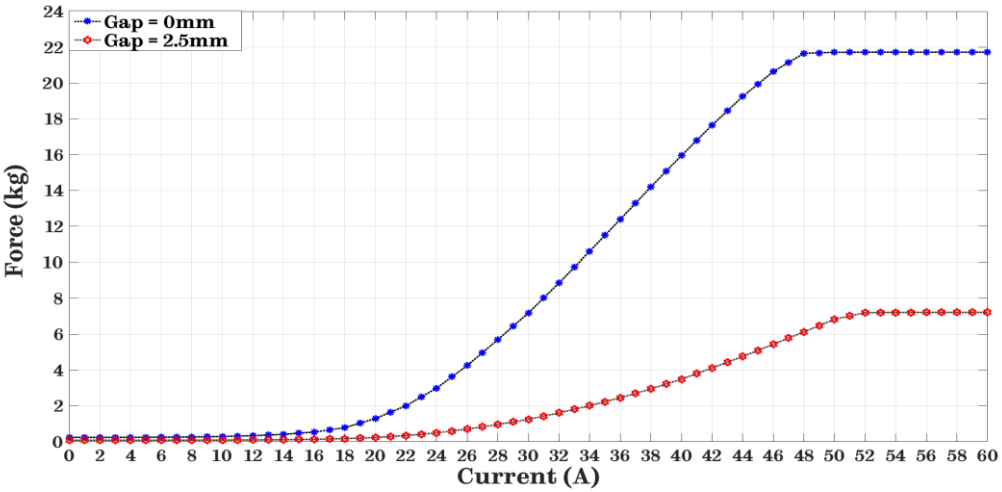

Figure 5.14: Force vs current flowing through the coil. The maximum possible adhesive forces is reach with a 50A current. Blue dot line shows the simulation results for the case of 0mm gap. Red dot line shows the simulation results for a 2.5mm gap.

Customised components

Once the final design is selected, the components are manufactured in order to build a physical EPMAM to be integrated in a wheel design. Figure 5.15 shows the customised components: half cylinder Alnico5 PM with 12mm radius, coiled with AWG 26 enamelled wire, Figure 5.15(a); half cylinder Neodymium PM, with 12.5mm radius, Figure 5.15(b); mild steel keeper, Figure 5.15(c).

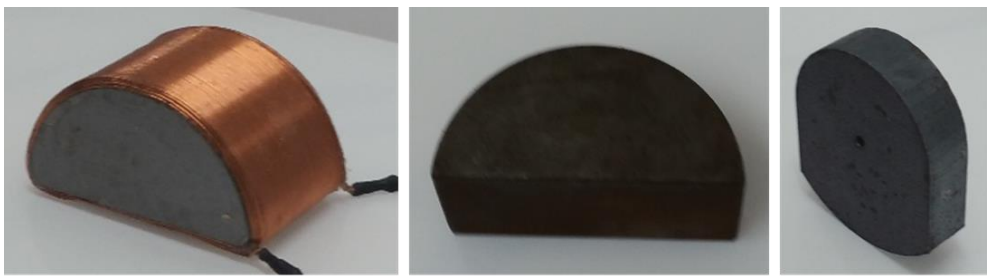

(a) (b) (c)

Figure 5.15: EPAM customised and manufactured components. (a) Anilco5 PM, coiled with 424 turns of AWG 26 enamelled wire. (b) Neodymium N48 PM. (c) Steel keeper.

Once the EPMAM components are manufactured and the windings around the Alnico5 coiled, the actual EPMAM is built and the corresponding CAD model drawn Figure 5.16.

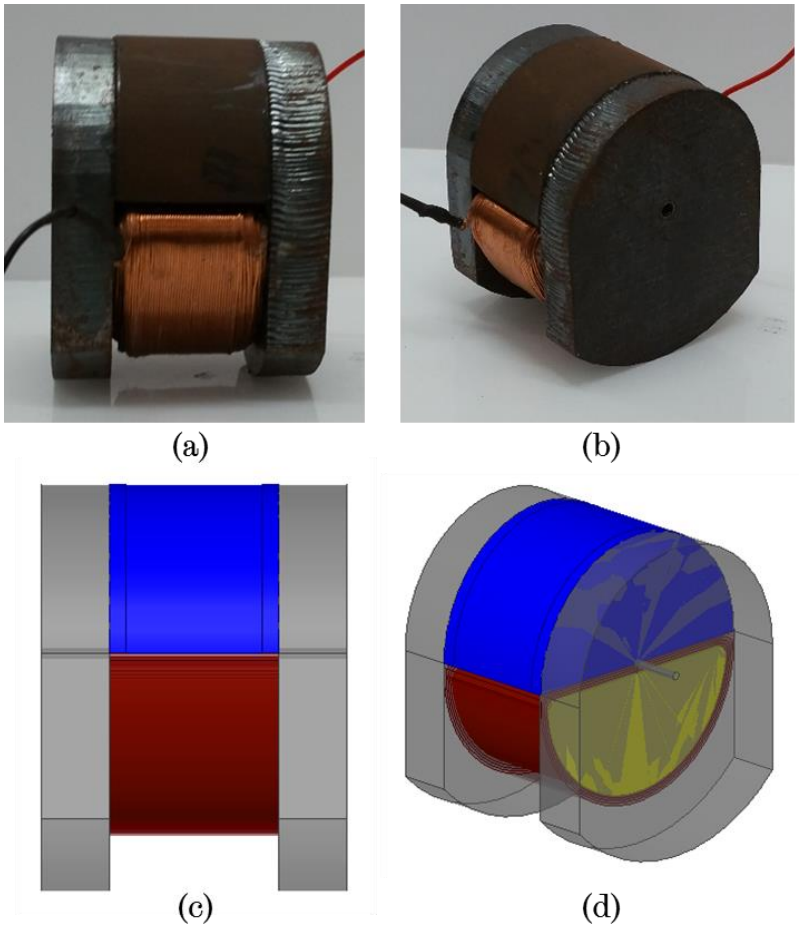

Figure 5.16: EPMAM device built with customasied components. Physical design (a) front view and (b) isometric view. CAD model (c) front view and (d) isometric view.

5.4. Simulation and experimental results from the customised EPMAM

After the EPMAM device is built, the next step is to validate the FEA simulation results presented in Figure 5.14. Using the equipment and setup presented in Section 3.3.2, the corresponding experiments are performed in order to measure the adhesive force produced by applying different electric pulses. Results from the experiments are presented in Figure 5.17 and Figure 5.18.

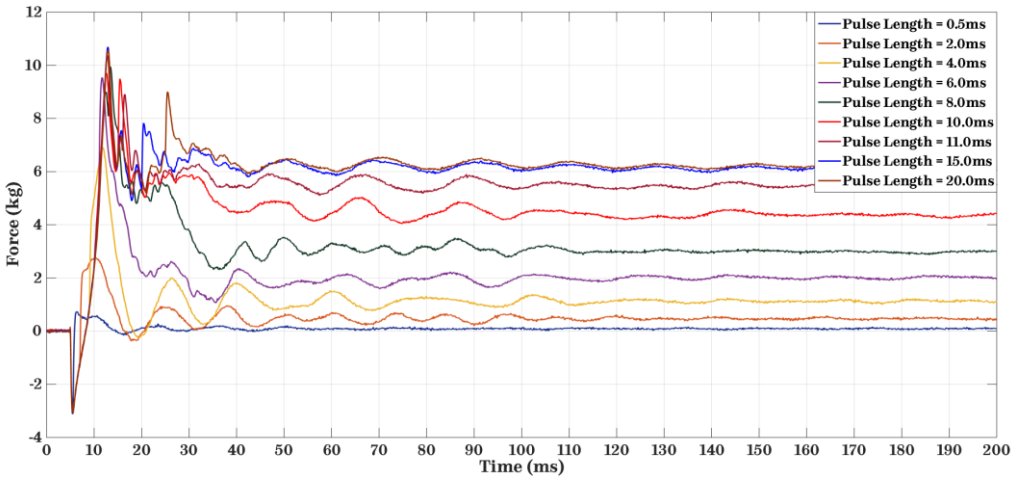

Figure 5.17: Experimental results from different electric pulses. Graphs presented correspond to the resulting OFF-ON transition for different electric pulse lenghts.

For the case of the OFF-ON switching different pulse lengths are applied to the windings. The transient response, shown in Figure 5.1, presents a similar behaviour to the discussed in Section 3.3.4. From these results is observed that the maximum adhesive force is reached with 15ms electric pulse.

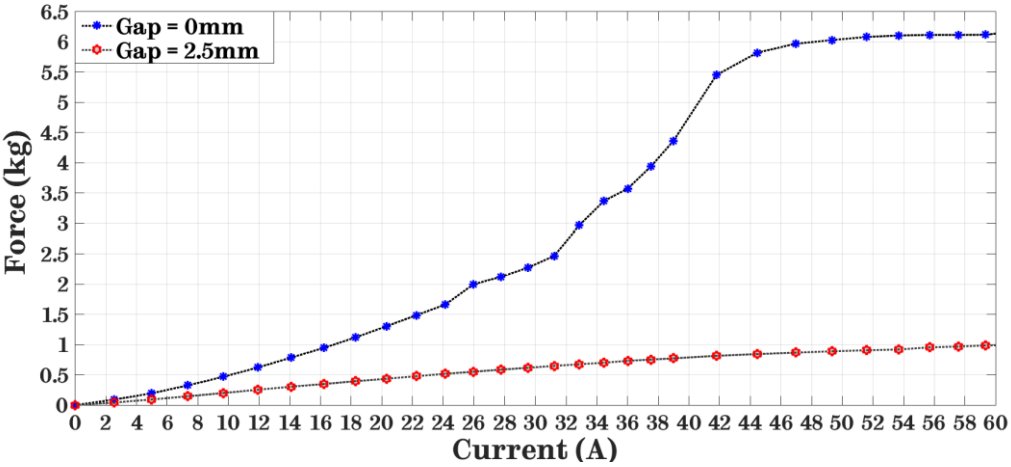

Figure 5.18: Force vs current obtained by experimental mesaurments. Blue dot line shows the experimental mesaurments for the case of 0mm gap. Red dot line shows the experimental mesaurments for a 2.5mm gap.

Figure 5.18 presents the results from an increasing electric pulse that range from 0 to 20ms, after the initial transient effects from the pulse have settled. After comparing the results from the simulations presented in

Figure 5.14 with the experimental results, a big discrepancy in the maximum possible adhesive forces is observed.

Table 5.1: Comparison of simulation and experimental results for the customised EPMAM.

Gap	**Simulation results (kg)**	**Experimental results (kg)**	**Difference %**
0 mm	21.72	6.12	255
2.5 mm	7.22	1.56	363

Although experimental measurements show a considerable deviation from the simulation results, which might dismiss the feasibility of the proposed EPMAM, a search for possible causes is performed.

Due to the higher magnetic fields produced by bigger PMs and stronger solenoid, compared to the ones employed for the concept validation in Chapters 3 and 4, the non-linear magnetic characteristics of the EPMAM components must be taken into account. It is found out that a stronger magnetic field drives the mild steel of the keepers to saturation, which did not happen in the concept validation experiments.

Moreover, magnetic characterises of mild structural steel vary considerably from the chemical composition of each steel type. When produced for structural purposes, mild steel is not magnetically characterised when fabricated. However, MagWeb[6] produce the magnetic BH curves for different types of steel. After analysing the mild steel BH curve data provided by MagWeb, and the generic BH curve from ANSYS Maxwell, a difference is observed. The mild steel saturation points from MagWeb and Maxwell are 2.085Teslas and 1.72Teslas respectably. A lower magnetic BH saturation point means a lower magnetic flux flowing through the material after reaching saturation.

[6] http://magweb.us/free-bh-curves/

Additionally, in order to obtain a more accurate simulation, the actual BH curve for the PM were requested to Arnold Magnetic Technologies[7], which is the manufacturer of the PM. Using the data from the more accurate magnetic BH curves for the components of the EPMAM simulations are performed again. Results are presented in Figure 5.19 and a comparison is presented in Table 5.2. The experiments were repeated five times and the results averaged.

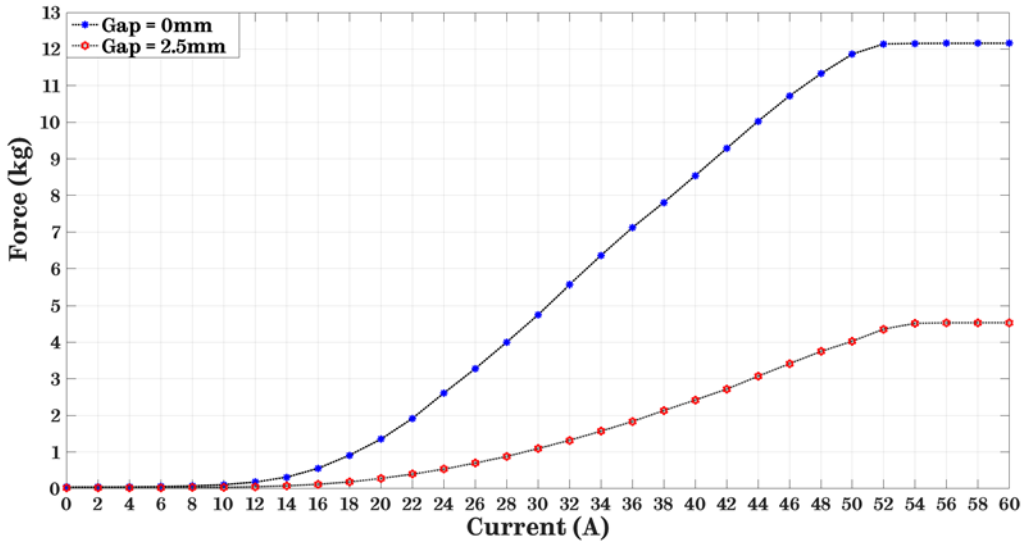

Figure 5.19: Force vs current flowing through the coil, with magnetising BH curves obtained from manufacturers. The maximum possible adhesive forces is reach with a 50A current. Blue dot line shows the simulation results for the case of 0mm gap. Red dot line shows the simulation results for a 2.5mm gap.

Table 5.2: Comparison of simulation and experimental results for the customised EPMAM with magnetising BH data from manufacturers.

Gap	Simulation results (kg)	Experimental results (kg)	Difference %
0 mm	12.16	6.12	99
2.5 mm	4.53	1.56	190

[7] http://www.arnoldmagnetics.com/en-us/

Results from FEA simulation, performed with magnetising BH curves obtained from the PMs and mild steel manufacturers, show a more realistic behaviour of the EPMAM performance. Qualitative results exhibit a similar behaviour between simulation and experimental results. However, in terms of the quantitative results still there exist a significant deviation between the FEA simulation and experimental results. There are several factors that affect the outcomes from experiments that were not considered in the simulations setup, which could be answer for this discrepancy. These factors are:

- **Environmental variables:** Temperature and humidity, which can reduce the saturation points, specifically in the regular neodymium magnets. These magnets are sensitive to changes in temperature.
- **Painting coating**: Coating on the steel plate used as target where the EPMAM was adhered. Paintings, coatings and even small corrosion affect the magnetic properties of the steel.
- **Load cell and test bench:** As discussed in Section 3.3.4 the load cell used for measuring the pulling of the EPMAM when the adhesion was ON has a spring transient behaviour. This created oscillations along the measurement axis (up and down), which although lasted approximately 1ms could have affected the initial gap. Hence affecting the measurement of the force.

These factors might not have big impact in the outcomes if considered individually, however when combined could a considerable influence in the results. Another thing to considered is the accuracy of FEA software, which only allow to perform a relative performance comparison, specially when demagnetization process is involved

Overall, experimental results still demonstrate the feasibility of the proposed novel adhesion mechanism, which can be further enhance by exploring use of alternative materials with higher magnetic saturation points. As well as further optimization of the components.

5.4.1. Discussion

Results from the FEA simulations and experiments, although presented a similar qualitative behaviour, showed significant discrepancies in terms of the quantitative results. After analysing the possible causes for the differences, it was determined that magnetising BH curves used initially were generic, which caused the simulation results to be inaccurate.

As a result, the actual BH curves, provided by the manufacturers of the PMs and mild steel were used to perform the simulations, again. Quantitative results, although exhibit a more realistic outcome, still had a significant difference form the once obtained on the experiments. As result the most probable reasons for the discrepancies between experimental and simulations were presented.

Finally, despite the differences between simulations and experiments, the EPMAM was considered feasible and potential based on the experimental results. Even though the adhesive forces from the real device were significantly smaller compared to the obtained in simulations, these forces still are strong enough to maintain the EPMAM wheel design attached to a vertical ferric structure. Furthermore, the EPMAM has the enough strength to hold its own weight and the weight of a MR, in which it is implemented.

In the next section the final EPM wheel prototype is presented. The prototype is built to fit an off-the-shelf MR.

5.5. EPMAM Integration into a Functional Wheel Design

In the present section, the EPMAM device built in Section 5.3.1 is integrated into a functional wheel design with the purpose to be implemented in an off-the-shelf MR. The EPMAM is set at the core of the wheel in a fix position with respect to the main frame of the MR. To allow the rotation of the wheel a customised bearing and a planetary gear were integrated to the design as it can be seen in Figure 5.22. Both, the gear and bearing, are non-ferric 3D-printed components in order to not interfere with the performance of the adhesion mechanism.

5.5.1. Wheel design with an internal fixed EPMAM

The final wheel complementary components are integrated in order to allow the rotation of the wheel whilst keeping the EPMAM in a fixed position, Figure 5.20 presents the wheel design with the EPMAM as fixed core. Figure 5.21 shows the interaction of the internal EPMAM for both OFF and ON states.

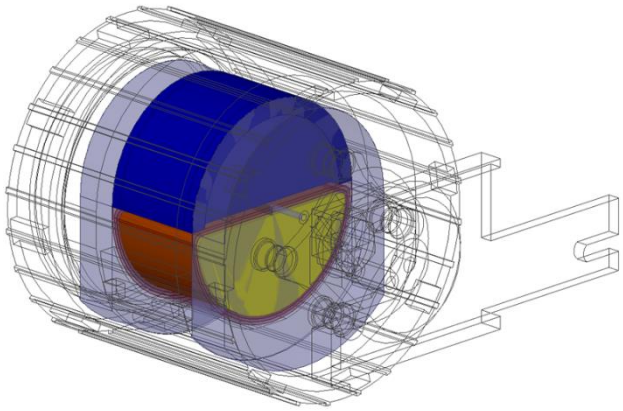

Figure 5.20: Wheel desing with a fixed EPMAM as core of the wheel.

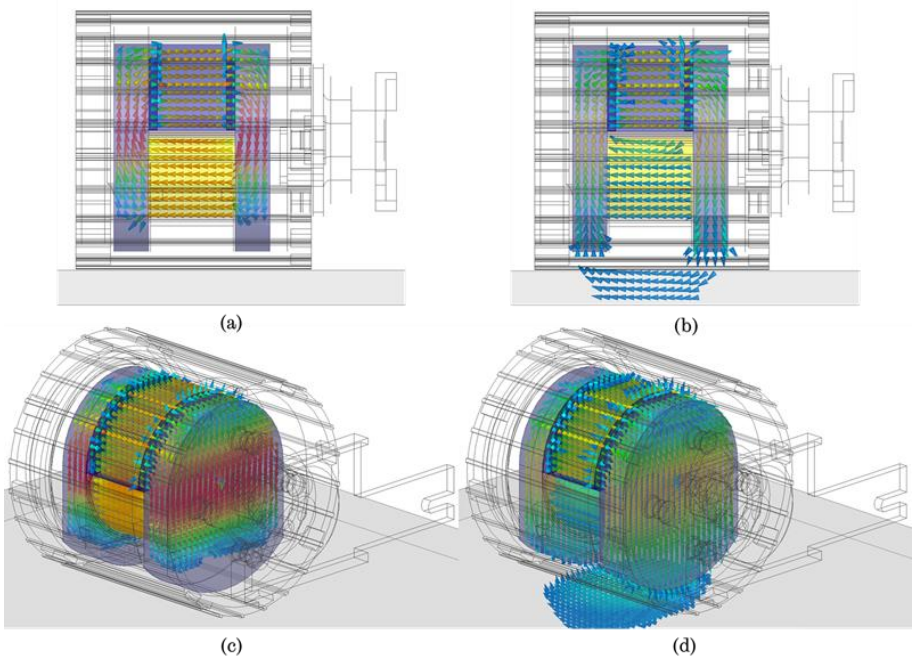

Figure 5.21: Magnetic field interaction for the OFF and ON states, inside the EPM wheel. (a) Front view for the OFF state. (b) Front view for the ON state. (c) Isometric view for the OFF state. (d) Isometric view for the ON state.

For the case of the rest of the wheel components, apart from the EPMAM, must be fabricated with non-ferric materials to avoid interferences between them and the magnetic fields produced by adhesion mechanism. Figure 5.22 presents the final CAD design for the final prototype, with an exploded view of all internal components.

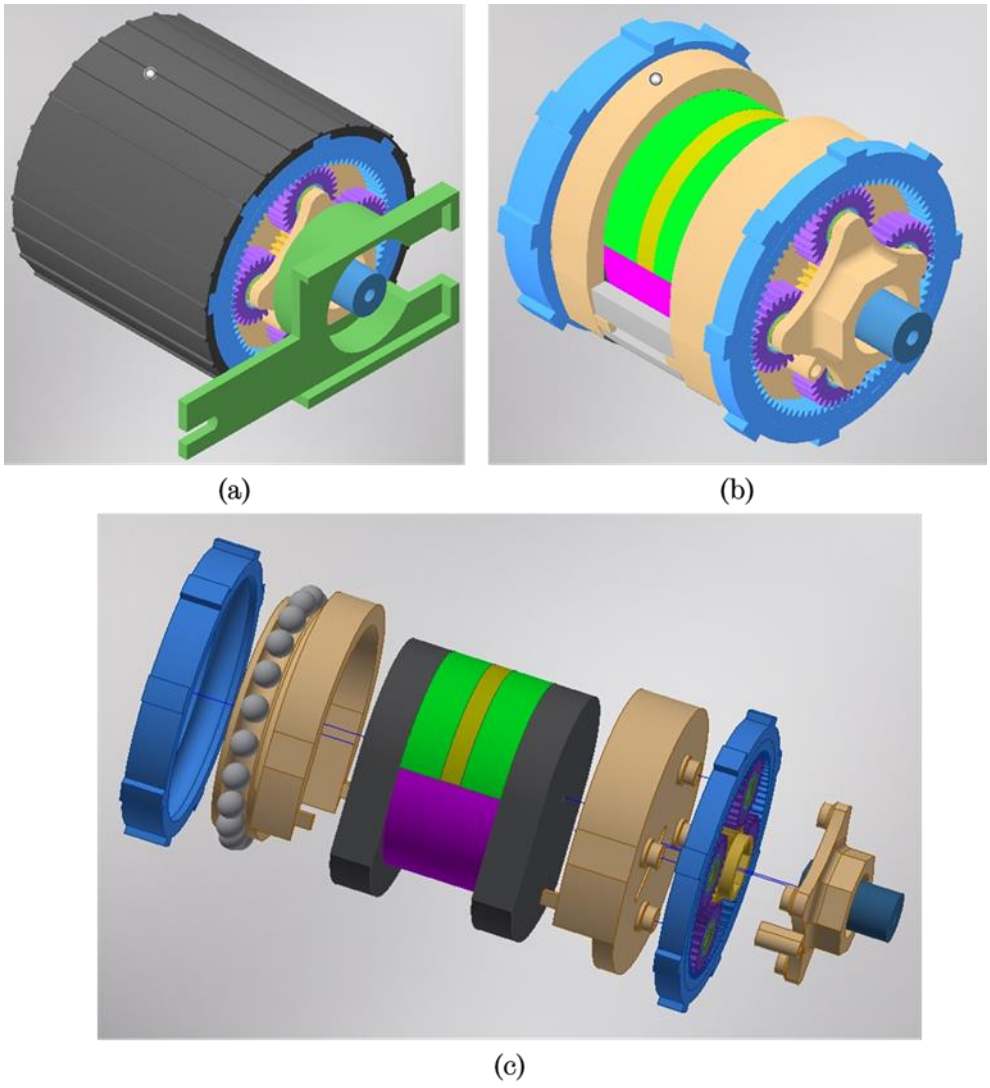

Figure 5.22: Final wheel design to be implemented in a of-the-shelf MR. (a) Isometric view of the full wheel. (b) Isometric view of the internal components of the wheel. (c) Exploded view of all the internal components of the wheel.

All the components of the wheel prototype, apart from EPMAM, are customised 3D printed plastic components. The final assembled EPM wheel using these components is presented in Figure 5.23.

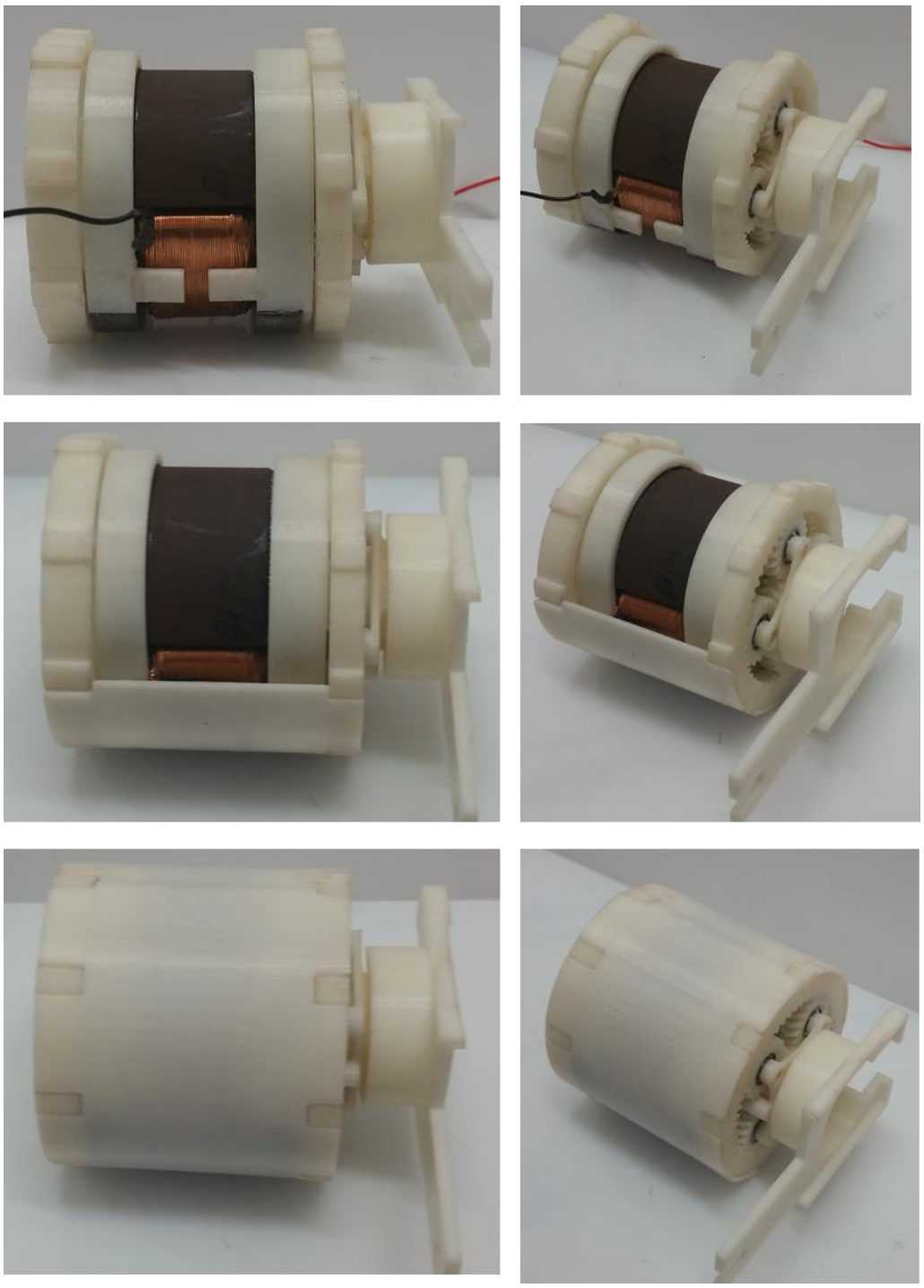

Figure 5.23: Final EPM wheel prototype constructed using customised 3D printed components. The EPMAM is placed as core of the wheel in a fixed position. The rotating outer part and the EPMAM are connected with a customised 3D printed bearing on the left and a 3D printed planetary gear on the right.

In order to verify adhesion capabilities, the prototype is tested in two scenarios: 1. with the EPMAM in direct contact with target surface, Figure 5.24(a). For this case, the wheel was able to support its own weight (0.848kg) plus 2kg pay load; and 2. with the outer part of the wheel in between the EPMAM and the surface target, which generated a 3.2mm gap them. In this scenario, the wheel was able to support its own weight plus a 0.314kg payload, Figure 5.24(a).

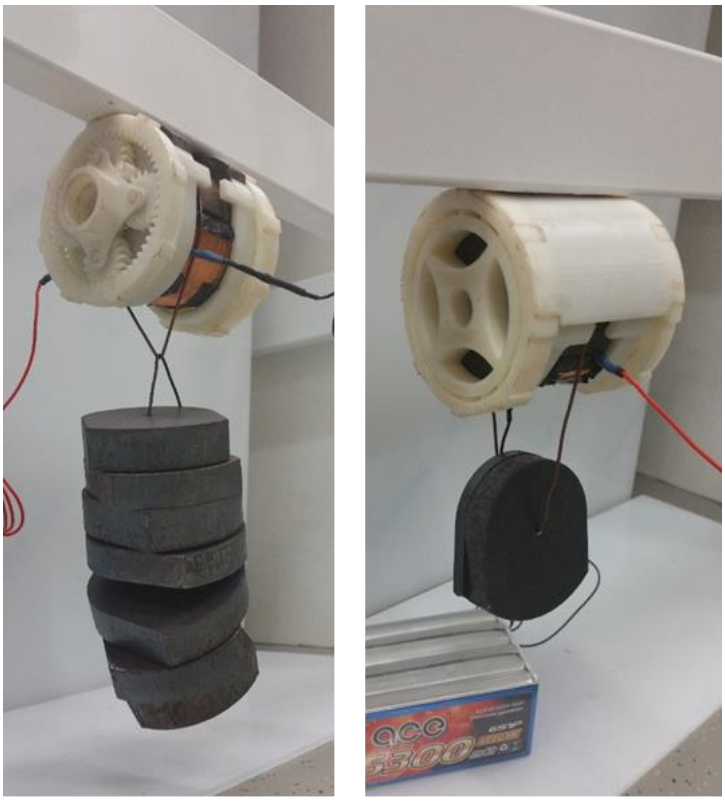

(a) (b)

Figure 5.24: Desmostration of the adhesion strenght of the final EPM wheel prototype. (a) Direct contact between the EPMAM and the target surfase. The wheel eseally withstand a payload with a 2kg weight plus its own weight, which is 0.848kg. (b) EPM wheel attached to a steel target with the outer part of wheel in between. Wheel withstanded its own weithg plus a 0.314kg payload.

5.5.2. Discussion

From the experimental results obtained in Sections 5.4 and 5.5.1 demonstrate the viability of EPMAM integrated into a wheel. Although there

exist differences between the experimental and simulation results, these differences can be explained by: 1. exist variables that were not included in the simulations in order to save computational power and time. These variables (temperature, humidity, external magnetic fields, proximity of ferric components) by themselves cannot be meaningful in the results, but all of them combine might be; 2. limitations of the software (ANSYS Maxwell) used, it was not able to perform the ON-OFF transition.

Results for the magnetic force of the final wheel design, presented in Section 5.5.1, show that each wheel is able to hold a pay load of 0.314kg. If implemented in a MR, four wheels will be able hold a 1.2kg MR. Furthermore, if the thickness of the outer part of the wheel (that separates the EPMAM from the structure surface) is reduced, the strength of the magnetic force can be increased. The maximum magnetic force that this specific design can generate is 2kg, in a direct contact of the EPMAM with the ferric structure.

In terms of energy consumption for performing the switching between states, each transition pulse consumes 5.27mWh from the battery. This power is determined using maximum current (≈55A) and pulse length (15ms) needed for the switching.

$$P_{Switching} = VIt_{pulse} = (23V)(55A)(4.17x10^{-6}h) = 5.27mWh$$

Considering the battery used for the experiments, which has a 5300mWh capacity, ≈1,000 switching pulses can be delivered by fully charged battery.

5.6. Concluding remarks

In the present chapter, a detailed analysis an EPMAM wheel design, using customised components, was performed. The impact of the thickness of the steel keepers, the gauge of enamelled wire and the presence of an air gap were examined in order to determine optimum component configuration. Once the most suitable component's size was selected the most feasible configuration, for integrating the EPMAM in a wheel design,

was explored. The static EPMAM configuration was chosen over the rotating EPMAM, based on the discussed advantages and disadvantages.

Once the customised components and EPMAM wheel configuration were established, an EPMAM wheel design was presented based on manufacturability and fabrication cost considerations. After building the selected EPMAM design, a set of simulations and experiments were presented with the aim to verify the performance of the final device. The outcomes of the simulations and experiments were compared in both, qualitative and quantitative, ways. In terms of the qualitative results, FEA simulations and experiments exhibit similar behaviour for the OFF and ON states, as well as the OFF-ON and ON-OFF switching. However, when compared a quantitative way, FEA simulations presented a significant deviation from the experimental outcomes. Some of the main reasons for the difference was due to the magnetization BH curves, initially used by the FEA software. For this reason, the magnetization BH curves from the actual PMs and mild steel materials were requested to the manufacturers. Using the new magnetisation BH data simulations were repeated, and the results obtained were more realistic, however, the still were significantly different from the experimental results. After analysing the possible factors that might have affected the simulation and based on the experimental results, it was determined the proposed Novel adhesion mechanism still was feasible and has potential for being implemented in WCMR.

Finally, an EPM wheel prototype was presented and built using customised 3D printed plastic components. The final wheel prototype was tested for to scenarios with a holding payload, which verify that the wheel remained adhered to the target surface, holding its own weight plus the added payload.

Chapter 6

Conclusions and Future Work

Inspection and maintenance tasks of ferric structures are crucial preserve the functionality of existing infrastructure. In order to reduce the risk for humans that have been performing these task, along with the costs and times for such activities WCMR have been studied in the last decades. Most of the MR developed for the specific case of ferric structures use magnetic adhesion mechanism in order to climb vertical structures performing against gravity. These WCMR use PM magnets as the main source of magnetic adhesion. However, PMs have a fixed adhesive force, which means the adhesive force cannot be modified once the MR has been fabricated. Moreover, if the strength of the adhesion mechanism is not selected carefully the final adhesive performance could be significantly affected. A weak adhesive force can result in WCMR not being able to adhere to the structure. On the other hand, a strong adhesive force reduces considerably the manoeuvrability of the MR and increases the power consumption need to move around the structure.

The work presented in this thesis explores a novel magnetic adhesion mechanism for WCMR used for inspection and/or maintenance tasks in ferric structures and its implementation in a wheeled locomotion mechanism.

This chapter presents the final conclusions from the work presented and explores the possible future work for further optimisation of this novel adhesion mechanism. Throughout the present thesis the following subjects where covered:

- The current state-of-the-art on MR used for inspection tasks was presented throughout Chapter 2. Inspection robots were classified base on their domain and it was established that the most suitable MR domain for inspection tasks in vertical ferric structures was the ground domain. Within the ground MR were further examined base on the type of locomotion and adhesion mechanism. These analysis showed that the most suitable locomotion mechanism for WCMR used in ferric structures, due its advantages, was the wheeled mechanism. In terms of the adhesion mechanism the most feasible mechanism was determined to be the magnetic adhesion mechanism. Finally, in order to overcome the limitations of current magnetic adhesion mechanisms, a novel active magnetic adhesion mechanism using EPMs was proposed.

- The EPM were explored in more detailed throughout Chapter 3. Their theory and working principles were presented and their OFF and ON configurations were examined. Furthermore, the novel characteristic that allows the EPMs to vary their adhesive force was presented. In order to validate the feasibility of EPMs as an adhesion mechanism a preliminary device was constructed using off-the shelf components. This EPM device was subject of different experiments and corresponding FEA simulations with the aim to verify its adhesive capabilities and behaviour for the OFF, ON and variable adhesion states. Results from both, FEA simulations and experiments validated the feasibility of the concept and set the basis for more detailed examination of the concept.

- In Chapter 4, an analysis of the locomotion mechanism for implementing the EPM as an adhesion mechanism were explored. After a detailed analysis it was determined that the wheeled

locomotion was the most suitable, based in some predefined requisites. Having selected the locomotion mechanism, different possible configurations for integrating the EPMAM into a wheeled locomotion mechanism were explored. After selecting most appropriate configuration, similarly to Chapter 3, a preliminary device was constructed using again the same off-the-shelf components. Again a set of FEA simulations and experiments were performed to the proposed EPMAM wheel device. Results from both, experiments and simulations demonstrated the feasibility of a wheel design with an EPMAM as the main adhesion mechanism.

- In Chapter 5, based on results obtained in Chapter 4, a customised EPMAM was presented and the influence of each of the individual components on the performance of the EPMAM was explored. Based on the results from analysis performed to each of the components a final EPMAM was built using the customised components. Finally a set of FEA simulations and experiments were performed and compared in a quantitative and qualitative way. Qualitative results had similar outcomes, however quantitative results differed considerably. The possible causes for the differences were explored and, although significant difference between experiments and simulations, based on experimental results the EPMAM was proven to be feasible and with potential in the WCMR field. Next, a complete wheel prototype was designed and constructed using 3D printed components. The final prototype was tested under load scenarios with positive results. Finally the built prototype was mounted on an off-the-shelf MR.

6.1. Future work

Based on the results obtained through Chapter 5, it was determined that further work must be performed for selecting which parameters should be included into the FEA setup for obtaining simulation results close to real life. The achievements presented in this thesis can be used as base line to

extend the research on active magnetic adhesion mechanisms using EPMs with the following list of possible future work:

- A more detailed examinations of the parameters that have potential influence on the final performance of the EPMAM, such as temperature or humidity. Additionally, including effects of motion into the FEA simulation to explore the impact of the transient oscillations present in the experiments measurements.
- Design and use of a more robust test bench in order to minimize external transient effects in the experimental measurements.
- The use of different materials for the keepers. Using materials with higher magnetic saturations points might enable to increase magnetic adhesive forces and reducing the total weight of the EPMAM. Some of the material can be the electrical or silicon steel, permalloy or Mu-metal.
- Testing the wheel on a MR. As shown in Figure 6.1, building 4 identical EPM wheels in order to mount them into a MR and testing them in a real scenario.

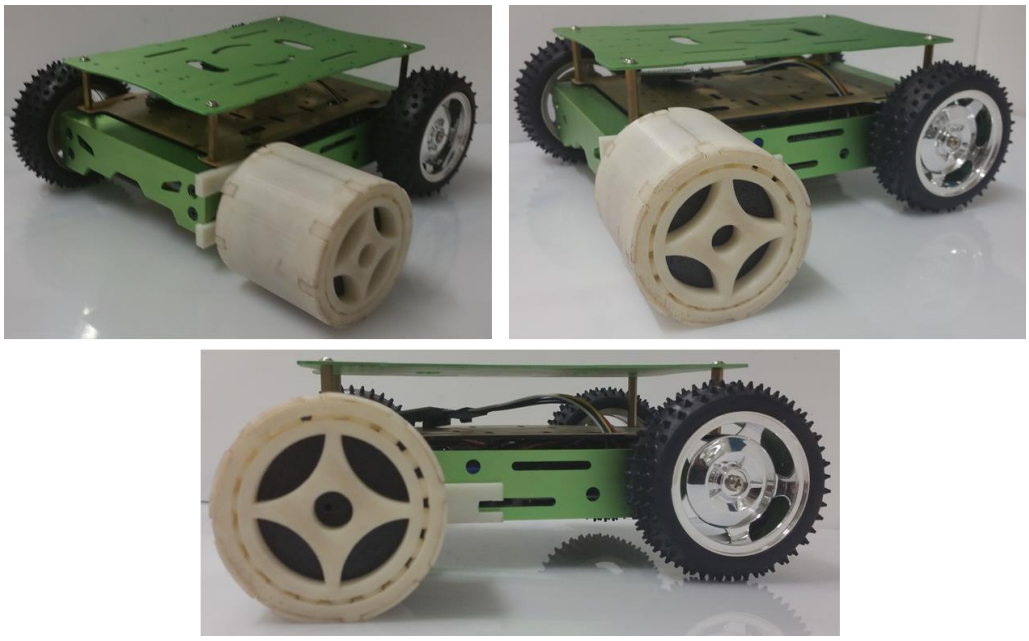

Figure 6.1: Final EPM wheel prototype installed ifn a off-the-shelf MR

REFERENCES

Agoros, C., 1994. US Navy Unmanned Undersea Vehicle Navigation. In *1994 IEEE Oceans*. Brest: IEEE, p. III/372-III/377. Available at: http://ieeexplore.ieee.org/lpdocs/epic03/wrapper.htm?arnumber=364227 [Accessed March 28, 2014].

Asano, K. et al., 1983. Multijoint Inspection Robot. *IEEE Transactions on Industrial Electronics*, IE-30(3), pp.277–281. Available at: http://ieeexplore.ieee.org/lpdocs/epic03/wrapper.htm?arnumber=4180472.

Autumn, K. et al., 2005. Robotics in Scansorial Environments. In G. R. Gerhart, C. M. Shoemaker, & D. W. Gage, eds. *Proceedings of SPIE - Unmanned Ground Vehicle Technology VII*. Orlando, pp. 291–302. Available at: http://proceedings.spiedigitallibrary.org/proceeding.aspx?articleid=864272 [Accessed March 21, 2014].

AUVIS, 2013. Unmanned Maritime Vehicles: Core Capabilities and Market Background. *The Association for Unmanned Vehicle Systems International*, 100, pp.1–16.

Bahr, B., Li, Y. & Najafi, M., 1996. Design and suction cup analysis of a wall climbing robot. *Computers and Electrical Engineering*, 22(3), pp.193–209.

Balaguer, C., Gimenez, A. & Jordon, A., 2005. Climbing robots' mobility for inspection and maintenance of 3D complex environments. *Autonomous Robots*, 18(2), pp.157–169.

Bannon, R.T., 2000. Remotely Operated Vehicles Evolution for Maintenance and Repair of Fiber Optic Systems. In *2000 IEEE Oceans*. Providence, RI, RI: IEEE, pp. 489–496. Available at: http://ieeexplore.ieee.org/xpl/articleDetails.jsp?arnumber=881304%5Cnhttp://ieeexplore.ieee.org/lpdocs/epic03/wrapper.htm?arnumber=881304 [Accessed March 28, 2014].

Bovim, K., 2014. *Design of a wall-climbing robot system*.

Briones, L., Bustamante, P. & Serna, M.A., 1994. Robicen: A wall-climbing pneumatic robot for inspection in nuclear power plants. *Robotics and Computer Integrated Manufacturing*, 11(4), pp.287–292.

Bruch, M.H. et al., 2005. Advances in Autonomy for Small UGVs. In *SPIE Proc. 5804 Unmanned Gr. Veh. Technol. VII*.

Bruzzone, L. & Fanghella, P., 2014. Mantis: hybrid leg-wheel ground mobile robot. *Industrial Robot: An International Journal*, 41(1), pp.26–36.

Bruzzone, L. & Quaglia, G., 2012. Review article: locomotion systems for ground mobile robots in unstructured environments. *Mechanical Sciences*, 3(2), pp.49–62. Available at: http://www.mech-sci.net/3/49/2012/ [Accessed February 26, 2014].

Burri, M. et al., 2012. Aerial Service Robots for Visual Inspection of Thermal Power Plant Boiler Systems. In *2012 2nd International Conference on Applied Robotics for the Power Industry (CARPI)*. pp. 70–75.

Byrd, J.S. & DeVries, K.R., 1990. A Six-Legged Telerobot for Nuclear Applications Development. *The International Journal of Robotics Research*, 9(2), pp.43–52. Available at: http://ijr.sagepub.com/cgi/doi/10.1177/027836499000900204 [Accessed November 22, 2013].

Caprari, G. & Breitenmoser, A., 2012. Highly Compact Robots for Inspection of Power Plants. In *2010 1st International Confconference on Applied Robotics for the Power Industry*. Montreal, Canada, pp. 1–6. Available at: http://onlinelibrary.wiley.com/doi/10.1002/rob.21411/full.

Carrara, G., De Paulis, A. & Tantussi, G., 1992. SSR: a mobile robot on ferromagnetic surfaces. *Automation in Construction*, 1(1), pp.47–53. Available at: http://linkinghub.elsevier.com/retrieve/pii/092658059290036J [Accessed May 22, 2015].

Carroll, D.M., Mikell, K. & Denewiler, T., 2004. *Unmanned ground vehicles for integrated force protection*, Available at: http://proceedings.spiedigitallibrary.org/proceeding.aspx?articleid=844163.

Cassing, W., Pohl, T. & Steger, F., 2008. Using electro-permanent magnets to lift loads in modern logistics networks. *ThyssenKrupp techforum*, (1), pp.80–85. Available at: http://cat.inist.fr/?aModele=afficheN&cpsidt=20617234 [Accessed March 7, 2014].

Cho, K.H. et al., 2013. Inspection robot for hanger cable of suspension bridge: Mechanism design and analysis. *IEEE/ASME Transactions on Mechatronics*, 18(6), pp.1665–1674. Available at: http://ieeexplore.ieee.org/lpdocs/epic03/wrapper.htm?arnumber=6612676 [Accessed March 27, 2014].

Chu, B. et al., 2010. A survey of climbing robots: Locomotion and adhesion. *International Journal of Precision Engineering and Manufacturing*, 11(4), pp.633–647.

Clapper, J.R. et al., 2009. *FY2009-2034 Unmanned Systems Integrated Roadmap*, Available at: http://scholar.google.com/scholar?hl=en&btnG=Search&q=intitle:FY2009+?+2034+Unmanned+Systems+Integrated+Roadmap#0 [Accessed February 21, 2014].

Damus, R. et al., 2002. Design of an Inspection Class Autonomous

Underwater Vehicle. In *2002 IEEE Oceans*. IEEE, pp. 180–185. Available at: http://ieeexplore.ieee.org/lpdocs/epic03/wrapper.htm?arnumber=1193268.

Debenest, P. et al., 2008. Sensor-arm - Robotic Manipulator for Preventive Maintenance and Inspection of High-voltage Transmission Lines. In *2008 IEEE/RSJ International Conference on Intelligent Robots and Systems, IROS*. IEEE, pp. 1737–1744. Available at: http://ieeexplore.ieee.org/lpdocs/epic03/wrapper.htm?arnumber=4650964 [Accessed March 27, 2014].

Defense, U.D. of, 1992. *Unmanned Ground Vehicle Master Plan* D. O. F. D. W. DC, ed.,

Degani, A. et al., 2007. A dynamic single actuator vertical climbing robot. In *2007 IEEE International Conference on Intelligent Robots and Systems*. San Diego, CA, USA: IEEE, pp. 2901–2906. Available at: http://ieeexplore.ieee.org/lpdocs/epic03/wrapper.htm?arnumber=4399200 [Accessed March 27, 2014].

Desbiens, A.L., Asbeck, A. & Cutkosky, M., 2010. Hybrid aerial and scansorial robotics. In *2010 IEEE International Conference on Robotics and Automation*. IEEE, pp. 72–77. Available at: http://ieeexplore.ieee.org/lpdocs/epic03/wrapper.htm?arnumber=5509397 [Accessed March 21, 2014].

Elliott, M. et al., 2007. City-Climbers at Work. In *Proceedings 2007 IEEE International Conference on Robotics and Automation*. IEEE, pp. 2764–2765.

Fernández, R. et al., 2010. A wall climbing robot for tank inspection. An autonomous prototype. In *IECON Proceedings (Industrial Electronics Conference)*. IEEE, pp. 1424–1429. Available at: http://ieeexplore.ieee.org/lpdocs/epic03/wrapper.htm?arnumber=5675473 [Accessed February 22, 2014].

Fischer, W. et al., 2010. Foldable magnetic wheeled climbing robot for the inspection of gas turbines and similar environments with very narrow access holes. *Industrial Robot: An International Journal*, 37(3), pp.244–249. Available at: http://www.emeraldinsight.com/journals.htm?issn=0143-991X&volume=37&issue=3&articleid=1858511&show=html [Accessed November 22, 2013].

Fischer, W. et al., 2011. Locomotion system for a mobile robot on magnetic wheels with both axial and circumferential mobility and with only an 8-mm height for generator inspection with the rotor still installed. *IEEE Transactions on Industrial Electronics*, 58(12), pp.5296–5303. Available at: http://ieeexplore.ieee.org/lpdocs/epic03/wrapper.htm?arnumber=5762597 [Accessed February 22, 2014].

Fischer, W., Tache, F. & Siegwart, R., 2007. Inspection system for very thin and fragile surfaces, based on a pair of wall climbing robots with magnetic wheels. In *2007 IEEE International Conference on Intelligent Robots and Systems*. San Diego, CA, USA: IEEE, pp. 1216–1221. Available at: http://ieeexplore.ieee.org/lpdocs/epic03/wrapper.htm?arnumber=4399060 [Accessed March 27, 2014].

Fischer, W., Tache, F. & Siegwart, R., 2007. Magnetic Wall Climbing Robot for Thin Surfaces with Specific Obstacles. In *6th International Conference on Field and Service Robotics (FSR)*. pp. 551–561. Available at: http://hal.inria.fr/inria-00194494 [Accessed March 27, 2014].

Fish, S. & Sitzman, A., 2009. Unmanned vehicles for mobile electromagnetic launch platforms. *IEEE Transactions on Magnetics*, 45(1), pp.639–640. Available at: http://ieeexplore.ieee.org/lpdocs/epic03/wrapper.htm?arnumber=4773631 [Accessed March 28, 2014].

Fu, G., Menciassi, A. & Dario, P., 2012. Design of a miniature switchable connection system for stochastic modular robots. *Sensors and Actuators A: Physical*, 173(1), pp.267–276. Available at: http://linkinghub.elsevier.com/retrieve/pii/S0924424711005504 [Accessed March 27, 2014].

Fulbright, R. & Stephens, L.M., 1995. SWAMI: An autonomous mobile robot for inspection of nuclear waste storage facilities. *Autonomous Robots*, 2(3), pp.225–235. Available at: http://link.springer.com/10.1007/BF00710858 [Accessed March 27, 2014].

Gilbert, P. et al., 2007. *Miniature Mobile Robot for Inspection of Ferromagnetic Structures MagBot*, Lausanne. Available at: http://citeseerx.ist.psu.edu/viewdoc/download?doi=10.1.1.172.8780&rep=rep1&type=pdf [Accessed February 22, 2014].

Gilpin, K., Knaian, A. & Rus, D., 2010. Robot pebbles: One centimeter modules for programmable matter through self-disassembly. In *2010 IEEE International Conference on Robotics and Automation*. IEEE, pp. 2485–2492. Available at: http://ieeexplore.ieee.org/lpdocs/epic03/wrapper.htm?arnumber=5509817 [Accessed March 27, 2014].

Gogarty, B. & Robinson, I., 2011. *Unmanned Vehicles: A (Rebooted) History, Background and Current State-Of-the-Art*, Available at: http://heinonlinebackup.com/hol-cgi-bin/get_pdf.cgi?handle=hein.journals/jlinfos21&section=17.

Granosik, G., Hansen, M.G. & Borenstein, J., 2005. The OmniTread serpentine robot for industrial inspection and surveillance. *Industrial Robot: An International Journal*, 32(2), pp.139–148.

Grieco, J.C. et al., 1998. A six legged climbing robot for high payloads. In

1998 International Conference on Control and Applications. Trieste, Italy: IEEE, pp. 446–450. Available at: http://ieeexplore.ieee.org/xpls/abs_all.jsp?arnumber=728488 [Accessed May 22, 2015].

Gunetti, P., Thompson, H. & Dodd, T., 2011. Autonomous mission management for UAVs using soar intelligent agents. *International Journal of Systems Science*, 44(5), pp.831–852. Available at: http://www.tandfonline.com/doi/abs/10.1080/00207721.2011.626902 [Accessed February 22, 2014].

Guo, R. et al., 2010. A mobile robot for inspection of substation equipments. In *2010 1st International Conference on Applied Robotics for the Power Industry, CARPI 2010*. IEEE, pp. 1–5.

Haas, G.A. et al., 1997. *An Unmanned Ground Vehicle for Mine*,

Hadfield, D. & Mawson, D.L., 1952. Permanent Magnets for Spectrographs and Nuclear Physical Research. *British Journal of Applied Physics*, 3(6), pp.199–202.

Haraguchi, R. et al., 2005. The development of the mobile inspection robot for rescue activity, MOIRA2. In *2005 International Conference on Advanced Robotics, ICAR '05, Proceedings*. Seattle, WA, WA, pp. 498–505.

Hirose, S. & Tsutsumitake, H., 1992. Disk Rover: A Wall-climbing Robot Using Permanent. *1992 IEEE/RSJ International Conference on Intelligent Robots and Systems*, 3, pp.2074–2079.

Hobson, B. et al., 2001. Development of a Micro Autonomous Underwater Vehicle for Complex 3-D Sensing. In *2001 IEEE Oceans. An Ocean Odyssey*. Marine Technol. Soc, pp. 2043–2045. Available at: http://ieeexplore.ieee.org/xpl/articleDetails.jsp?arnumber=968311%5Cnhttp://ieeexplore.ieee.org/lpdocs/epic03/wrapper.htm?arnumber=968311 [Accessed March 28, 2014].

Hrabar, S., Merz, T. & Frousheger, D., 2010. Development of an autonomous helicopter for aerial powerline inspections. In *2010 1st International Conference on Applied Robotics for the Power Industry, CARPI 2010*. IEEE, pp. 1–6. Available at: http://ieeexplore.ieee.org/lpdocs/epic03/wrapper.htm?arnumber=5624432 [Accessed March 28, 2014].

Hu, B. et al., 2009. A Miniature Wall Climbing Robot with Biomechanical Suction Cups. *Industrial Robot: An International Journal*, 36(6), pp.551–561. Available at: http://www.emeraldinsight.com/journals.htm?issn=0143-991X&volume=36&issue=6&articleid=1819209&show=html%5Cnhttp://www.emeraldinsight.com/10.1108/01439910910994623 [Accessed October 31, 2013].

International, S.R.I., 2010. Electroadhesion for Industrial , Biomedical ,

Military , and Consumer Applications. *Power*. Available at: http://www.sri.com/research-development/robotics [Accessed March 2, 2014].

Jahanian, O. & Karimi, G., 2006. Locomotion Systems in Robotic Application. In *2006 IEEE International Conference on Robotics and Biomimetics, ROBIO 2006*. IEEE, pp. 689–696. Available at: http://ieeexplore.ieee.org/lpdocs/epic03/wrapper.htm?arnumber=4141949 [Accessed March 27, 2014].

Ji, C.H. et al., 2004. Electromagnetic 2 ?? 2 MEMS optical switch. *IEEE Journal on Selected Topics in Quantum Electronics*, 10(3), pp.545–550.

Kalra, L.P. & Gu, J., 2007. An autonomous self contained wall climbing robot for non-destructive inspection of above-ground storage tanks. *Industrial Robot: An International Journal*, 34(2), pp.122–127. Available at: http://www.emeraldinsight.com/journals.htm?issn=0143-991X&volume=34&issue=2&articleid=1597860&show=html [Accessed March 27, 2014].

Kalra, L.P., Gu, J. & Meng, M., 2006. A Wall Climbing Robot for Oil Tank Inspection. In *2006 IEEE International Conference on Robotics and Biomimetics, ROBIO 2006*. IEEE, pp. 1523–1528. Available at: http://ieeexplore.ieee.org/lpdocs/epic03/wrapper.htm?arnumber=4142092 [Accessed March 27, 2014].

Kato, I., 2005. Dynamics of Track - Wheel Systems on High Speed Vehicles. *Journal of Meehamcal Science and Technology*, 19(1), pp.328–335.

Katrašnik, J., Pernuš, F. & Likar, B., 2010. A survey of mobile robots for distribution power line inspection. *IEEE Transactions on Power Delivery*, 25(1), pp.485–493. Available at: http://ieeexplore.ieee.org/lpdocs/epic03/wrapper.htm?arnumber=5345712 [Accessed March 27, 2014].

Khirade, N.R., Sanghi, R.K. & Tidke, D.J., 2014. Magnetic Wall Climbing Devices - A Review. , 2014, pp.55–59.

Khurshid, J. & Bing-rong, H., 2004. Military robots-a glimpse from today and tomorrow. In *2004 8th International Conference on Control, Automation, Robotics and Vision*. p. 771–777 Vol. 1.

Kim, J.H., Sharma, G. & Iyengar, S.S., 2010. FAMPER: A fully autonomous mobile robot for pipeline exploration. In *2010 IEEE International Conference on Industrial Technology*. Ieee, pp. 517–523. Available at: http://ieeexplore.ieee.org/lpdocs/epic03/wrapper.htm?arnumber=5472748.

Kim, S. et al., 2008. Smooth vertical surface climbing with directional adhesion. *IEEE Transactions on Robotics*, 24(1), pp.65–74.

Knaian, A.N., 2010. *Electropermanent Magnetic Connectors and Actuators: Devices and Their Application in Programmable Matter*. Massachusetts Institute of Technology. Available at:

http://dspace.mit.edu/handle/1721.1/60151%5Cnhttp://hdl.handle.net/1721.1/60151 [Accessed March 27, 2014].

Knaian, A.N. et al., 2012. The Milli-Motein: A self-folding chain of programmable matter with a one centimeter module pitch. In *2012 IEEE International Conference on Intelligent Robots and Systems*. IEEE, pp. 1447–1453. Available at: http://ieeexplore.ieee.org/lpdocs/epic03/wrapper.htm?arnumber=6385904 [Accessed March 27, 2014].

Kolhalkar, N. & Patil, S., 2012. Wall Climbing Robots: A Review. *International Journal of Engineering and Innovative Technology*, 1(5), pp.227–229. Available at: http://ijeit.com/vol 1/Issue 5/IJEIT1412201205_44.pdf [Accessed February 26, 2014].

Koo, I.M. et al., 2013. Development of wall climbing robot system by using impeller type adhesion mechanism. *Journal of Intelligent and Robotic Systems: Theory and Applications*, 72(1), pp.57–72. Available at: http://link.springer.com/10.1007/s10846-013-9820-z [Accessed March 27, 2014].

Kwon, Y.-S.K.Y.-S. et al., 2010. A pipeline inspection robot with a linkage type mechanical clutch. In *2010 IEEE International Conference on Intelligent Robots and Systems*. IEEE, pp. 2850–2855. Available at: http://ieeexplore.ieee.org/lpdocs/epic03/wrapper.htm?arnumber=5652391 [Accessed March 27, 2014].

Lab, B.M., Biologically Inspired Synthetic Gecko Adhesives. Available at: http://robotics.eecs.berkeley.edu/~ronf/Gecko/.

Lee, B.J. et al., 2008. Optimal design of electro-permanent magnet lifter using improved auto-tuning niching genetic algorithm. In *2007 International Conference on Electrical Machines and Systems*. pp. 783–788. Available at: http://ieeexplore.ieee.org/xpls/abs_all.jsp?arnumber=4412219 [Accessed February 22, 2014].

Lee, D. et al., 2012. Novel mechanisms and simple locomotion strategies for an in-pipe robot that can inspect various pipe types. *Mechanism and Machine Theory*, 56, pp.52–68. Available at: http://www.sciencedirect.com/science/article/pii/S0094114X12001127 [Accessed March 27, 2014].

Liu, D.K. et al., 2008. A Robotic System for Steel Bridge Maintenance: Research Challenges and System Design. *2008 Australasian Conference on Robotics and Automation*. Available at: http://www.scopus.com/inward/record.url?eid=2-s2.0-84862909210&partnerID=tZOtx3y1.

Ltd, L.M.P., 2014. Electropermanent Plate Lifting Magnet. , pp.31–33. Available at: http://www.liftonmagnets.com/c-36-lifting-magnets-range.aspx.

M. Lauria; Y. Piguet and R. Siegwart, 2002. Octopus-an Autonomous

Wheeled Climbing Robot. In *5th International Conference onon Climbing and Walking Robots*. pp. 1–8. Available at: http://citeseerx.ist.psu.edu/viewdoc/download?doi=10.1.1.149.6526&rep=rep1&type=pdf.

Mae, Y. & Ohara, K., 2009. Wheel Hybrid Loeomotion for Multi Legged Robot. *The Japan Society fo Mechanical Engineers*.

Manley, J.E., 2008. Unmanned surface vehicles, 15 years of development. *Oceans 2008*, pp.1–4. Available at: http://ieeexplore.ieee.org/lpdocs/epic03/wrapper.htm?arnumber=5152052.

Marchese, A.D., Asada, H. & Rus, D., 2012. Controlling the locomotion of a separated inner robot from an outer robot using electropermanent magnets. In *2012 IEEE International Conference on Robotics and Automation*. IEEE, pp. 3763–3770. Available at: http://ieeexplore.ieee.org/lpdocs/epic03/wrapper.htm?arnumber=6225034 [Accessed March 27, 2014].

Marchese, A.D., Onal, C.D. & Rus, D., 2011. Soft robot actuators using energy-efficient valves controlled by electropermanent magnets. In *2012 IEEE International Conference on Intelligent Robots and Systems*. IEEE, pp. 756–761. Available at: http://ieeexplore.ieee.org/lpdocs/epic03/wrapper.htm?arnumber=6095064 [Accessed March 25, 2014].

Menon, C., Murphy, M. & Sitti, M., 2004. Gecko Inspired Surface Climbing Robots. In *2004 IEEE International Conference on Robotics and Biomimetics*. Ieee, pp. 431–436. Available at: http://ieeexplore.ieee.org/lpdocs/epic03/wrapper.htm?arnumber=1521817 [Accessed March 27, 2014].

Michaud, F. et al., 2003. AZIMUT, a leg-track-wheel robot. *2003 IEEE/RSJ International Conference on Intelligent Robots and Systems*, 3(October), pp.2553–2558. Available at: http://ieeexplore.ieee.org/lpdocs/epic03/wrapper.htm?arnumber=1249254.

Michaud, F. et al., 2005. Multi-modal locomotion robotic platform using leg-track-wheel articulations. *Autonomous Robots*, 18(2), pp.137–156.

Miyake, T., Ishihara, H. & Yoshimura, M., 2007. Basic studies on wet adhesion system for wall climbing robots. In *2007 IEEE International Conference on Intelligent Robots and Systems*. IEEE, pp. 1920–1925. Available at: http://ieeexplore.ieee.org/lpdocs/epic03/wrapper.htm?arnumber=4399417 [Accessed March 27, 2014].

Murphy, M.P. et al., 2011. Waalbot II: Adhesion Recovery and Improved Performance of a Climbing Robot using Fibrillar Adhesives. *The International Journal of Robotics Research*, 30(1), pp.118–133. Available at: http://ijr.sagepub.com/cgi/doi/10.1177/0278364910382862 [Accessed

October 31, 2013].

Nave, C.R., 2017. HyperPhysics. Available at: http://hyperphysics.phy-astr.gsu.edu/hbase/magnetic/magfie.html [Accessed March 29, 2017].

Nie, C., Pacheco Corcho, X. & Spenko, M., 2013. Robots on the move: Versatility and complexity in mobile robot locomotion. *IEEE Robotics and Automation Magazine*, 20(4), pp.72–82. Available at: http://www.nature.com/scientificamerican/journal/v295/n6/full/scientificamerican1206-57a.html [Accessed February 22, 2014].

Nishi, A., 1996. Development of wall-climbing robots. *Computers and Electrical Engineering*, 22(2), pp.123–149. Available at: http://www.sciencedirect.com/science/article/pii/0045790695000348 [Accessed March 27, 2014].

Okamoto, J. et al., 2012. Development of an autonomous robot for gas storage spheres inspection. *Journal of Intelligent and Robotic Systems: Theory and Applications*, 66(1–2), pp.23–35. Available at: http://link.springer.com/10.1007/s10846-011-9607-z [Accessed February 21, 2014].

Oliveira, A.L.C., Silva, M.F. & Barbosa, R.S., 2010. Architecture of an wheeled climbing robot with dynamic adjustment of the adhesion system. In *2010 8th IEEE International Symposium on Intelligent Systems and Informatics*. Ieee, pp. 127–132.

Ondreička, J. & Paľa, J., 2010. Design and Experimental Examination of New Type of Electro-Permanent Magnet Chuck. *Journal of Electrical Engineering*, 61(7), pp.152–155. Available at: http://iris.elf.stuba.sk/cgi-bin/jeeec?act=abs&no=7s_110&ttl=42 [Accessed March 7, 2014].

Online, K.& L., 2016. Tables of Physical & Chemical Constants. *16th edition 1995*. Available at: http://www.kayelaby.npl.co.uk/general_physics/2_6/2_6_6.html.

Palmer, L.R., Diller, E.D. & Quinn, R.D., 2009. Design of a wall-climbing hexapod for advanced maneuvers. In *2009 IEEE/RSJ International Conference on Intelligent Robots and Systems, IROS 2009*. IEEE, pp. 625–630. Available at: http://ieeexplore.ieee.org/lpdocs/epic03/wrapper.htm?arnumber=5354753 [Accessed March 27, 2014].

Pascoal, a. et al., 2000. Robotic ocean vehicles for marine science applications: the European ASIMOV project. In *2000 IEEE Oceans*. IEEE, pp. 409–415. Available at: http://ieeexplore.ieee.org/Xplore/cookiedetectresponse.jsp?reload=true [Accessed March 28, 2014].

Perhinschi, M.G.G., Napolitano, M.R.R. & Tamayo, S., 2010. Integrated Simulation Environment for Unmanned Autonomous Systems—Towards a Conceptual Framework. *Modelling and Simulation in Engineering*, 2010, pp.1–12.

Peyvandi, A., Soroushian, P. & Lu, J., 2013. A New Self-Loading Locomotion Mechanism for Wall Climbing Robots Employing Biomimetic Adhesives. *Journal of Bionic Engineering*, 10(1), pp.12–18. Available at: http://linkinghub.elsevier.com/retrieve/pii/S1672652913601948 [Accessed February 22, 2014].

Piranda, B. et al., 2013. A new concept of planar self-reconfigurable modular robot for conveying microparts. *Mechatronics*, 23(7), pp.906–915. Available at: http://www.sciencedirect.com/science/article/pii/S0957415813001633 [Accessed February 22, 2014].

Prahlad, H. et al., 2008. Electroadhesive robots - Wall climbing robots enabled by a novel, robust, and electrically controllable adhesion technology. In *2008 IEEE International Conference on Robotics and Automation*. IEEE, pp. 3028–3033. Available at: http://ieeexplore.ieee.org/lpdocs/epic03/wrapper.htm?arnumber=4543670 [Accessed December 1, 2013].

Pranoto, T. et al., 2007. Vibration suppression device using permanent-electromagnet and MRF shear damper. *Journal of Materials Processing Technology*, 181(1–3 SPEC. ISS.), pp.235–240. Available at: http://www.sciencedirect.com/science/article/pii/S0924013606001749 [Accessed March 7, 2014].

ROCHAT, F. et al., 2010. DESIGN OF MAGNETIC SWITCHABLE DEVICE (MSD) AND APPLICATIONS IN CLIMBING ROBOT. In *Clawar 2010*. World Scientific Publishing Co. Pte. Ltd., pp. 375–382. Available at: http://www.worldscientific.com/doi/10.1142/9789814329927_0047.

Roman, H.T., 1991. Robots Cut Risks and Costs in Nuclear Power Plants. *IEEE Computer Applications in Power*, 4(3), pp.11–15. Available at: http://ieeexplore.ieee.org/lpdocs/epic03/wrapper.htm?arnumber=85957 [Accessed March 27, 2014].

Sahay, R. et al., 2015. A State-of-the-Art Review and Analysis on the Design of Dry Adhesion Materials for Applications such as Climbing Micro-robots. *RSC Advances*, 5(1), pp.50821–50832. Available at: http://pubs.rsc.org/en/Content/ArticleLanding/2015/RA/C5RA06770G.

Santos, D. et al., 2008. Gecko-inspired climbing behaviors on vertical and overhanging surfaces. In *2008 IEEE International Conference on Robotics and Automation*. IEEE, pp. 1125–1131. Available at: http://ieeexplore.ieee.org/lpdocs/epic03/wrapper.htm?arnumber=4543355 [Accessed March 27, 2014].

Santos, M.F. et al., 2013. Development of an Underwater Riser Inspection Robot. *Industrial Robot: An International Journal*, 40(4), pp.402–411. Available at: http://www.emeraldinsight.com/10.1108/01439911311320895 [Accessed December 1, 2013].

Schmidt, D. & Berns, K., 2013. Climbing robots for maintenance and

inspections of vertical structures - A survey of design aspects and technologies. *Robotics and Autonomous Systems*, 61(12), pp.1288–1305.

Schoeneich, P. et al., 2011. TRIPILLAR: a miniature magnetic caterpillar climbing robot with plane transition ability. *Robotica*, 29(7), pp.1075–1081. Available at: http://www.journals.cambridge.org/abstract_S0263574711000257 [Accessed April 2, 2014].

Shen, Z.H. & Seipel, J.E., 2012. A fundamental mechanism of legged locomotion with hip torque and leg damping. *Bioinspiration & Biomimetics*, 7(4), p.46010.

Shirazee, N.A. & Basak, A., 1995. Electropermanent suspension system for acquiring large air-gaps to suspend loads. *IEEE Transactions on Magnetics*, 31(6 pt 2), pp.4193–4195. Available at: http://ieeexplore.ieee.org/lpdocs/epic03/wrapper.htm?arnumber=489923 [Accessed March 27, 2014].

Shiroma, N. et al., 2006. Development and control of a high maneuverability wheeled robot with variable-structure functionality. In *2006 IEEE International Conference on Intelligent Robots and Systems*. pp. 4000–4005.

Smith, H., 2001. U-99 Uninhabited Tactical Aircraft Preliminary Systems Design. *Aircraff Engineering and Aerospace Tecnology*, 73(3), pp.244–267. Available at: http://www.emeraldinsight.com/journals.htm?issn=0002-2667&volume=73&issue=3&articleid=876537&show=html.

Smith, J.A., Sharf, I. & Trentini, M., 2006. Bounding gait in a hybrid wheeled-leg robot. In *2006 IEEE International Conference on Intelligent Robots and Systems*. pp. 5750–5755.

De Sousa, J.B. & Andrade Gonçalves, G., 2011. Unmanned vehicles for environmental data collection. *Clean Technologies and Environmental Policy*, 13(2), pp.369–380. Available at: http://link.springer.com/10.1007/s10098-010-0313-5 [Accessed February 15, 2014].

Tache, F. et al., 2007. Adapted magnetic wheel unit for compact robots inspecting complex shaped pipe structures. *IEEE/ASME International Conference on Advanced Intelligent Mechatronics, AIM*, pp.1–6.

Tavakoli, M. et al., 2013. OmniClimbers: Omni-directional magnetic wheeled climbing robots for inspection of ferromagnetic structures. *Robotics and Autonomous Systems*, 61(9), pp.997–1007. Available at: http://linkinghub.elsevier.com/retrieve/pii/S0921889013001024 [Accessed November 22, 2013].

Tavakoli, M. et al., 2015. The hybrid OmniClimber robot: Wheel based climbing, arm based plane transition, and switchable magnet adhesion. *Mechatronics*, 36, pp.136–146.

Tavakoli, M., Marques, L. & Almeida, A.T. De, 2010. Development of an industrial pipeline inspection robot. *Industrial Robot: An International Journal*, 37(3), pp.309–322. Available at: http://www.emeraldinsight.com/journals.htm?issn=0143-991X&volume=37&issue=3&articleid=1858520&show=html [Accessed March 27, 2014].

Ting Wang, Yuechao Wang & Chen Yao, 2005. Study on Mechanism of a Mobile Robot Used Unstructured Environment. In *2005 IEEE International Conference on Robotics and Biomimetics - ROBIO*. IEEE, pp. 201–205. Available at: http://ieeexplore.ieee.org/lpdocs/epic03/wrapper.htm?arnumber=1708622 [Accessed March 27, 2014].

US DoD, 2013. Unmanned Systems Integrated roadmap 2013-2038 O. O. F. T. H. E. U. S. O. F. D. (ACQUISITION T. A. N. D. L. W. DC, ed. *FY*, p.168.

Wang, H. et al., 2010. Development of an inspection robot for 500 kV EHV power transmission lines. In *2010 IEEE International Conference on Intelligent Robots and Systems*. pp. 5107–5112.

Wang, H., Yamamoto, A. & Higuchi, T., 2012. Electrostatic-motor-driven electroadhesive robot. In *2012 IEEE International Conference on Intelligent Robots and Systems*. Ieee, pp. 914–919. Available at: http://ieeexplore.ieee.org/lpdocs/epic03/wrapper.htm?arnumber=6385758 [Accessed March 27, 2014].

Wang, Z. & Gu, H., 2007. A review of locomotion mechanisms of urban search and rescue robot. *Industrial Robot: An International Journal*, 34(5), pp.400–411. Available at: http://www.emeraldinsight.com/10.1108/01439910710774403 [Accessed February 22, 2014].

Ward, P. & Liu, D., 2012. Design of a high capacity Electro Permanent Magnetic adhesion for climbing robots. In *2012 IEEE International Conference on Robotics and Biomimetics, ROBIO 2012 - Conference Digest*. Ieee, pp. 217–222. Available at: http://ieeexplore.ieee.org/lpdocs/epic03/wrapper.htm?arnumber=6490969 [Accessed March 27, 2014].

Winkvist, S., Rushforth, E. & Young, K., 2013. Towards an Autonomous Indoor Aerial Inspection Vehicle. *Industrial Robot: An International Journal*, 40(3), pp.196–207. Available at: http://www.emeraldinsight.com/journals.htm?issn=0143-991X&volume=40&issue=3&articleid=17086376&show=html%5Cnhttp://www.emeraldinsight.com/10.1108/01439911311309870 [Accessed November 14, 2013].

Xiao, J. et al., 2006. Climber: A New Generation of Mobile Robot with Wall-climbing Capability G. R. Gerhart, C. M. Shoemaker, & D. W. Gage, eds. *Proceedings of SPIE - The International Society for Optical Engineering*, 6230 II(October), p.62301D–62301D–10. Available at: http://www.scopus.com/inward/record.url?eid=2-s2.0-

33748552307&partnerID=tZOtx3y1 [Accessed December 1, 2013].

Xiao, J. & Zhu, Z., 2009. *Cooperative Wall-climbing Robots in 3D Environments for Surveillance and Target Tracking*, New York. Available at: http://find.shef.ac.uk/primo_library/libweb/action/search.do?dscnt=0&vl(38298075UI4)=00&scp.scps=primo_central_multiple_fe&tab=remote&dstmp=1395933932126&vl(38298080UI0)=title&srt=date&mode=Advanced&vl(38298077UI4)=Year&vl(1UIStartWith1)=contains&tb=t&ind [Accessed March 27, 2014].

Xingguang, D. et al., 2006. MOBIT, A small wheel -track- leg mobile robot. In *6th World Congress on Intelligent Control and Automation*. pp. 9159–9163.

Xu, Z.Y. et al., 2015. Design and optimization of magnetic wheel for wall climbing robot. In *2010 EEE International Conferenece on Mechatronics and Automation*. Ieee, pp. 619–629. Available at: http://ieeexplore.ieee.org/lpdocs/epic03/wrapper.htm?arnumber=5589061.

Yoon, K.H. & Park, Y.W., 2012. Design, fabrication, and characterization of in-pipe robot with controllable magnetic force. In *8th IEEE International Conference on Automation Science and Engineering*. Seoul, Korea: Ieee, pp. 786–789. Available at: http://ieeexplore.ieee.org/lpdocs/epic03/wrapper.htm?arnumber=6386443 [Accessed March 27, 2014].

Yoshida, Y. & Ma, S., 2010. Design of a wall-climbing robot with passive suction cups. In *2010 IEEE International Conference on Robotics and Biomimetics, ROBIO 2010*. IEEE, pp. 1513–1518. Available at: http://ieeexplore.ieee.org/lpdocs/epic03/wrapper.htm?arnumber=5723554 [Accessed April 2, 2014].

Yun, H.B. et al., 2013. Development of inspection robots for bridge cables. *The Scientific World Journal*, 2013(ii), p.967508. Available at: http://www.pubmedcentral.nih.gov/articlerender.fcgi?artid=3888749&tool=pmcentrez&rendertype=abstract [Accessed March 27, 2014].

Zhang, Y. & Dodd, T., 2011. Systematic design of flexible magnetic wall and ceiling climbing robot for cargo screening. In R. Groß et al., eds. *Lecture Notes in Computer Science (including subseries Lecture Notes in Artificial Intelligence and Lecture Notes in Bioinformatics)*. Lecture Notes in Computer Science. Springer Berlin Heidelberg, pp. 414–415.

Zwicker, E., Zesch, W. & Moser, R., 2010. A modular inspection robot platform for power plant applications. In *2010 1st International Conference on Applied Robotics for the Power Industry, CARPI 2010*. IEEE, pp. 1–6. Available at: http://ieeexplore.ieee.org/lpdocs/epic03/wrapper.htm?arnumber=5624429 [Accessed February 22, 2014].